Ministry of Higher Education and Scientific Research
Abou Bekr Belkaid University, Tlemcen
Faculty of Technology

Ahlem Benazzouz

A Dissertation submitted for the degree of Doctor of Philosophy
in Biomedical Engineering
Specialty: Biomedical Instrumentation

Extraction of Electromyogram (EMG) characteristics for classification

---

Defended on July 2, 2020

Mohammed-Amine CHIKH	Professor	Tlemcen University	President
Zine-Eddine HADJ SLIMANE	Professor	Tlemcen University	Supervisor
Farid AMIROUCHE	Professor	University of Illinois at Chicago, USA	Co-supervisor
Lotfi MERAD	Professor	ESSA Tlemcen	Examiner 1
Benaoumeur AOUR	Professor	ENP Oran	Examiner 2
Abdelghani DJEBBARI	MCA	Tlemcen University	Examiner 3

“ Learning never exhausts the mind ”

— Leonardo da Vinci —

(1452-1519)

I dedicate this dissertation to:
The soul of my grandmother
My mother and father
My sisters and brother.

Ahlem Benazzouz
December, 2019

Acknowledgements

My PhD journey was such a wonderful experience that I will treasure for many years to come. Throughout these four years of study, I've learned how to sail in this immense scientific world of research, acquired new skills, learnt to be patient, committed, work continuously days and nights, walking forward and never look back to achieve my main goals. Keeping in mind the guidance, support, and persistent help and advice that I've received from many people who earned my deep gratitude, without them this dissertation would not have been possible.

First and foremost I would like to express my sincere thanks to my supervisor Prof. Zine-Eddine HADJ SLIMANE for giving me the opportunity to work on Electromyogram processing and classification, for providing me the resources I needed and for being patient with me. His kindness, encouragement, and his motivation during my PhD study were formidable.

My heartfelt appreciation goes to my mentor Prof. Farid AMIROUCHE, Director of orthopaedic research at University of Illinois at Chicago, USA. His immense knowledge in bioengineering and orthopedics help me a lot in my research and it was a truly great experience working with polymath. Because of his generous support, his insightful advice and suggestions, his motivation and his encouragement, I finished this dissertation. I really owe him too much!

In addition to my supervisors, I would like to extend my special thanks to my dissertation committee members, Prof. Mohamed Amine CHIKH, Dean of faculty of Technology, Dr. Abdelghani DJEBBARI, Director of Biomedical Engineering laboratory-Tlemcen University, Prof. Lotfi MERAD from Ecole supérieure en Sience Appliquées-Tlemcen, and Prof. Benaoumeur AOUR from Polytechnic School of Oran, for providing insightful comments and suggestions to improve the outcome of this dissertation.

Special mention goes to Prof. José Joaquin RIETA from Universitat Politecnica de Valencia, for offering me the fall internship opportunity, his expertise in biomedical signal processing, his friendly guidance, and kindness have been invaluable during my internship and after.

My deepest thanks to Prof. Abdelbaki BENZIANE, Rector of University of Oran1, for his support and guidance, and especial thanks and gratitutde goes to

a well appreciated Prof. Kebir BOUCHERIT, Rector of of University of Tlemcen.
I would also like to extend my deep gratitude and love to my family and all my friends including those in Spain for their continuous support, and encouragement during the course of my research and internship.
I would particularly like to thank my lab-mate and true friend: Rima GUILAL for standing by my side in hardest moments, for all the nights we spent on campus working together, and for all the fun we had. These are wonderful memories that I will keep with me for years to come.
Last but not least, my profound appreciation goes to my mother and father, for their unbelievable support in my whole life, their encouragement and motivation and in believing in me. Many thanks to my sisters, brother, nephew, and my little nieces for everything. "I owe you so much!".

—Ahlem Benazzouz
December, 2019

Abstract

Electromyography is a technique for recording the electrical activity of skeletal muscles by means of either surface electrodes or concentric needles. The non-invasive technique surface electromyography sEMG has received significant attention in the past decade: in biomechanics, rehabilitation, control of prosthetic devices, for the development of emotion recognition systems, sports activities, and the science of exercise. On the other hand, the invasive technique in electromyography is employed for diagnosing neuromuscular disorders such as neuropathy and myopathy. The stochastic nature of these EMG signals complicates the interpretation, so it needs advanced methods for detection, processing, feature extraction, and classification.
This dissertation aims to extract the pertinent characteristics which are essential in the diagnosis and lead to correct prediction.
During gait, the muscular activation interval, onset and offset timings are very important parameters used for studying the function of the muscle in healthy patients and detecting the abnormalities when the gait data is abnormal.These parameters have been precisely extracted by S-Transform.
We have also developed two automatic diagnosis approaches, one for soft tissue knee injuries i.e. Anterior Cruciate Ligament ACL and Meniscus MN injuries using surface electromyographic sEMG and goniometric signals, and the other one for neuromuscular disorders i.e. neuropathy and myopathy using intramuscular electromyogram iEMG. These signals (sEMG/EMG) were collected and preprocessed for extracting the newly developed parameters associated with the different pathologies. The relevant features were selected using different criteria and methods classified by supervised classifiers. The newly developed algorithms are provided and shown through different applications and case studies.

Index Terms— Anterior ligament injury, classification, Electromyogram, feature extraction, feature selection, iEMG, knee injuries, meniscus injury, myopathy, neuromuscular disorders, neuropathy, sEMG, S-Transform.

Contents

Acknowledgements **iii**

Abstract **v**

List of Figures **x**

List of Tables **xiii**

Nomeclature **xiv**

Introduction **1**
Scope of the dissertation 1
Motivation and Objectives 1
Structure of the dissertation 2

1 Basics of Electromyography **4**
1.1 Introduction 4
1.2 Structure and function of skeletal muscle 4
1.2.1 Structure of skeletal muscle 7
1.2.1.1 Muscle fiber structure 8
1.2.1.2 Motor unit structure 9
1.2.2 Physiology of skeletal muscle 10
1.2.2.1 Action potential and motor unit action potential 10
1.2.2.2 Contraction and relaxation of muscle 14
1.2.2.3 Type of muscle contractions 16
1.3 Electromyography 16
1.3.1 Intramuscular and surface EMG 17
1.3.1.1 Intramuscular and surface electrodes 17
1.3.1.2 The electrode sites and skin preparation 19
1.3.2 EMG applications 20

1.4 Conclusion 21

2 Development of real-time sEMG system 22
2.1 Introduction 22
2.2 sEMG acquisition system 22
2.2.1 Hardware part 23
2.2.1.1 Sensor 23
2.2.1.2 Analog conditioning circuit 24
2.2.1.3 Microcontroller 28
2.2.2 Software part 29
2.2.2.1 Arduino Uno software 29
2.2.2.2 Matlab graphical user interface (GUI) 30
2.3 The effect of fatness, age, gender, handedness, and diabetes on sEMG 33
2.3.1 Data collection 33
2.3.1.1 Subjects 34
2.3.1.2 Protocol 34
2.3.2 Digital signal processing 35
2.3.2.1 Temporal analysis 35
2.3.2.2 Spectral analysis 36
2.3.3 Statistical parameters 37
2.3.3.1 Temporal parameters 37
2.3.3.2 Frequency parameters 38
2.4 Results and Discussion 38
2.5 Limitation and recommendations 42
2.6 Conclusion 42

3 Muscular activation detection using sEMG signals during dynamic contractions 44
3.1 Introduction 44
3.2 Literature review of muscular activation detection methods . . . 44
3.3 S-transform-based muscular activation detection method 45
3.3.1 S-transform technique 46
3.3.1.1 The short-time Fourier transform (STFT) 46
3.3.2 The ST-STFT relationship 46
3.3.3 The Discrete S-Transform 46
3.3.4 S-Transform Matrix 47
3.3.5 The binary image of the S-transform matrix 47
3.3.6 Binary signal 47
3.4 Experimental setup 48

3.4.1 Methods for Comparison 48
3.4.1.1 Teager-Kaiser Energy Operator 48
3.4.1.2 Integrated Profile 49
3.4.1.3 Sample Entropy 49
3.4.2 Performance evaluation metric 51
3.4.3 Muscle activation interval and onset timing-knee flexion correlation 51
3.4.3.1 The muscle activation interval (MAI) 51
3.4.3.2 Correlation between onset timing and maximum flexion of the knee 51
3.5 Result and discussion 52
3.6 Conclusion and future scope 55

4 An automatic diagnosis of knee injuries using sEMG and goniometric signals 56
4.1 Introduction 56
4.2 Knee Joint 56
4.2.1 Knee Joint Anatomy 57
4.2.1.1 Bones 57
4.2.1.2 Articular Cartilages 57
4.2.1.3 Meniscus 58
4.2.1.4 Ligaments 58
4.2.1.5 Tendons and Muscles 58
4.2.2 Knee Joint Biomechanics 59
4.2.3 Knee joint biomechanics and muscle activation during gait 59
4.2.4 Knee injuries and diagnosis techniques 62
4.3 Problem statement and motivation 63
4.4 Literature review 64
4.5 Methodology 65
4.5.1 Lower Limb sEMG Dataset description 65
4.5.2 Data pre-processing 65
4.5.2.1 Independent Component Analysis (ICA) 66
4.5.3 Feature extraction 66
4.5.3.1 Time Domain features 66
4.5.3.2 Autocorrelation and linear correlation 68
4.5.3.3 Frequency Domain features 70
4.5.4 Feature Vector 70
4.5.5 Feature Selection 71
4.5.5.1 ReliefF 71
4.5.6 Classification 72

4.5.7 Performance evaluation 72
4.6 Results and discussion 73
4.7 Conclusion 77

5 An automatic diagnosis of neuromuscular disorders using iEMG 78

5.1 Introduction 78
5.2 Neuropathy and myopathy 78
5.3 Literature review 79
5.4 Methodology 81
5.4.1 Databases Description 81
5.4.1.1 Simulated EMG Database Description 81
5.4.1.2 Clinical EMG Database 81
5.4.2 Feature extraction based on Wavelet Transform methods . 82
5.4.2.1 Discret Wavelet Transform 83
5.4.2.2 Wavelet Packet Transform 84
5.4.3 Feature Extraction 84
5.4.4 Feature Selection 85
5.4.4.1 ReliefF 85
5.4.4.2 Fast Correlation-Based Filter method (FCBF) . 86
5.4.5 Classification 86
5.4.6 Performance evaluation 87
5.5 Results and Discussion 87
5.6 Conclusion 91

Conclusion 92
Future Directions 93

Appendix A 94
Publications 94
International Journal Papers 94
International Conference Papers 94
National Conference Papers 95

Bibliography 96

List of Figures

1.1 Types of muscle tissue [1]. 5
1.2 Shapes and fiber arrangements for skeletal muscles [2]. 5
1.3 Anterior and posterior skeletal muscles of the body [2]. 6
1.4 Agonistic and antagonistic muscles for flexion and extension of the knee joint 7
1.5 Structure of skeletal muscle[3]. 8
1.6 Structure of a single skeletal muscle fiber [4]. 9
1.7 Structure of the motor unit[5]. 10
1.8 Structure of myelinated Neuron [6]. 11
1.9 Ion channels [7]. 12
1.10 Action potential. 12
1.11 Neuromuscular junction and chemical synapse. 13
1.12 An example of triphasic motor unit action potential [8]. 14
1.13 Cross-bridge cycle [9]. 15
1.14 Sliding filament theory [4]. 15
1.15 Types of muscle contractions. 16
1.16 Types of EMG electrodes. 17
1.17 Types of needle electrodes. 18
1.18 Fine wire electrode. 18
1.19 Example of pre-gelled disposable sEMG electrodes. 19
1.20 Anatomical position of fine wire and surface electrode sites [10]. . 20

2.1 Block diagram of EMG measurement system. 23
2.2 Lessa electrode patches. 24
2.3 sEMG signal amplification and feedback loop circuit (drawn in NI Multisim). 25
2.4 Circuit (a) and bode diagram (b) of the first order passive high pass filter. 26
2.5 Fourth order Sallen-Key lowpass filter. 26
2.6 Bode diagram of lowpass Sallen-Key filter. 27
2.7 DC-offset adjustment circuit. 27

2.8 Power supply circuit. 28
2.9 Arduino Uno board. 29
2.10 Arduino IDE. 30
2.11 EMG graphical user interface. 31
2.12 sEMG measurement system design. 31
2.13 Acquired sEMG by Matlab interface. 32
2.14 An example of MAT and TXT sEMG files. 32
2.15 Protocol of the experimental setup. 34
2.16 sEMG baseline wander correction and envelope detection. 36
2.17 Welch's PSD of sEMG signal. 37
2.18 The sEMG signals detected from healthy male athlete (20 years old) and their PSDs. 39
2.19 Comparison between left-handers and right-handers(temporal statistical parameters). 40
2.20 Statistical comparison of sEMG parameters between diabetics and healthy subjects. 40
2.21 Statistical comparison of sEMG parameters between young, adults and elderly subjects (only for healthy subjects). 41
2.22 Statistical comparison of sEMG parameters between thin and obese subjects (only for healthy subjects). 41

3.1 Scheme of the proposed ST image segmentation method. 48
3.2 Onset and offset timing detection using ST, IP, SampEn and TKEO methods. 50
3.3 Comparison of MAI detection using ST, IP, SampEn and TKEO method. 52
3.4 Statistical comparison of onset offset detection performance. . . . 53
3.5 Detection of sEMG muscle activation and knee flexion peaks for normal (a) and abnormal (b) subjects. 54

4.1 The knee joint anatomy [11]. 57
4.2 Six degrees of freedom of the knee [12]. 59
4.3 The phases and the knee angle of normal gait. 61
4.4 ACL injury [13]. 62
4.5 Meniscus tear. 62
4.6 Block diagram of the knee injuries classification method. 65
4.7 Knee angle and angular velocity signals. 67
4.8 Integrated profile and autocorrelation of sEMG (from RF) and goniometric signal (healthy subject) 69
4.9 Autocorrelation-based goniometric features. 70
4.10 Ranking features of ACL injuries database. 74

4.11 Ranking features selection of MN injuries database. 74
4.12 Ranking features selection of Knee injuries database. 76

5.1 Neuropathic and myopathic disorders. 79
5.2 Block diagram of neuromuscular diseases classification. 81
5.3 Example of iEMG signals for normal, neuropathic and myopathic subjects. 82
5.4 Discrete wavelet decomposition at 2^{nd} level. 83
5.5 Wavelet packet decomposition at 2^{nd} level. 84
5.6 Ranking of relevant features using ReliefF and FCBF algorithms. 89

List of Tables

2.1 AD620 specifications 25
2.2 sEMG statistical parameters at different dumbbell weights 39

3.1 Statistical results of the sEMG-knee relationship and MAI diversity. 54

4.1 Muscle activation during Gait cycle 61
4.2 Feature vector description 71
4.3 Classification performance of ACLI, and MNI databases with and without feature selection. 75
4.4 Classification performance of knee injuries database with and without feature selection. 76
4.5 Confusion matrix of classification results for random forest classifier and reliefF 76

5.1 The LDA overall classification accuracy (in %) of DWT and WPT methods for simulated EMG signals. 88
5.2 The LDA overall classification accuracy (in %) of DWT and WPT methods for simulated EMG signals. 88
5.3 The confusion matrix for LDA classifier 89
5.4 The classification performance for five supervised classifiers using clinical EMG signals 90
5.5 Comparison of feature extraction methods of other studies 90

Nomeclature

Acronyms/ Abbreviations

AChE	Acetylcholinesterase
ACh	Acetylcholine
ACL	Anterior cruciate ligament
AMV	Absolute Mean Value
AP	Action Potential
ATP	Adenosine Triphosphate
CT-scan	Computed Tomography scan
CWT	Continuous Wavelet Transform
DAMV	Difference Absolute Mean
DWT	Discrete Wavelet Transform
ECG	Electrocardiogram
EEG	Electro-Encephalography
EMG	Electromyography
EPSP	Excitatory Postsynaptic Potentials
FCBF	Fast Correlation-Based Filter
FF	Foot Flat
GPL	General Public License
HO	Heel Off
HPF	high pass filters
HS	Heel Strike
iEMG	intramuscular Electromyography
IP	Integrated Profile
IPSP	Inhibitory Postsynaptic Potentials
K-NN	K-Nearest Neighbor
LCL	lateral collateral ligament
LDA	linear discriminant analysis
LPF	Low Pass Filter
MAI	muscle activation interval
MAV	Mean Absolute Value
MCL	medial collateral ligament
Med-F	Median frequency
MFAP	Muscle Fiber Action Potential
MF	Mean frequency
MN	Meniscus
MRI	Magnetic Resonance Imaging
MUAP	Motor Unit Action Potential
NMJ	Neuro-Muscular Junction
PCL	posterior cruciate ligament
PF	Peak frequency
PSD	Power spectral Density
QMF	quadrature mirror filter
RAM	Random-Access Memory
RMS	Root Mean Square
SampEn	Sample entropy
SD	Standard deviation
sEMG	surface Electromyography
SRAM	Static Random-Access Memory
STFT	Short Time Fourier Transform
ST	Stockwell Transform

SU	Symmetrical Uncertainty
SVM	Support Vector Machine
SWE	Shannon Wavelet Entropy
SWPE	Shannon Wavelet Packet Entropy
TFR	Time-Frequency Representation
TKEO	Teager-Kaiser Energy Operator
TO	Toe Off
TP	Total Power
TXT	Text
USB	Universal Serial Bus
V	Volt (s)
WPT	Wavelet Packet Transform
WT	Wavelet Transform

Greek Symbols

μF	micro-Farad
ω	Ohm
π	Ratio of the circumference of a circle to its diameter ≈ 3.14
$\psi(t)$	window function
Σ	Sum function
τ	Latency
$M\omega$	Mega-Ohm

Other Symbols

Ca^{2+}	Calcium ion
Cl^{-}	Chloride ion
Na^{+}	Sodium ion
K^{+}	Potassium ion
abs	Absolute value
AD620	Instrumentation Amplifier
AgCl	Silver chloride
Ag	Silver
arg	Argument
ATmega328	Microcontroller
G	Gain
ICL7660	Integrated circuit invert the positive input voltage
max	Maximum value
R	Resistor

Introduction

Scope of the dissertation

The biomechanics of human movement has been studied for several decades, to understand the mechanics of the human body, how it moves, how joint movements are controlled so one can measure, and diagnosis in real time joint problems and their relation to pain. This process of data analysis and modeling allows for identifying pathologies that are otherwise not seen by x-rays or current imaging techniques. Indeed, the understanding of human joints kinematics/kinetics allows for the design of better prostheses, clinical robots and improve the patient quality of life. These voluntary movements are controlled by a nerve impulse that travels along the axons to trigger the specific muscles. The signal or signals can be measured by an Electromyogram.
In kinesiology, the electromyogram plays an important role in studying and evaluating the muscle function during movement, and in orthopedics it is used to diagnose and discover the source of pain and injuries. The majority of knee injuries that affect the elite athletes are anterior cruciate ligament (ACL) and meniscus tear.
The EMG can be used as a detection technique to measure muscle feedback using surface EMG, and for the neuromuscular disorders, intramuscular EMG is most appropriate for detection of Myopathy and neuropathy.

Motivation and Objectives

The Early detection of diseases increases the patient's survival and increase its longevity; hence the computer-aided diagnosis plays an important role in the future of medicine; assists the physicians and enhance their decision making in the treatment of their patients.
To develop this new system, we need to address its integration and reliability as well as the computation time and user interface to make accessible and useful. For the patient, the cost is always an important criteria. As a researcher

in biomedical engineering, we should study carefully these criteria before implementing these newly developed technologies.
In this dissertation, we employed both sEMG and iEMG to develop an automatic detection method for knee injuries and neuromuscular disorders diagnosis. These EMG signals are weak in amplitude but contain rich information, using the advanced processing and analysis techniques proposed and extracting the relevant characteristics are key to correct prediction, whereas the low-cost of the computerized system depends on both hardware components and software tools that have an impact on the quality of data collection and processing. EMG is a powerful technique when addressing its cost.

Structure of the dissertation

This dissertation consists of five chapters. In the two first chapters, I provided the basics information needed to understand the use of electromyograms including anatomy, physiology, biomechanics, instrumentation recording technology, digital signal processing, and analysis. The last chapters provides three applications of EMG in clinical and orthopedic diagnostic techniques. Here's a short description of each chapter:
Chapter 1 provides the basic anatomy and physiology of skeletal muscle needed for understanding the origin and the source of electromyogram and outlines the fundamental concept of EMG, its types i.e. Intramuscular and surface EMG and its applications.
Chapter 2 details the hardware and software used to develop the real-time sEMG measurement system with low cost and in a simple manner, the signal processing techniques used to extract statistical features in order to facilitate the interpretation. This chapter also gives you a glance at the effect of age, gender, handedness, diabetes, obesity, and others on sEMG and how it influences on sEMG characteristics.
Chapter 3 reviews in depth the interesting aspect of muscular activation onset/offset timing detection. The recent detection methods i.e. Teager-Kaiser Energy Operator, Integrated Profile, Sample Entropy have been employed and compared with our proposed method "S-transform technique". The aim of onset/offset timing detection is to increase the detection performance, reduce the error and extract the muscle activation intervals (MAIs) parameter to detect the knee pathology during dynamic contraction as well.
Chapter 4 provides an automatic method for knee injury diagnosis using sEMG and knee kinematics during gait. The features were extracted in time-domain and frequency-domain then selected for classification. This chapter details the basic anatomy and biomechanics of the knee joint, and the different injuries that affect

the knee. The existing diagnosis techniques to understand clearly our concept, the muscle activity, and the knee function during gait are described in detail.
Chapter 5 is devoted to the clinical application of EMG using iEMG. This chapter reviews the decomposition methods apply on iEMG signal to extract features and classify the neuromuscular disorders i.e. neuropathy and myopathy. A comparative study was made between two wavelet-transform techniques i.e. discrete wavelet transform and packet wavelet transform using two databases i.e. simulated database for evaluating and clinical database for validating the results.
Finally, the conclusion and future research provide a brief summary of these chapters and potential research based on the developed techniques that could have benefits on our future research.

1

Basics of Electromyography

1.1 Introduction

The perfect integration of the brain, nervous system, and muscles appears clearly in human body motion, these movements and gestures are controlled by electrical signals which are transmitted from the brain to muscles via the peripheral nervous system. The analysis of human movements and the study of these electrical signals aid in discovering and diagnosing the abnormalities.
Electromyography is the recording of the electrical activity of muscle by means of electrodes regarded as a diagnostic technique also as a tool for rehabilitation and prosthetics control.
The focus of this chapter is on the anatomy and physiology of electromyography. We will describe the structure of skeletal muscle and explain how the electrical signals (action potential waves) are generated and transmitted for exciting the muscles to contract and move the body. This chapter also will describe the types of electromyographic techniques and their applications.

1.2 Structure and function of skeletal muscle

The muscle tissues are assists in moving the body or materials inside the body. It exists three types of muscle tissue i.e. smooth muscle, cardiac muscle, and skeletal muscle(see Figure.1.1).
Smooth muscle is found in the walls of internal organs and tubes such as intestines, stomach, blood vessels, and internal passageways; and also, in the follicles at the skin. the cardiac muscle is found in walls of heart in order to pump the blood through the circulatory system; both cardiac and smooth muscles can be excited and controlled by the nervous system or by the other stimuli such as hormones,

chemical signals like autocrine and paracrine agents. Whereas skeletal muscle is concerned with voluntary control which completely relies on exciting from the nervous system to contract and move the skeleton[14].

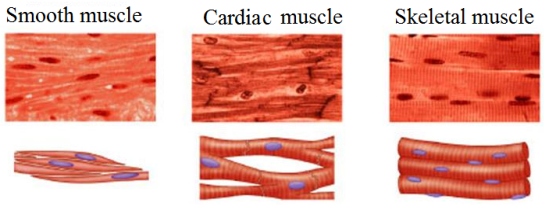

Figure 1.1: Types of muscle tissue [1].

Besides the excitability and contractility, the muscle tissue has other proprieties i.e. extensibility and elasticity. The extensibility allows the muscle tissues to extend and due to elasticity, the muscles recoil to their original length.
The skeletal muscles represent 40% of body mass, named according to their shapes, their fascicles or fibers arrangements i.e. parallel, fusiform, convergent, triangular, circular, pennate (see Figure.1.2); to their location in body e.g. orbicularis oculi muscle which has an orbicular shape situated in the orbit; or to their location in the bone like temporalis which is located on top of the temporal bone [14].

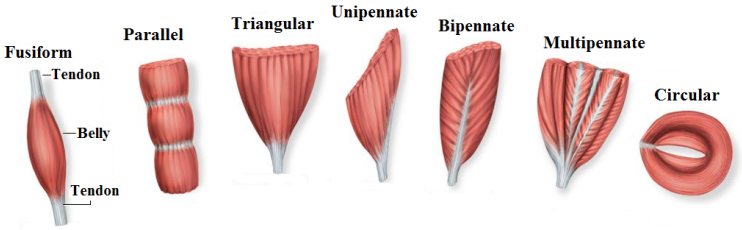

Figure 1.2: Shapes and fiber arrangements for skeletal muscles [2].

Also, they can be determined by their size, i.e. minimus meaning minimum, medius (medium), and maximus (maximum) for example gluteus maximus; or identified by their length: longus for long muscle and brevis for short muscle e.g. radialis brevis. Other muscle's names indicate their origins and or insertions like biceps brachii that has two origins, and triceps brachii (three origins). Some of the others are related to their position, for example, tibialis posterior, tibialis anterior, rectus (straight) femoris, and vastus medialis (toward the midline), or to their action e.g. flexor /extensor, abductor/adductor muscles (see Figure.1.3).

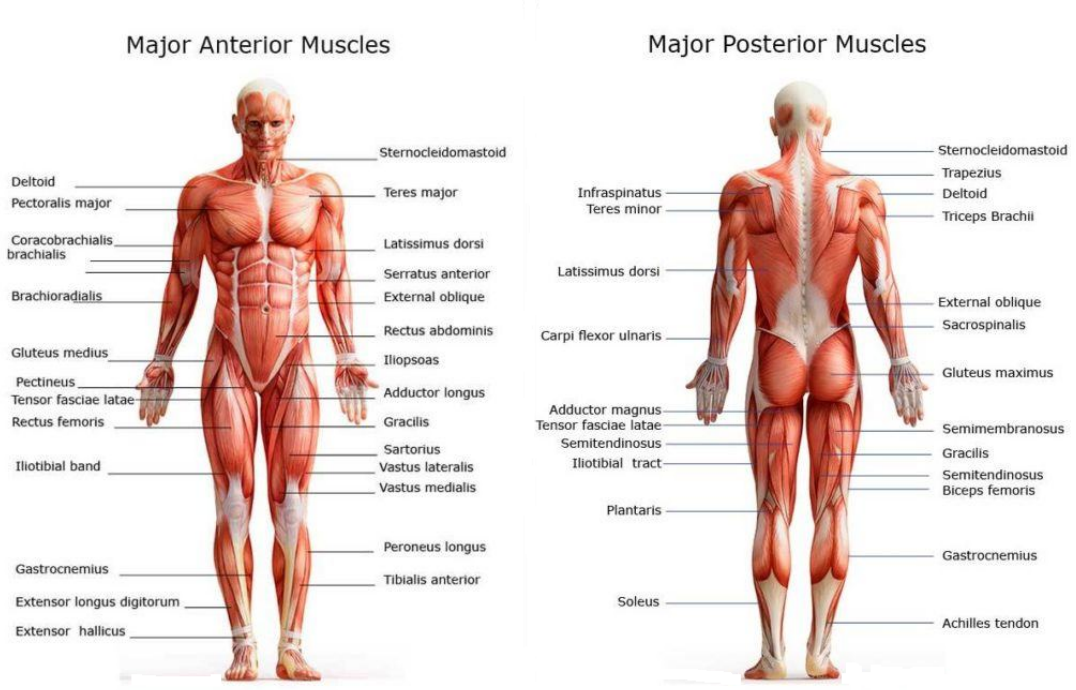

Figure 1.3: Anterior and posterior skeletal muscles of the body [2].

The skeletal muscles are also classified according to their action into four types i.e. agonist, antagonist, synergist, and fixator. Agonistic muscle is the prime mover that contracts and generates most of the force to produce the movement, meanwhile, the antagonistic muscle opposes the action in order to maintain a smooth movement; in the same time, the synergist contracts directly to action and complement the prime mover in order to facilitate the movement. The fourth type is the fixator, acting on joints to stabilize and provide posture, it can be considered as a synergist type because it assists the agonistic muscle in movement. In Figure.1.4, the agonistic muscle for flexion of knee joint are the hamstrings and the antagonistic muscles are quadriceps because the hamstrings are contracted to flex the knee meanwhile, quadriceps muscles are relaxed. However, for knee joint extension, the quadriceps are the agonists and hamstrings are the antagonists.

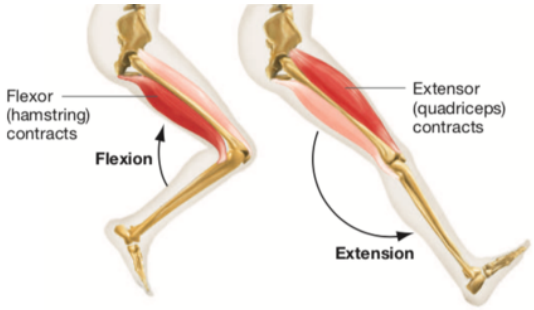

Figure 1.4: Agonistic and antagonistic muscles for flexion and extension of the knee joint

The skeletal muscles act not only to move the body but also to stop and control the movement, to stabilize the joints and maintain posture, act as a protective shield against the exterior trauma for the internal organs and support their weights, contribute to homeostasis processes by generating and balancing the heat in the whole body as well.

1.2.1 Structure of skeletal muscle

Skeletal muscles differ in size, shape, and function, but their main structure is basically the same (see Figure.1.5). Each muscle is wrapped in protective sheath or layer called **epimysium** which separates the muscle from neighbor muscles and protects it from the friction against the other tissues, organs and bones, it also continues to the end of muscle and inter-meshes with bundles of collagen fibrous tissue (**fascia**), and **tendon** in order to connect muscles with bones. Inside each muscle, there are a number of bundles of muscle fibers called **fasciculus** which is surrounded by another layer tissue called **perimysium**. A bundle of muscle fibers contains 10 to 100 fibers, a large number of fibers are found generally in the large strong muscles e.g. the muscles of quadriceps group, whereas a few numbers of fibers found in small muscles those in hand which used for precision movements. Each **muscle fiber** is covered by a connective tissue layer called **endomysium**, which in turn insolate each fiber[6].
These three-layer tissues i.e. epimysium, perimysium, and endomysium provide two main functions. They allow the whole skeletal muscle to exert tensile forces due to muscle layer tissues-tendon connection; secondly, they group the units of fibers or fasciculus together to integrate their action.
In addition, the skeletal muscle is also rich by nerve for innervation and blood vessels to deliver the oxygen, nutrients e.g. glucose, and waste removal.

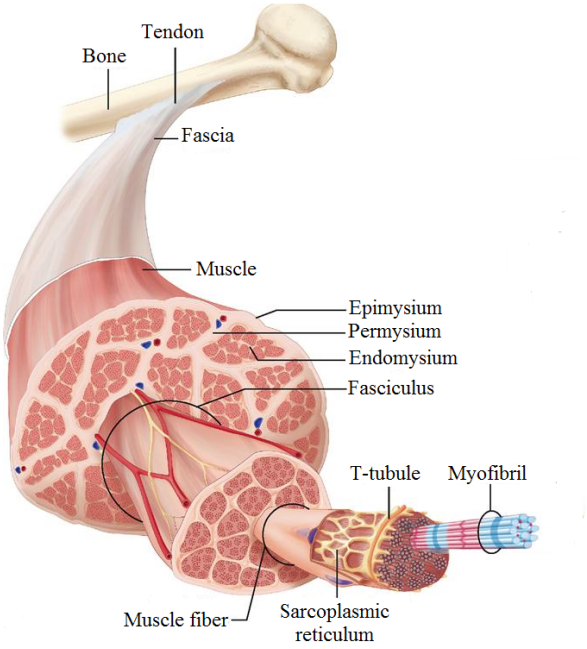

Figure 1.5: Structure of skeletal muscle[3].

1.2.1.1 Muscle fiber structure

The individual muscle fiber is made of the multinucleated cell membrane called the **sarcolemma**, and sarcoplasm which is the cytoplasm of muscle fiber contained gelatinous fluids i.e. glycogen and fat, as well as mitochondria to produce the energy, and surrounds many of cylindrical myofibrils.
Each **myofibril** is about 1μm in diameter and has the length of muscle fiber, surrounded by a network of tubules and channels called sarcoplasmic reticulum which store the calcium and controls the contraction/ relaxation of myofibrils. Within the myofibril, there are a series of sarcomeres composed of thick and thin filaments i.e. **myosin** and **actin** proteins, respectively (see Figure.1.6); and two regulatory proteins: tropomyosin and troponin.
The sarcomere is the basis for the sliding filament theory of muscle contraction, that's because the interaction between myosin and actin proteins causes a sarcomere contraction which in turn contracts the muscle fiber.

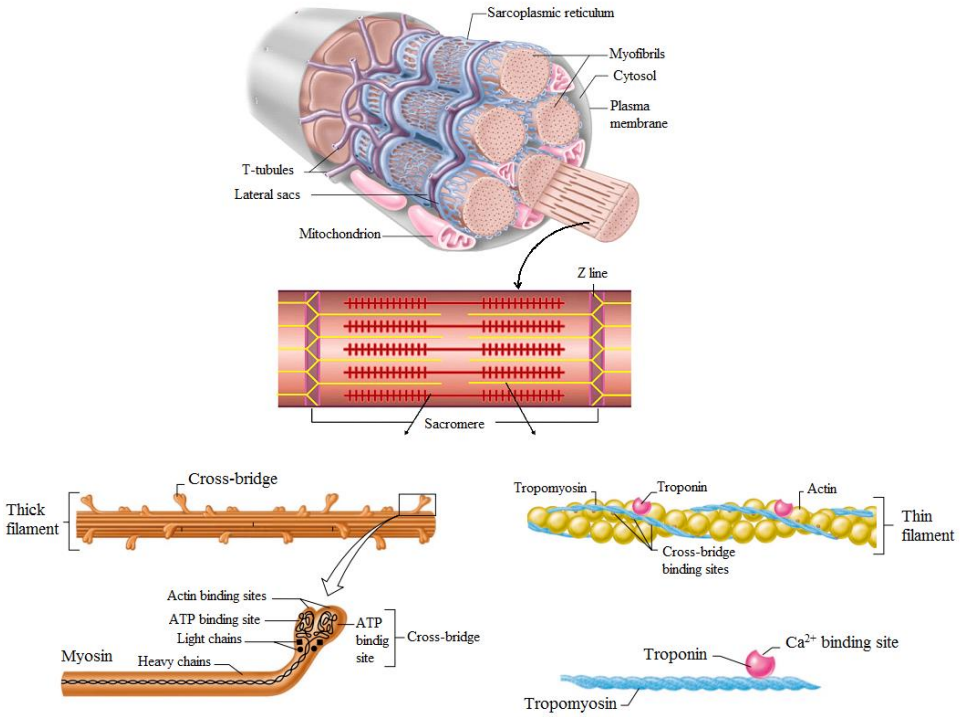

Figure 1.6: Structure of a single skeletal muscle fiber [4].

The muscle fibers are classified on the base of their metabolic, histochemical, and mechanical proprieties into two categories: slow-twitch fibers and fast-twitch fibers[15].
The slow-twitch fibers or type I are red fibers with high resistance to fatigue, they are appropriate for long term sustained contractions and product the energy by using aerobic metabolism.
The fast-twitch fibers or type II is divided into two types: fast-twitch oxidative (type IIA) and fast-twitch glycolytic (type IIB) Type IIA fibers are pale with a low resistance to fatigue compared to type I, use both aerobic and anaerobic metabolisms to produce energy and generate sustained contractions of the short term. While type IIB fibers are white and fatigue faster than type IIA, use only the anaerobic metabolism to produce energy and generate quick contractions.

1.2.1.2 Motor unit structure

Motor unit is a number of muscle fibers innervated by one α motor neuron via a neuromuscular junction (NMJ) (see Figure.1.7). The α motor neuron located in the spinal cord transmits an electrical signal along its axon to NMJ. at the NMJ, the motoneuron termini and sarcolemma are connected by chemical synapses.

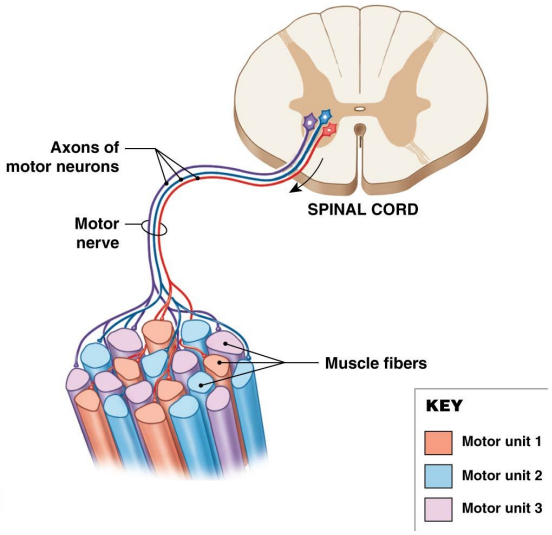

Figure 1.7: Structure of the motor unit[5].

The size of the motor unit effects the strength and the degree of muscle movements. In the small motor unit, the single motor neuron supplies a few numbers of muscle fibers to produce precise movements such as the muscles of the extraocular eye that move the eyeballs. For the large motor unit, the single motor neuron is connected to a large number of muscle fibers in order to produce gross movements such as the quadriceps muscle that move the thigh. As strong contraction is needed, the nervous system excites more than one motor unit, these stimulated motor units increase the strength of contraction known as **recruitment**.

1.2.2 Physiology of skeletal muscle

1.2.2.1 Action potential and motor unit action potential

Before stimulation, the neuron potentials are negatively polarized, it means that the intracellular fluid has a high concentration of potassium K^+ and large anions compared with extracellular fluid that has a high concentration of sodium Na^+ and chloride ion Cl^-. These ions and anions distributions create a positive charge on the outside and a negative charge on the inside. During the resting state, two specific channels work to establish the resting potential. The leakage channels allow to slowly flow Na^+ into the cell membrane or K^+ out the cell, also the Na^+/K^+pump is powered by metabolic energy i.e. adenosine triphosphate (ATP) to pump Na^+ outside and restore K^+, this aid to maintain the resting potential (-70 mV typical value in human neuron cell).[6].
The neurons are excitable cells divided into two portions: soma and dendrites

designed as analog portion, and the digital portion consists of axon, from axon hillock to axon terminals (see Figure.1.8), their dendrites are received information from other neurons synapses i.e. electrical synapses with direct connection and chemical synapses which release the neurotransmitters to open up the chemically-gated channels and generate the graded potentials. Some of these transmitters and postsynaptic receptors are excitatory, allow the Na^+ or Ca^{2+} to come in the cell, pushing the membrane potential toward the threshold and depolarize the neuron. Others are inhibitory, allow the K^+ to leave the cell or Cl^- to enter the cell, and generate the hyperpolarizing graded potentials that move away from the threshold. The summation of all these signals i.e. Excitatory and inhibitory postsynaptic potentials (EPSP and IPSP) leads the neuron to fire an action potential if their sum reaches the threshold [14].

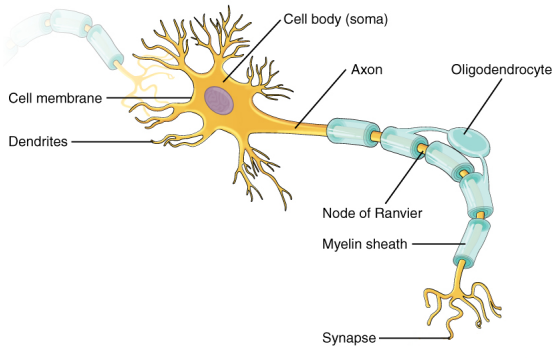

Figure 1.8: Structure of myelinated Neuron [6].

The neurons always obey ' *all or no law*', depend on threshold not on the strength of stimuli, that is, when a stimuli with sub-threshold intensity (less than -55 mV) is applied to axon hillock, no action potential is fired; when the stimuli hit the threshold even if the strength of stimuli is much more than threshold value, the produced action potential is looking exactly the same with no increase in the amplitude.
At the threshold -55 mV, the Na^+ voltage-gated channels open up and allow a rush of sodium to enter the cell membrane, this large amount of sodium causes a depolarization and increase the voltage to +30 mV when the Na^+ voltage-gated channels become inactivated, the K^+ voltage-gated channels open and allow the passage of potassium to outside which causes repolarization. During this phase, the Na^+ voltage-gated channels close at -55 mV, while potassium continues to rush the cell until the closing of K^+ voltage-gated-channel at -50 mV. During this short delay, the influx of K^+ results in undershoot (hyperpolarization). The

leakage channels and Na^+/K^+ pump (Figure.1.9) re-establish that overshoot gradient to -70 mV in order to return to resting state.

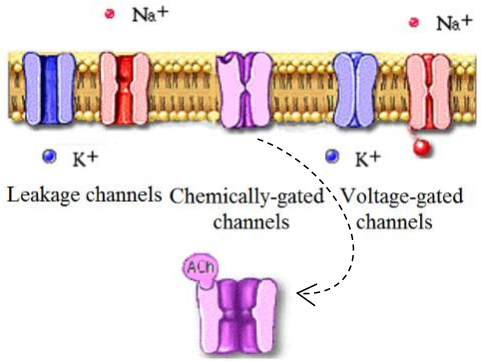

Figure 1.9: Ion channels [7].

The period in which the Na^+ voltage-gated channels are inactivated is known as the absolute refractory period, during this period, the neuron does not respond to any stimulus no matter how strong it may, and another action potential cannot be fired. Once the Na^+ voltage-gated channels close, the neuron can respond only to the stimulus that has a greater threshold than the normal threshold, this is because of the rush of K^+ , the amount Na^+ that should depolarize the neuron will only retain it from hyperpolarizing (see Figure.1.10).

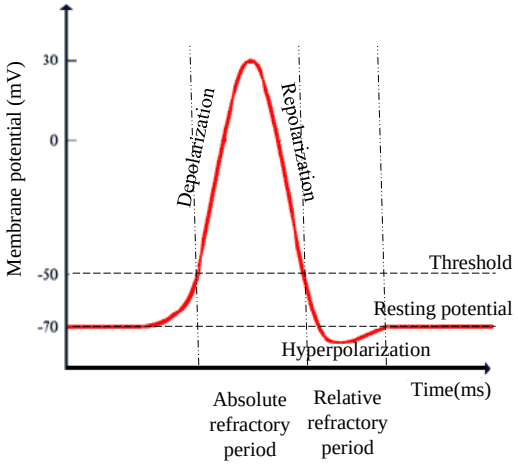

Figure 1.10: Action potential.

The action potential generated at the axon hillock travels down towards the axonal termini in order to excite the muscle fiber. As the Na^+ voltage-gated channels of the current section close, the action potential propagates to the adjacent section and moves along the axon. Due to the absolute refractory period, the action potential does not move in the reverse direction. These continuous propagations are found in unmyelinated axons (the short axon). The long axons are insulated by myelin sheath to speed up the transmission of the action potential. In these myelinated axons, the action potential jumps from one Ranvier node to the next, this sort of propagation is termed saltatory conduction.
When an action potential reaches the motoneuron termini, it depolarizes the synaptic end bulb membrane (see Figure.1.11), opens the voltage-gated calcium channels and allows the calcium ions (Ca^{2+}) to enter inside. These Ca^{2+} ions dock with the surface of synaptic vesicles to maintain the connection of vesicles with docking proteins and facilitate their merging with the presynaptic membrane.
As the vesicles merge with the presynaptic membrane, they start to release neurotransmitters acetylcholine (Ach) through the synaptic cleft. These neurotransmitters bind to ACh receptors at the motor end-plate of the sarcolemma and trigger a depolarization. Then, they are quickly dissociated and recycle back to the synaptic vesicles or degraded and hydrolyzed by acetylcholinesterase (AChE) enzyme in order to prevent an excessive firing of the action potential, and regulate the timing and the degree of contraction as well.

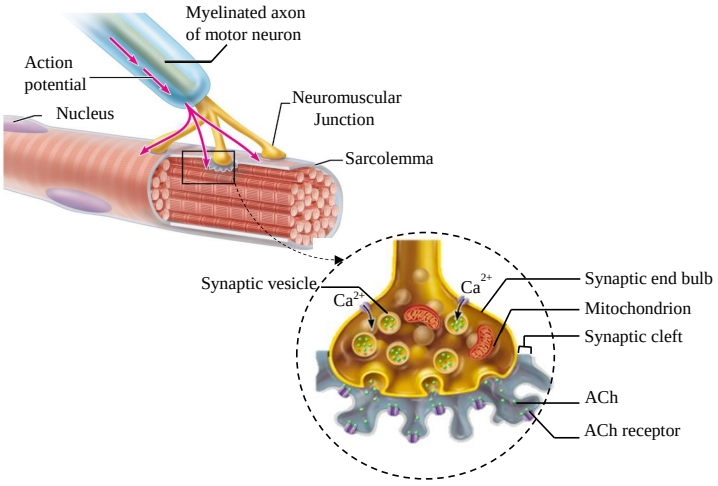

Figure 1.11: Neuromuscular junction and chemical synapse.

As known that all the neuromuscular junctions' potentials that depolarized the sarcolemma are excitatory. While the sarcolemma is depolarized, the sodium and

potassium voltage-gated channels become activated to trigger an action potential that propagates in both directions along the muscle fiber, called the muscle fiber action potential (MFAP). The Spatio-temporal summation of these potentials of the same motor unit called motor unit action potential MUAP (Figure.1.12).

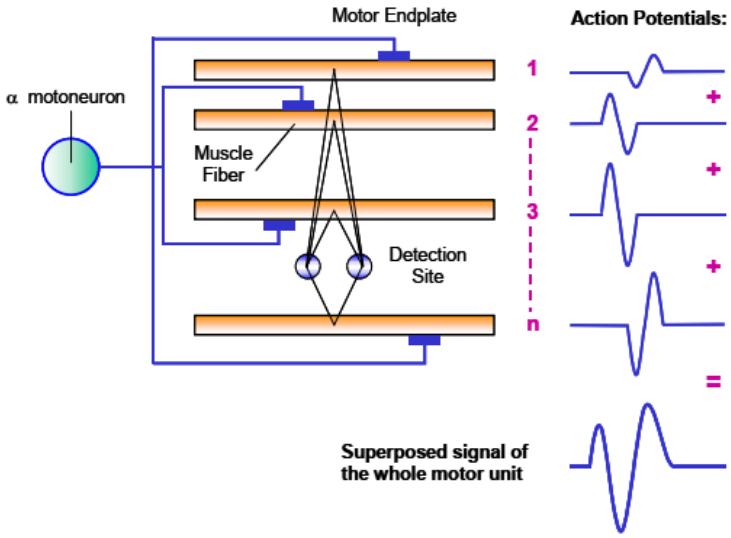

Figure 1.12: An example of triphasic motor unit action potential [8].

1.2.2.2 Contraction and relaxation of muscle

The muscle contraction begins when the muscle fiber action potential propagates along the sarcolemma and penetrates into the transverse network of tubules (T-tubules) to stimulate the sarcoplasmic reticulum. Once the sarcoplasmic reticulum is excited, the Ca^{2+} voltage-gated channels open and allow the Ca^{2+} to move into the sarcoplasm. The released Ca^{2+} ions bind to troponin, which in turn forces the tropomyosin to move away from binding sites and allow the myosin and actin to bind and form the cross-bridges. Then myosin heads start to pull the actin filaments but only for a short distance, and to reach the sarcomere center, they must be detached, reattach to other binding sites and pull again. This repeated action is known as the cross-bridge cycle (Figure.1.13) that cannot be accomplished without ATP and ATP Hydrolysis that used for detaching and reattaching of the cross-bridges, respectively.

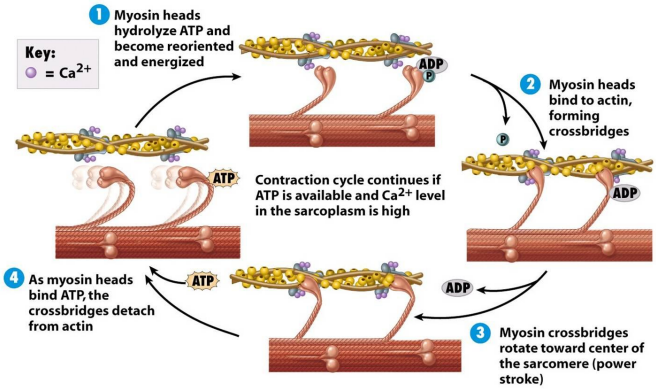

Figure 1.13: Cross-bridge cycle [9].

This procedure results in sliding filament theory (Figure.1.14), sarcomere shortens , and the muscle contracts.

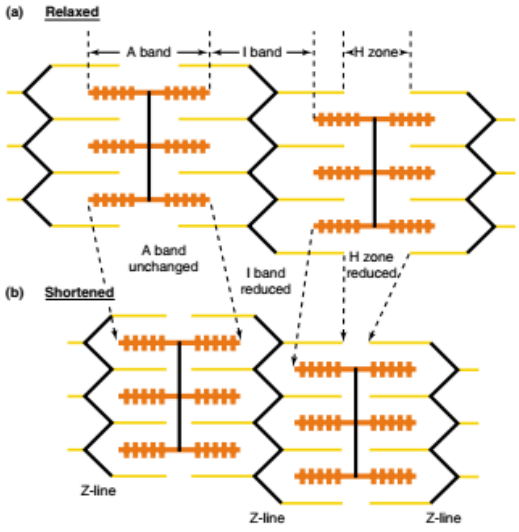

Figure 1.14: Sliding filament theory [4].

When the action potential ends, the muscle fiber membranes repolarize, and the voltage-gated Ca^{2+} channels close. The Ca^{2+} ions are then restored to sarcoplasmic reticulum by ATP-driven pumps. Without these ions, the myosin-action binding is broken down, meanwhile, the tropomyosin recovers the binding-sites. As a consequence, the sarcomere returns to its resting state and the muscle relaxes.
In resting state, the muscles don't become flaccid because of muscle tone which

is a random asynchronous contraction that provides a closely constant state of low-level tension and resistance to stretch, maintain posture and stabilize the joints.

1.2.2.3 Type of muscle contractions

The muscle contractions are characterized by tension across the muscle, the length of the muscle, and the amount of energy required by the muscle. There are three types of contractions: isotonic, isometric, and isokinetic contractions.

- Isotonic contractions are the regular weight loading contractions, while the length of the muscle and the required energy change, the muscle tension stay the same. It is also divided into two types of contractions: concentric and eccentric contractions.
- Concentric contraction occurs when the tension across the muscle is greater than the load, and the muscle shortens.
- Eccentric contraction occurs when the tension across the muscle is less than load, and the muscle lengthens.
- Isometric contraction: the muscle length stays the same meanwhile the tension across the muscle and the energy may change.

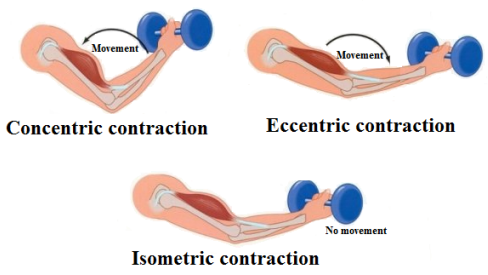

Figure 1.15: Types of muscle contractions.

1.3 Electromyography

The electromyography is an electrodiagnostic technique for measuring and evaluating the electrical activities of skeletal muscle. its records are known as electromyograms or electromyographic signals which represent the sum of motor unit action potentials at a given area, detected either by intramuscular electrodes or

surface electrodes. The choice of these electrodes types i.e. invasive or non-invasive depends on the domains of application, and the needs of clinicians as well.

1.3.1 Intramuscular and surface EMG

There are two types of EMG: intramuscular electromyography (iEMG) and surface electromyography (sEMG). The iEMG signals are recorded by invasive electrodes whereas the non-invasive electrodes are used for sEMG (Figure.5.3). The quality of EMG signals is related to the shape, the size, and the placement of electrodes, and also to the proper skin preparation.

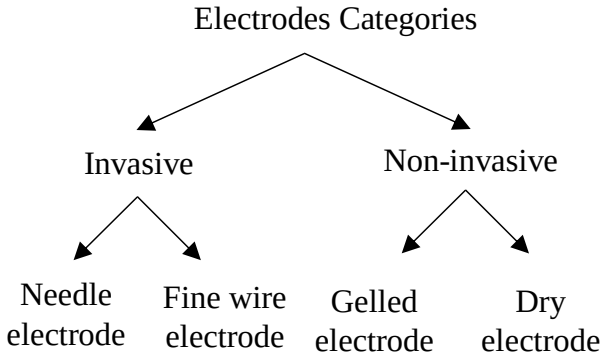

Figure 1.16: Types of EMG electrodes.

1.3.1.1 Intramuscular and surface electrodes

The intramuscular electrodes i.e. needle, and fine wire are applied on thin, and deeper muscles to evaluate the single motor unit action potentials (MUAPs), can be used in a clinical investigation such as neuromuscular disorders diagnosis.

1.3.1.1.1 Needle electrode It exists three types of needle electrodes.

- The monopolar needle is manufactured from stainless steel cover by Teflon, his small diameter and finely sharpened point decrease the level of pain during the implantation. However, the distance between the needle (active electrode) and the surface electrode used for reference increase the background of noise.
- The concentric needle contains an insulated wire used as an active electrode in the cannula with a diameter of 0.5 mm. and the reference outside of

it, these small active electrode-reference distances reduce the background noise. But it is painful due to its large diameter.

– The single-fiber needle consists of a fine platinum wire with a diameter of 25μm inside the stainless-steel cannula (0.5-0.6 mm of diameter).

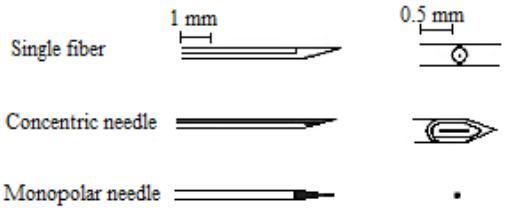

Figure 1.17: Types of needle electrodes.

1.3.1.1.2 Fine wire electrode It's produced by inserting two insulate fine wires with a small diameter of 0.025 mm through the cannula of a hypodermic needle. The preferable alloys which are used for wires are 90% platinum and 10% iridium to ensure the rigidity of wires and make them handle easily. Also, the nylon, polyurethane, and Teflon are used as insulations. This kind of electrode is more comfortable than needle electrodes.

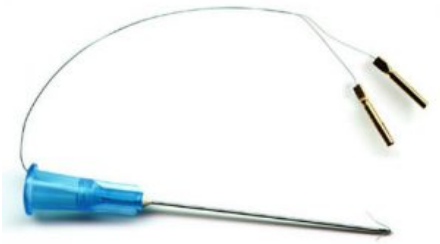

Figure 1.18: Fine wire electrode.

Whereas, the surface electrodes are applied to the surface of the skin and measure only the superficial muscles. The choice criteria of their materials depend on electrode-skin contact, electrode-skin impedance, stability, and allergic reaction. There are three sorts of material: silver, conductive polymer and gold described below.

– Silver/silver chloride electrode: The Ag/AgCl is a non-polarized electrode with low junction potentials and high stability. It can be manufactured easily, hence it is not expensive.

– Conductive polymer electrode: it has conductive and adhesive properties, which means that it doesn't need for gel or adhesive, also it becomes conductive when joining to Silver foil or Aluminum. However, it is not appropriate for low noise due to its high resistivity and has not a good connection compared to Ag/AgCl electrode.

– Gold electrode: its conductivity is very high with low impedance, and more expensive compared to Ag /AgCl where is often used for EEG.

Figure 1.19: Example of pre-gelled disposable sEMG electrodes.

1.3.1.2 The electrode sites and skin preparation

To obtain a high quality of EMG signals, the EMG recording electrodes should be well positioned and required on cleaned skin. For iEMG, the intramuscular electrodes insert into cleaned skin away from nerve trunks, blood vessels, and viscus at 45° angle, approximately. Whereas, the pair of sEMG electrodes or more are placed on the surface of the skin parallel to the muscle fibers at the belly of muscle with detecting surface of 1-2 cm measuring from the center of electrodes in order to reduce the electrical cross-talk from the adjacent muscles. Also, the skin should be prepared beforehand by removing the body hair and using alcohol to clean the skin; for the dry electrodes, the gel should be used to reduce the electrode-skin impedance. Figure.1.20 shows the different sites for surface electrode and fine wire electrode.

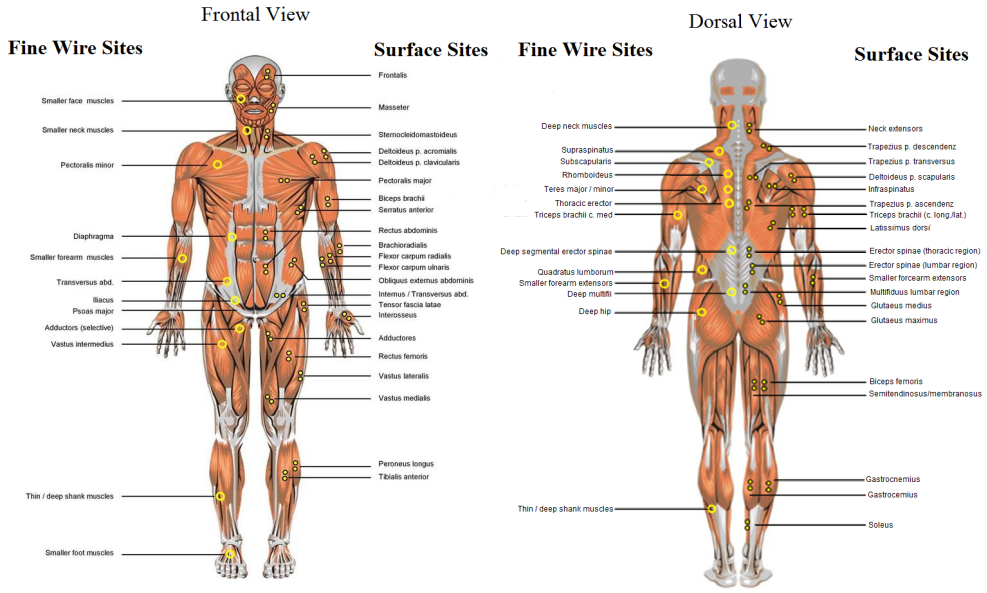

Figure 1.20: Anatomical position of fine wire and surface electrode sites [10].

The iEMG and sEMG do not differ only in recording electrodes but also in bandwidths. The iEMG bandwidth ranges from 0 -1000 Hz, whereas the sEMG bandwidth ranges from 20 to 600 Hz [16].

1.3.2 EMG applications

The sEMG is very comfortable during movement and easy to use, hence it has recently received significant attention in medical research, sports science, biometry, and ergonomics.

- Medical research such as gait and posture analysis [17] [18][19][20][21], control of prosthetics [22][23][24][25], pregnancy Monitoring by measuring uterine EMG [26] [27][28], orthopedics . . . etc.
- Rehabilitation: Post-surgery, physical therapy, neurological rehabilitation [29] [30]. . . etc.
- Sports medicine: Biomechanics [31], movement analysis, sports rehabilitation [30][29]. . . etc.
- Biometrics: personal identification [32][33], gait analysis, pattern recognition [34] . . . etc.
- Ergonomics: analysis of demand, ergonomics design [35][36] . . . etc.

The iEMG measures the deep and specific muscles, used for diagnosing neuromuscular disorders such as neuropathy and myopathy [37].

1.4 Conclusion

In this chapter, the basic physiology and anatomy of skeletal muscle, the mechanism of muscle contraction are described to understand the origin and the source of electromyographic signals. The action potential travels down from the neuron located in the brain to muscle through the myelinated axon in order to excite the contractile unit i.e. sarcomere. the sliding of thin and thick filaments results in the muscle contractions. The spatiotemporal summation of these potentials is recorded by EMG electrodes.
Two different EMG techniques are used to detect these motor unit action potentials: intramuscular EMG and surface EMG. The iEMG is used for specific muscle especially for the deep and thin muscle whereas the sEMG is used on the surface of the skin and measure the activity of many motor units. Recently, the EMG technique is widely applied to different applications not only in studying the muscle state.
In the next chapter, we will present the sEMG measurement system which is developed in order to recover and analysis the sEMG signals and studying the effect of the muscle weakness on sEMG.

2

Development of real-time sEMG system

2.1 Introduction

Nowadays various commercial sEMG systems are available with high quality and precision. Our aim is to develop a low-cost real-time sEMG acquisition system with a single channel and collect real sEMG data. These collected data are used for studying the effect of age, gender, patient's health status, and handedness on skeletal muscles and sEMG signals. This chapter is divided into four main sections. Here's a quick summary of these sections:
— The hardware part describes the analog circuit and the Arduino Uno acquisition board.
—The software part includes the firmware and the Graphical user interface (GUI).
— Collection of surface Electromyographic data.
— Finally, the digital signal processing and sEMG signals analysis.

2.2 sEMG acquisition system

The sEMG measurement system consists of different blocks designed to perform specific tasks. Starting with the sensor, the quality of raw sEMG signals depends on the location of surface electrodes, and skin preparation (refer to Chapter 1). These acquired sEMG signals are low in amplitude and noised, hence the signal conditioning circuit is used. The signals are firstly amplified by instrumentation amplifier then filtered using the analog pass-band filter. The DC offset adjustment circuit is utilized to prepare these bipolar signals for ADC. A laptop (DELL core

i5-2450M, 2.5 GHz, 6GB RAM, Win7, 64 bit) is used to upload the firmware in the Arduino Uno card and digitalize the analog sEMG signal at a frequency of 2000Hz with a resolution of 10 bits. These sEMG data are transmitted via the USB port and stored. To facilitate this task, we developed an interface (GUI) in the Matlab environment. The overall block diagram of this sEMG-DAQ system is shown in Figure.2.1

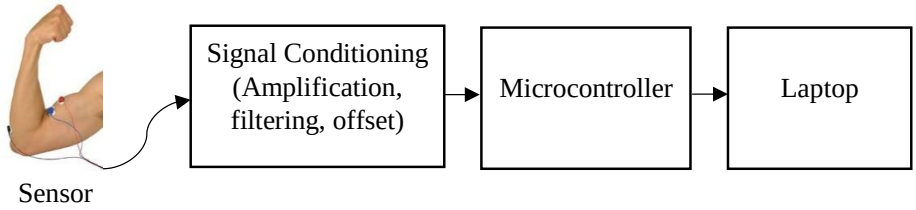

Figure 2.1: Block diagram of EMG measurement system.

2.2.1 Hardware part

The hardware part consists of two boards. The first board developed to acquire the analog sEMG signals including the instrumentation amplifier, analog filters, and DC-offset adjustment circuit. and the second board i.e. the Arduino Uno card used to digitalize the analog signals. In this section, we will describe in detail the main parts of these boards and their functionality.

2.2.1.1 Sensor

Dry and gelled electrodes are both used for detecting sEMG. the dry electrodes are appropriate for long term use especially for a prosthetic device meanwhile, the gel electrodes are disposable and used for a short term, but due to adhesive gel, they have a low electrode-skin impedance and make more stable skin contact. The Ag/AgCl electrode patches shown in Figure.2.2 are used in this study; a pair of these electrodes are placed in the middle of the belly of biceps brachii muscle with an interelectrode distance of 2 cm, and the ground reference electrode is placed on the elbow.

Figure 2.2: Lessa electrode patches.

2.2.1.2 Analog conditioning circuit

The sEMG signals are low in amplitude (0 to 10 mV) and can be contaminated by various noises or artifact sources that impact on their quality and lead to misinterpretation and erroneous diagnosis. Among these artifacts, the mechanical artifacts causing by skin-electrode interface or cables movements during dynamic activity; these artifacts are of a low-frequency range from 1 to 10 Hz, may occur when one or all of the electrodes detach, when the reference electrode is not utilized, when the wire is damaged, or when the electrodes change their sites. Also, the electrodes may pick up the crosstalk produced by the activity of neighboring muscles. As well as, the electromagnetic radiation of external devices such as the power sources (50 or 60 Hz), light bulbs especially the fluorescent lights, phone lines and ethernet cables ...etc. The ECG artifact influences on sEMG signals detected from the close muscle to the heart.
These artifacts and noises can be reduced by using a differential amplifier with high common-mode rejector ratio, choosing the right electrode design, respecting the inter-electrode distances, reducing the skin-electrode impedance by applying the gel layer, fixing the electrode correctly in the skin, utilizing the reference electrode, and also minimizing the number of devices connecting concurrently in order to avoid the ground loops, as well as the use of the battery, is recommended to reduce the Interfering power.

Amplification —The weak amplitude of sEMG that is acquired from the sensor is amplified through an amplifier circuit that consists of the instrumentation amplifier (AD620). This type of device has many desirable characteristics in medical applications, among these characteristics, AD620 provides a high common-mode rejection ratio (CMRR), it has a high input impedance, high gain, and optimal bandwidth. Furthermore, the low bias currents and low current noise coupled with the low voltage noise improve the dynamic range and achieve better performance [38].
Table.2.1 summarizes the main characteristics of AD620.

Table 2.1: AD620 specifications [38].

Parameter	Value
Gain	$[0 - 1000]$
Bandwidth at G = 100	120 kHz
Input voltage noise	9 nV/$\sqrt{}$Hz,@1 kHz
CMRR at 10 gain	100dB
Max input bias current	1 nA
Power supply	$[\pm 2.3 - \pm 18]$

The AD620's gain is resistor programmed by R_G, or more precisely, by whatever impedance appearing between Pins 1 and 8. For any arbitrary gain R_G can be calculated by using the following formula [38]:

$$R_G = \frac{49.4k\Omega}{G - 1} \tag{2.1}$$

Where G is the gain.
In our sEMG circuit, we use a resistor R_G with a value of 56Ω, this empirical selection has been obtained after several tests to get the gain of 883
The feedback loop circuit is used to reject the common-mode interference provoked by electrodes through the reference electrode in order to prevent instability and reduce the motion artifacts and noises.

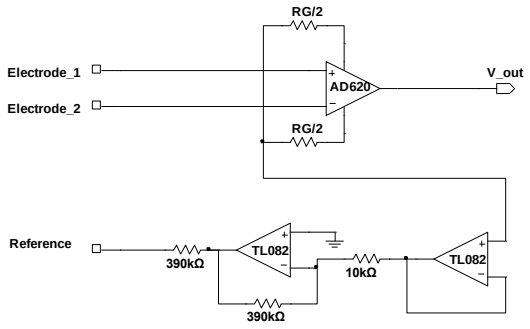

Figure 2.3: sEMG signal amplification and feedback loop circuit (drawn in NI Multisim).

Filtering — After the amplification stage, the EMG signal is still contaminated by noise and to reduce this interference we used two types of filters. A passive high pass filter and an active lowpass filter.

– **Passive high pass filter**
A first-order passive high pass filter with low cut-off frequency (Fc) of 0.04 Hz is applied to attenuate baseline noise. As shown below the used passive high pass filter with R= 1.6MΩ and C=2.2 μF.

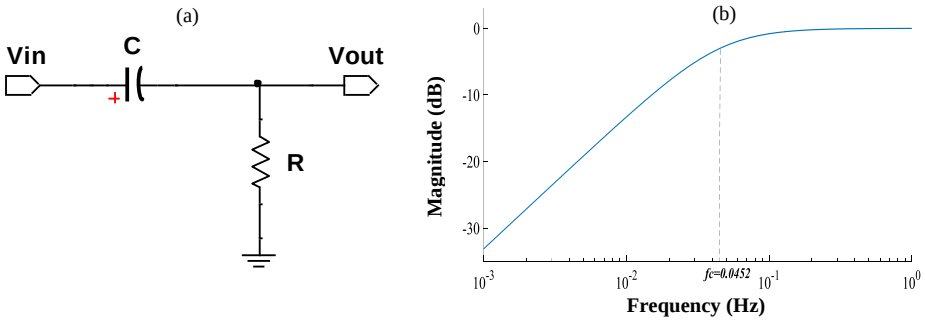

Figure 2.4: Circuit (a) and bode diagram (b) of the first order passive high pass filter.

– **Active low pass filter**
The impedance of each RC network impacts on the next stage, so cascading several RC networks may degrade the desired signal. The use of op-amp can solve this problem due to its high input impedance and low out impedance. Sallen-Key is an active filter and unitary gain voltage amplifier, it was chosen because of its high-quality factor.
The sEMG bandwidth is 0-1000 Hz, however, the dominant energy is concentrated in the range of 20-500Hz. For that, we developed a 4^{th} lowpass Sallen-Key filter with a cut-off frequency of 600 Hz in order to filter the high frequencies. The fourth-order of Sallen-Key structure is shown in Figure.2.5.

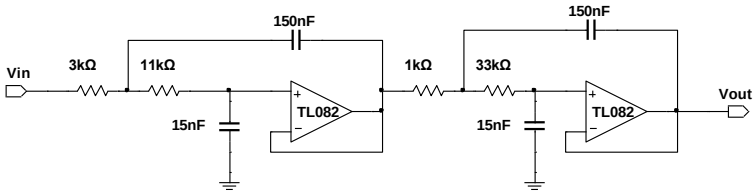

Figure 2.5: Fourth order Sallen-Key lowpass filter.

As shown in figure.2.6, the 4th order Sallen-Key LPF has a steeper roll-off near the Fc compared to the 2^{nd} order. This steep attenuation allows reducing the noise without degrading our sEMG signals.

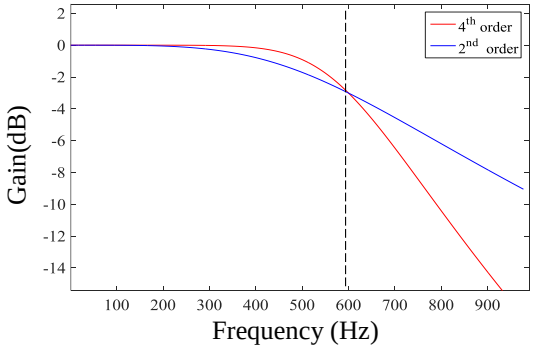

Figure 2.6: Bode diagram of lowpass Sallen-Key filter.

DC-offset adjustment circuit — sEMG is a bipolar signal, has positive and negative voltages. Otherwise, the analog-digital converter digitalizes only the positive input voltages, to solve this problem we added an offset adjustment circuit. This circuit adds a bias voltage to the input signal and thus to make it swing only positive. As shown in Figure.2.7, The output voltage can be determined by the following equation(2.2).

$$V_{out} = V_{in}\frac{Pot * 20\%}{Pot} * V_{cc} \tag{2.2}$$

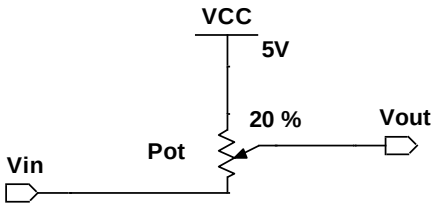

Figure 2.7: DC-offset adjustment circuit.

Power supply circuit — The use of the battery is recommended in order to design a portable sEMG measurement system. The ICL7660 integrated circuit is used to invert the positive input voltage, the supply circuit is shown in Figure.2.8.

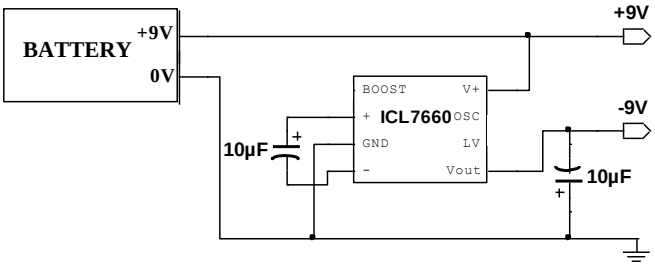

Figure 2.8: Power supply circuit.

2.2.1.3 Microcontroller

The analog sEMG signals are continuous in time and must be digitalized for further digital processing. For this purpose, we used microcontroller Arduino Uno. The choice of this type of card depends on our needs and also because it is an open-source license, and it is not expensive [39]. This board based on ATmega 328 carries an 8-bit processor and running at 16 MHz. As shown in Figure.2.9, the Arduino Uno board contains:
— 6 analog inputs named A0-A5.
— 14 digital input/output pins named (D0-D13). Six of the digital pins (D3, D5, D6, D9, D10, and D11) can be programmed to send pulse width modulation (PWM).
— 10-bit analog to digital converter which converts the analog data into entire numbers between 0 to 1023 (2^{10}-1) corresponds to [0-5] V of analog input values.
— The maximum transmission speed expressed in baud is about 115,200 bps (bits per second).
— Random Access Memory RAM of 2 kilobytes.
— Storage Random Access Memory SRAM of 32 kilobytes used for storing the program.
— EEPROM memory of 1 kilobyte used for storing variable's data generated within a sketch .
— 2 ground pins (GND) to share it with the external devices.
— 2 power supply 3V3 and 5V to supply the connected external devices with 3.3V or 5V.
— The reset button for reinitializing and storing the program again.
— Power jack with an input voltage range of [7-12]V.
— USB port to connect the Arduino board with computer.
The USB port connects to the computer for various purposes:
— Upload the new program to Arduino board,
— Communicate with computer and Arduino board,
— Supply the Arduino board with 5V only but for more power supply plug AC

adapter or battery 9V into the power jack.

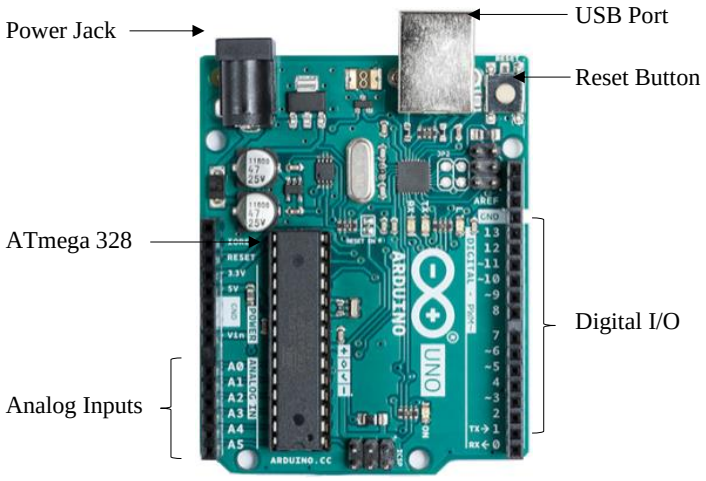

Figure 2.9: Arduino Uno board.

2.2.2 Software part

The software part consists of two programs. The first program developed in Integrated Development Environment (IDE) and upload it into the Arduino Uno board in order to convert the analog sEMG into a digital signal. The second one developed in Graphic User Interface using Matlab programming language in order to simplify the storage and the digital processing of sEMG data.

2.2.2.1 Arduino Uno software

The Arduino software is available on the website at `www.arduino.cc`, its latest versions can be downloaded freely with General Public License (GPL), running on Mac OS, Linux, and on all Microsoft Windows versions from Windows XP onwards i.e. Windows Vista, Windows 7, 8 and 10. After installing the Arduino software and its USB driver, the writing, compiling, and uploading of sketches to the Arduino board become easier.

Arduino Uno Firmware — The Arduino IDE used for writing sketches in C programming language, verifying and saving them before uploading into the Arduino board. As shown in Figure.2.10, the IDE contains a bar of menus, toolbar, text editor to write code, message area to display the actual action, and text console to display the compilation results.

The basic functions for writing sketches are setup() and loop(). The function setup() used to configure the I/O pins and all the used variables, it is only run once when the Arduino starts booting up. Conversely, the function loop() used for the main code, it repeats the execution of code until the Arduino is powered off.
After writing a sketch and connecting the Arduino board, the next step is to select the type of used board and the serial port, then, press the reset button to initialize and finally upload the program.

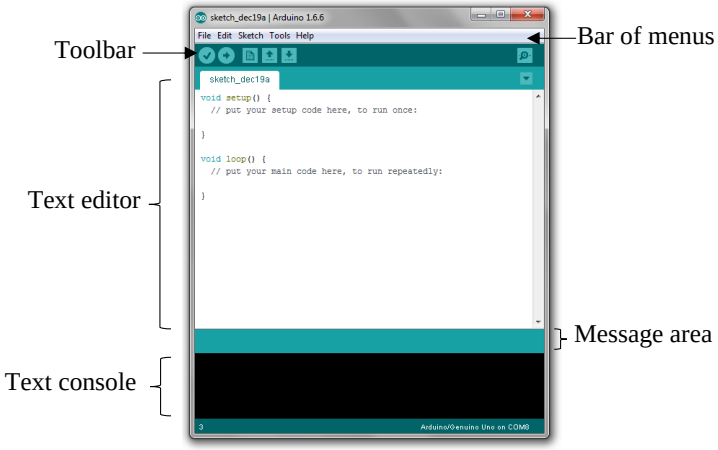

Figure 2.10: Arduino IDE.

2.2.2.2 Matlab graphical user interface (GUI)

There are various environments to create a graphical interface such as $C^{\#}$, Matlab, LabVIEW.... etc. We picked the Matlab environment in order to use its available toolbox which facilitates digital signal processing. Our purpose from creating an interface is to facilitate and simplify the storage, visualization, and processing of sEMG data without spending a lot of time understanding the Matlab programing language.
As shown in Figure.2.11, the sEMG GUI contains:
— The bar of menus: file, sEMG signal processing including digital filtering, spectral analysis, and statistical parameters; the help menu used to explain how to use this interface.
— Toolbar contains the essential tools such as open file, save the current results, creating a new file, print, zoom out, zoom in, and pan.
— Patient's info box used to insert the subject or patient information such as name, age, weight, height, and to select the gender.

— Diagnosis area to insert the patient health status.
— The acquisition box is assigned to insert the transmission speed, select the USB port, start and stop the acquisition, save the sEMG data and patient information in format .mat and .txt, respectively.
— Axes box for plotting the sEMG signal.

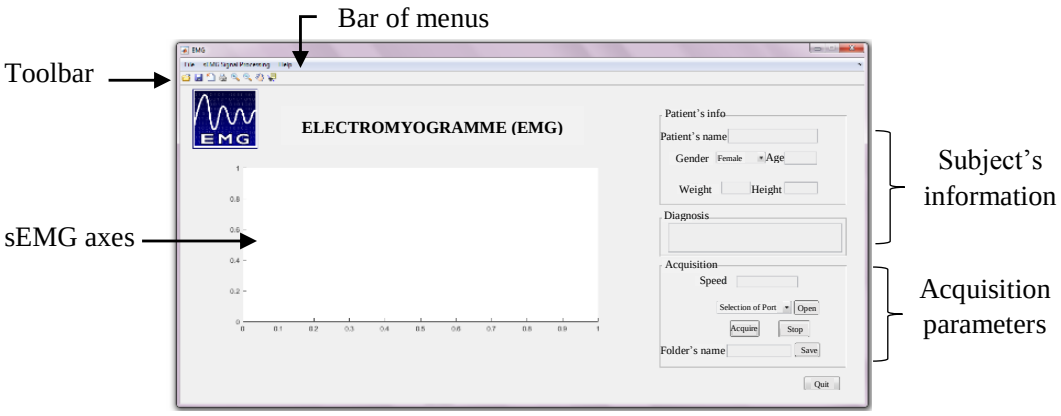

Figure 2.11: EMG graphical user interface.

The final design of our sEMG measurement system is illustrated in Figure.2.12. The sEMG signal acquired from the analog circuit is connected to analog input A0 of Arduino Uno card. This signal is sampled by DAC at a sampling rate of 2000 Hz respecting the Nyquist sampling theorem [40]: $f_s \geq 2\, f_{max}$, that because the sEMG signal is strictly bandlimited $[0 - 1000]$Hz, where the highest frequency f_{max} is 1000Hz, So we used the Nyquist rate fs=2 *1000 Hz in order to avoid the aliasing and the loss of information. The transmission speed was set at 9600 baud.

Figure 2.12: sEMG measurement system design.

During the acquisition, the Matlab GUI plots the sEMG signal in real-time as shown in Figure.2.13. As we can use the signal processing menu for digital filtering, spectral analysis, and extraction of statistical parameters.

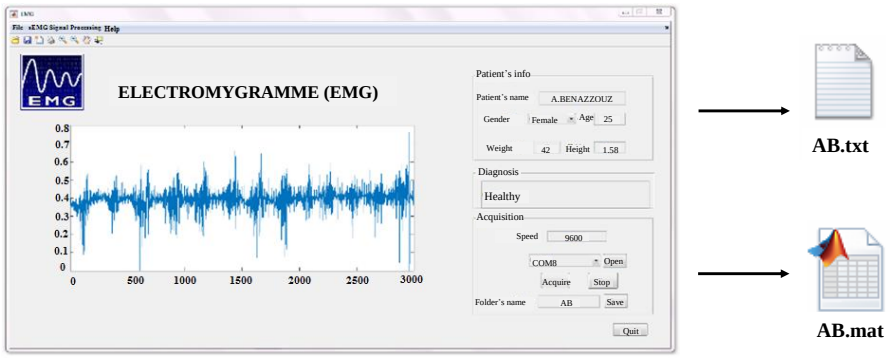

Figure 2.13: Acquired sEMG by Matlab interface.

Figure below shows an example of sEMG data file (.mat and .txt format).

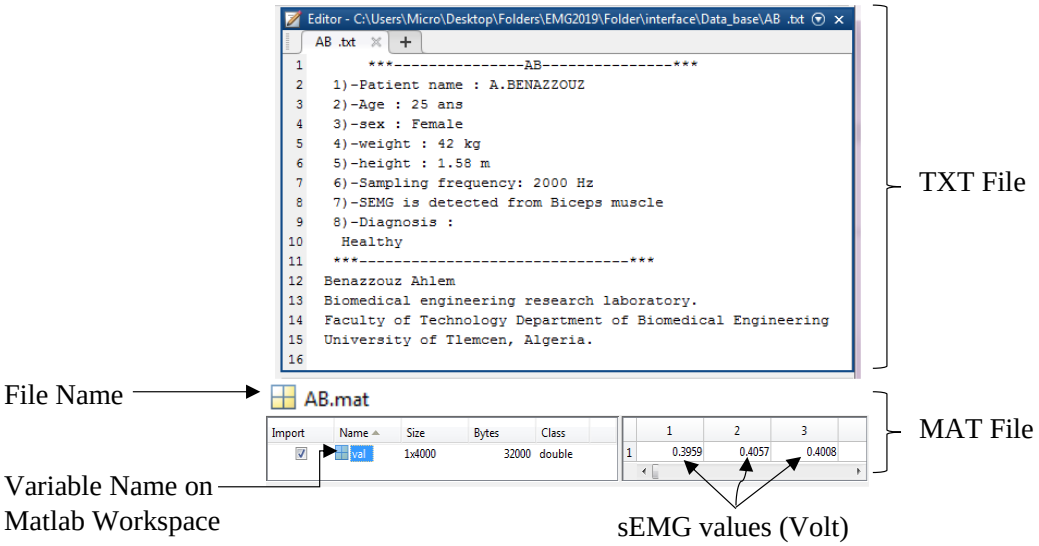

Figure 2.14: An example of MAT and TXT sEMG files.

2.3 The effect of fatness, age, gender, handedness, and diabetes on sEMG

Skeletal muscle strength, structure and function are influenced by different factors such as gender, age, weight, and health condition status . . . etc.
Diabetes mellitus caused by insufficient secretion of the pancreatic hormone insulin which controls the level of sugar in the blood, and thus causes serious damage to small blood vessels and nerves [41]. Because of damaged small blood vessels, an amount of glucose cannot reach skeletal muscles to fuel them and that can lead to muscle atrophy. Also, the nerve damage causes a dysfunction in the muscle fibers because of being uncontrolled.
Even for the healthy people, the skeletal muscles start the change from the fourth decade of life, the muscle fibers shrink, and their tissues are replaced by connective and adipose tissues [42]. Because of these tissues, the muscles fail to contract powerfully and generate a strong force. As well as the loss of muscle mass results in the loss of strength which affects mainly locomotion balance and posture [43].
The female and male differ in body structure and that may reflect on the strength of muscle [44]. besides gender, there are other characteristics that influence the human body and muscle functions such as obesity, handedness . . . etc.
Aging and obesity are the major cause of locomotion imbalance and instability, increasing the risk of diseases and injuries [43][45][46]. The age-related muscle atrophy can be delayed to some extent and obesity can be reduced by physical exercise.
In sports science and medicine, the effect of physical exercises on muscles, posture, and gait received the attention of many researchers. Where the relationship between force and muscle activity have been studied in order to improve the control of muscle and stability of the joint. sEMG is also used to measure muscle fatigue.
So, *how can gender, aging, obesity, and diabetes influence on sEMG signals?; if these factors affect the muscle structure and function, how can impact on sEMG temporal and spectral parameters?*
For this purpose, we used our sEMG measurement system and collected the sEMG data from different subjects and these data were analyzed in order to extract the temporal and spectral parameters and facilitate the implementation of the results.

2.3.1 Data collection

The sEMG data were collected from different age groups using our real-time sEMG measurement system. The folder .mat and .txt facilitate the analysis

of sEMG signals and study the effect of age, fatness, gender, handedness, and diabetes on sEMG signals.

2.3.1.1 Subjects

Twenty volunteers were recruited in this study. From all those volunteers, 02 left-handers and all the rest are right-handers. These collected data include:

- Six elderly subjects (mean ± SD; age= 72.33± 11.99 years). From those subjects, we have 02 diabetics type II (one male and one female) and the others are healthy (01 male and three females);
- Eight healthy adults (age= 34.75± 10.18 years; 02 males and 6 females);
- Three healthy youths (age= 19.33 ± 2.89 years; 01 male and 01 pregnant woman);
- And three healthy children (03 male; age= 8.33 ± 4.16 years).

2.3.1.2 Protocol

After skin preparation, the electrodes were placed on the belly of Biceps Brachii, respecting the inter-electrode distance (2cm). Six subjects were asked to load a dumbbell curl of 1 kg to 6 kg. During isotonic contraction, the sEMG of each dumbbell curl was acquired in order to determine the relationship between force and sEMG. The same exercise was repeated with the other arm to compare between left-handers and right-handers.

Figure 2.15: Protocol of the experimental setup.

Secondly, the sEMG signals were acquired from elderly subjects, children and housewives, healthy subjects and diabetics in order to study the effect of diabetes

mellitus on sEMG. The records were taken in two positions: relaxation and contraction of brachial biceps and the volunteers were asked to contract until their maximum.

2.3.2 Digital signal processing

The digital signal processing is a very essential step and Matlab programming language facilitate this task. In this context, the sEMG signals were filtered and analyzed using the specific functions of the Matlab toolbox, and then the relevant statistical parameters were extracted to evaluate the effect of subject characteristics and healthy condition on sEMG.
This Processing was made by the following procedures i.e. digital filtering, temporal and spectral analysis.

2.3.2.1 Temporal analysis

The digital sEMG signals acquired from the Arduino board contain the DC offset component that should be removed. We applied the 3rd order Butterworth high-pass filter with a cutoff frequency of 20 Hz for two purposes:

- Deleting the genitive DC voltage.
- Baseline wander correction.

The sEMG signal (s) is usually processed by firstly rectifying the raw signal, this is involved by taking the absolute value of the signal point, the full-wave rectification is all above zero can be calculated by the following formula.

$$rect\_sEMG_i = abs(s_i) \tag{2.3}$$

With i=1,2...,N.
Where N is the length of sEMG signal.
After that, the envelope (e) of sEMG signal (s) is determined by calculating the magnitude of the analytic sEMG signal. This complex signal contains two parts i.e. real and imaginary parts; the real part represents the original sEMG signal while the imaginary part ($\hat{s}$) is the Hilbert Transform [47]. Mathematically the envelope detection is defined as follows.

$$e\,(i) = \sqrt{s(i)^2 + \hat{s}(i)^2} \tag{2.4}$$

Finally, the sEMG envelope is smoothed by the moving average filter with a span of 1.5%.

Figure.2.16 shows the application of digital signal processing mentioned above on sEMG. the raw sEMG acquired from the healthy subject during contraction and relaxation of biceps brachii muscle. (a) represents the raw sEMG signal with DC offset component (black curve) and horizontal baseline (red dashed line). (b) represents sEMG signal without DC offset component and without baseline wander. (c) represents the sEMG envelope (blue curve) and smooth (red curve) sEMG envelope.

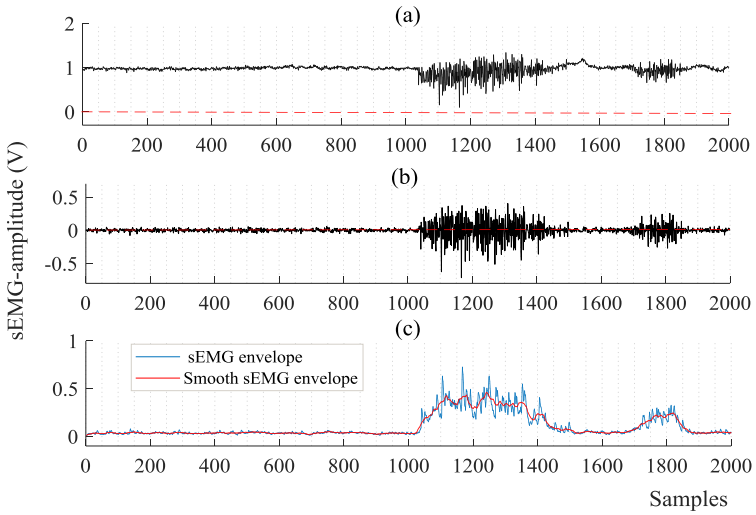

Figure 2.16: sEMG baseline wander correction and envelope detection.

2.3.2.2 Spectral analysis

The frequency domain is widely used in the signal processing to measure the changes in the spectral content of signal and extract the spectral parameters based on Fourier transform. There two methods: parametric and non-parametric. In our study, we used a non-parametric method i.e. Welch's power spectral density compared to the parametric method i.e. periodogram is based on windowing technique using a window function such as hamming and thus reduce the noise and leakage obtained by periodogram. The estimate of the modified periodogram is calculated from each segment where the average of all these estimates results in Welch's PSD estimate.
Figure.2.17 shows The Welch's PSD of sEMG signal after removing the DC offset, using Hamming window of 1024 points and default overlap of 50%, where the dominant energy is concentrated in the range of 0-500Hz.

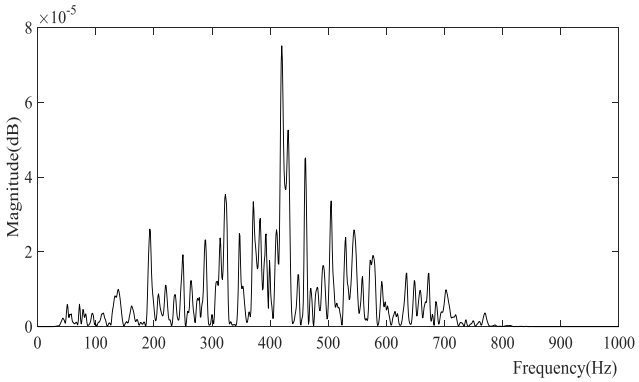

Figure 2.17: Welch's PSD of sEMG signal.

2.3.3 Statistical parameters

After the digital signal processing in both temporal and spectral domains, the statistical parameters were extracted in order to facilitate the interpretation of results.

2.3.3.1 Temporal parameters

– Root Mean Square Value **RMS** is defined as the square root of the mean of squared sEMG amplitudes, expressed as follows.

$$RMS = \sqrt{\frac{1}{N}\sum_{i=1}^{N} {s_i}^2} \tag{2.5}$$

– Mean Absolute Value **MAV** is the mean of rectified value, calculated as follows.

$$MAV = \frac{1}{N}\sum_{i=1}^{N} |s_i| \tag{2.6}$$

– Integrated EMG **IEMG** is the area under the smooth sEMG envelope. It is calculated using the Eq.(2.7):

$$IEMG = \sum_{i=1}^{N} |s_{smooth_i}| * \frac{1}{f_s} \tag{2.7}$$

2.3.3.2 Frequency parameters

– Total Power **TP**: is the total amount of the power spectrum density of sEMG signal.

$$TP = \sum_{i=1}^{F} PSD(i) \tag{2.8}$$

– Mean Frequency **MF**: is the average frequency calculated over the power spectrum as below.

$$MF = \frac{\sum_{i=1}^{F} iPSD(i)}{\sum_{i=1}^{F} PSD(i)} \tag{2.9}$$

– Median Frequency Med_F: is the frequency that divides the total power spectrum into two equal portions.

$$Med_f = imed\ \frac{f_s}{F} \tag{2.10}$$

$$\sum_{i=1}^{imed} PSD(i) = \sum_{i=imed}^{F} PSD(i) \tag{2.11}$$

– Peak Frequency **PF**: represents the frequency of peak power.

$$PF = arg\ \frac{f_s}{F} \max_{i=1....F} PS(i) \tag{2.12}$$

Where fs is the sampling frequency.
N is the total number of time data points.
And F is the total number of frequency data points.

2.4 Results and Discussion

During muscular contraction, the muscle can be recruited more than one motor unit simultaneously, in order to maintain the needed force. As shown in Figure.2.18, the sEMG acquired from athlete at different loading weight, we notice that the sEMG amplitude increases when the loading weight increase, and for the spectral density while loading 1 kg, the maximum power density is ranged from 70 to 125 Hz which is the slow-twitch units' frequency range, and this because 1 kg does not need great muscle tension to be lifted. Meanwhile, for 5 and 6 kg the maximum power density is ranged from 300 to 500 Hz means that the muscle recruits more motor units with both slow and fast-twitch fibers to load these weights.

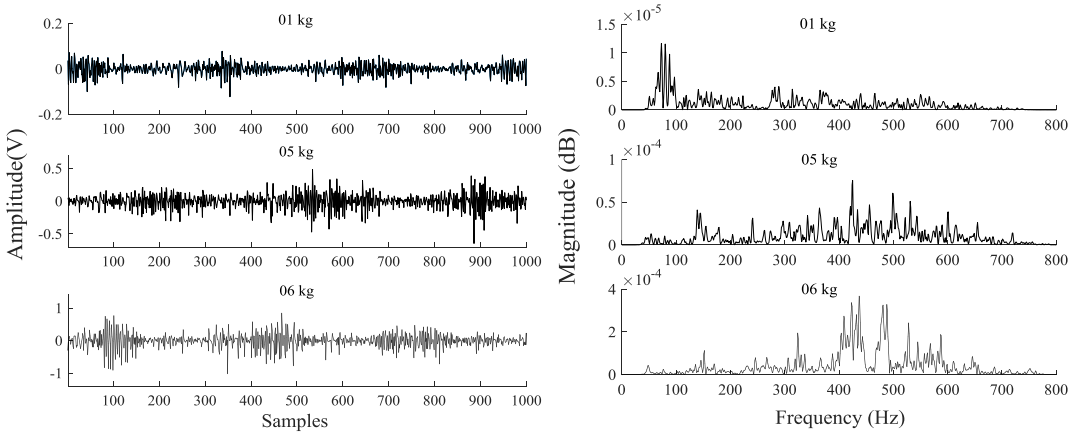

Figure 2.18: The sEMG signals detected from healthy male athlete (20 years old) and their PSDs.

In Table 2.19, the RMS, MAV, IEMG, and total power increase while increasing of dumbbell weight, for the mean, median and peak frequencies, they are shifted from 80-200 towards 500 Hz.

Table 2.2: sEMG statistical parameters at different dumbbell weights.

Dumbbell weight	**RMS (V)**	**MAV (V)**	**IEMG**	**MF (Hz)**	**Med$_F$ (Hz)**	**PF (Hz)**	**TP (dB)**
01kg	0.027	0.019	388.542	296.4740	288.509	80	0.001
05kg	0.094	0.069	533.597	412.327	427.289	425	0.008
06kg	0.173	0.122	568.922	433.048	437.562	437	0.033

The left-handers represent only 10% of the population [48], in this study we have two female left-handers and in order to compare their sEMG with right-handers, we chose two female right-handers of similar age. Figure.2.19 shows that the left hands of left-handers are stronger than their right hands. And for the right-handers, it can be noticed that the right hands are stronger than left hands. So, we conclude that the use of muscle can result in increased performance and muscle strength.

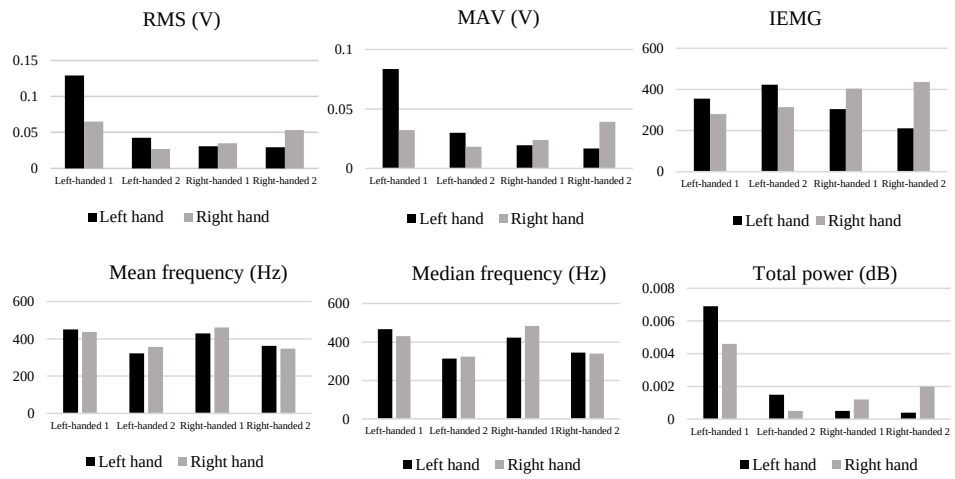

Figure 2.19: Comparison between left-handers and right-handers(temporal statistical parameters).

In Figure.2.20, it is observed that the RMS, MAV, IEMG and total power for diabetics are lower than healthy subjects, and also the strength of male are more than female for both diabetic and healthy subjects. This is Due to the elevation of sugar level in the blood that damages the vessels and nerves, which in turn leads to muscle atrophy and dysfunction. For that, EMG testing is an essential tool to evaluate and improve neuropathic changes.

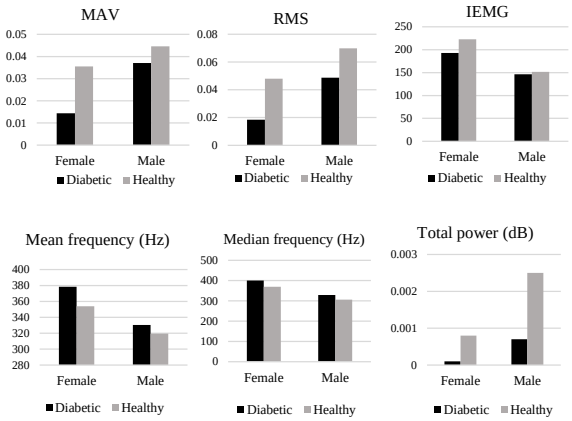

Figure 2.20: Statistical comparison of sEMG parameters between diabetics and healthy subjects.

As shown in Figure.2.21, the muscle strength increases from youth to adulthood and then decline at the aging phase.

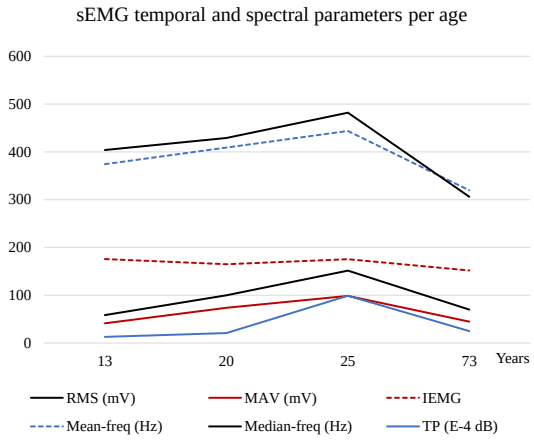

Figure 2.21: Statistical comparison of sEMG parameters between young, adults and elderly subjects (only for healthy subjects).

In order to study the effect of obesity on sEMG signals, we select 04 healthy subjects of similar age and different weights. The Body Mass Index BMI defined as weight-height ratio, is measured to compare between thin and obese subjects. As illustrated in Figure.2.22, the RMS, MAV, IEMG, and total power decrease when the weight-height ratio increases, hence the thick subcutaneous of fatty tissues increase the impedance even if the skin is well prepared. So, during sEMG recording, obesity should be taken into consideration, and for very overweight subjects, this technique may not be suitable.

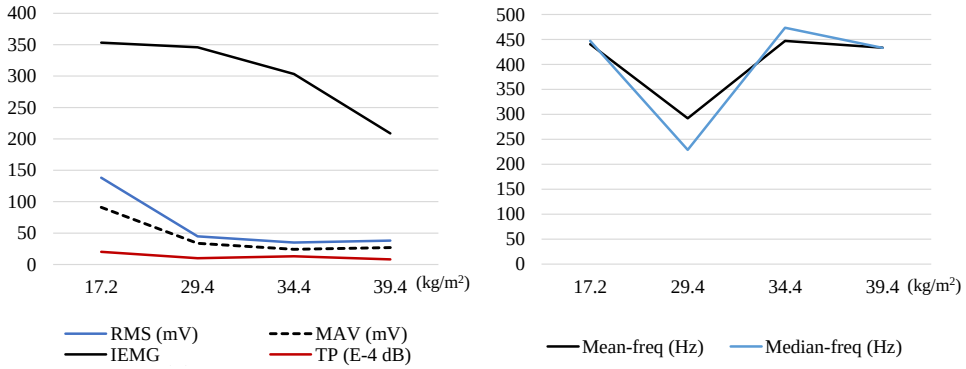

Figure 2.22: Statistical comparison of sEMG parameters between thin and obese subjects (only for healthy subjects).

The median and mean frequencies are more important in aging and disorders that affect the muscle, neuromuscular junctions, nerves, or spinal cords. These changes in muscle due to aging and disorders reduce the performance of muscle strength and sEMG characteristics. Also, for the detection of muscle fatigue, the mean and median frequencies shift towards the lower frequencies over time of submaximal isometric contractions.
Whereas, the adipose tissue is an additional high impedance that reduces the amplitude of sEMG signals but has no impact on the activity of muscle fibers or motor unit as a whole.

2.5 Limitation and recommendations

The current study involved some limitations and recommendations, which could be developed further. The number of volunteers in this study is limited, and for quantitative comparison of sEMG parameters, the fatty tissues, gender, and other physiological changes such as aging need careful consideration, because these factors vary from subject to another subject. So, we will collect more sEMG data.
Tingling in the hands, joint pain, and frozen shoulder syndrome are the more common in diabetics. Besides these syndromes, the obesity in diabetics subjects causes deformation of bone and joint instability and these problems become severe in aging. The physical exercise is helpful to reduce the weight and delay the aging as well as controlling diabetes, and sEMG technique can be used to evaluate and select effective exercises.
The endurance exercise e.g. marathon and resisting training e.g. muscle building, enhance the performance of muscle but may not be suitable for the female body. During pregnancy and after delivery, there are many changes in the body such as an increase in weight, difficulty in the movement that should be controlled by physical exercise to keep the joint and limbs flexible. In future work, we will focus on studying the effect of Pilates and some yoga asanas on sEMG for keeping the flexibility and stability of the female body.
We will develop a wireless and more sophisticated sEMG measurement system to facilitate the recording of signal during dynamic movement and adapt to any bodily posture during exercise.

2.6 Conclusion

In this chapter, the real-time sEMG measurement system is developed considering the cost and simplicity. The hardware and software of this system are described in

detail passing from sensor, amplification filtering and offset adjustment circuit to maintain the analog sEMG signal then digitalizing by Arduino Uno, the Matlab GUI was developed to facilitate the acquisition, storage, and digital processing. The sEMG data were collected for studying the effect of diabetes, age, gender, handedness on sEMG statistical parameters in both temporal and spectral domains. Sitting some limitations and recommendations at the end of this study. Besides the temporal and spectral parameters i.e. root mean square, mean absolute value, integrated EMG, mean and median frequencies and the total power spectrum density; the muscular activation Onset and offset timing parameters are very important in orthopedics, kinematic and kinetic. In the next chapter, the muscular activation detection based on S-transform will be described using sEMG signal during gait.

3

Muscular activation detection using sEMG signals during dynamic contractions

3.1 Introduction

The muscle activation onset/offset timing is a reliable parameter used in the diagnosis of abnormalities, measuring of nerve conduction velocity, and also in human movement analysis.
In this chapter, an automatic onset/offset timing detection method based on S-Transform was proposed using sEMG signals detected from lower limb muscles, during gait.
A comparative study was made with Sample Entropy, Teager–Kaiser Energy Operator, and integrated profile methods in order to validate the efficiency of our proposed method.
The main goal of this study is to detect muscle activation intervals (MAIs) and study their diversity in normal subjects and subjects with knee injuries.

3.2 Literature review of muscular activation detection methods

The onset/offset timing is widely used in kinesiology to study the role of each muscle in accomplishing movement, becomes insightful when deploying together

with kinetics for studying the body motion, joint moments [18], or with kinematics e.g. joint angles [49]. It has enormous potential in medical application such as orthopedics [50], neurology[51], gait analysis [52][53], diagnosis of cerebral palsy [54], measurement of conductive nerve velocity [55] and others, this because in regular conditions the muscle turns off, but if it still turns on when it is not needed, it indicates to muscular pathology, i.e., active muscle spasm, muscular hypertonicity, joint instability such as bad muscle coordination, and stress.
The amplitude of sEMG signal is influenced by different factors not only by motor unit action potentials which propagate the muscle fiber but also by the tissue characteristics (refer to chapter 2). During dynamic contraction, the EMG-force relationship is non-linear [56]means that the amplitude cannot express as an indicator of muscle force. In this context, the approach that based on sEMG amplitude is useless especially in dynamic conditions.
In the literature, to detect the muscle activation many methods have been proposed. Vannozzi et al. [57] proposed an approach for muscle detection intervals based on discontinuities detection in the wavelet domain
Recently, Solnik et al. [58] applied the Teager–Kaiser Energy Operator (TKEO) using sEMG signals to improve that the accuracy of the sEMG onset timing detection threshold, regardless of SNR signal-to-noise ratio.
Furthermore, Zhang et al. [59] used the Sample Entropy for onset detection using SEMG contaminated with Spurious Background Spikes. Zhou et al. [60] proposed also the Sample Entropy for muscle onset detection using sEMG signal keeping the ECG artifacts. Whereas, Liu et al. [61] used the integrated profile for muscle activation using EMG signals with spurious background spikes.

3.3 S-transform-based muscular activation detection method

This section describes the main steps of the S-transform-based muscle activation detection method that is used to pinpoint precisely the onset and offset timing. Here brief summarize of the S-Transform-based detection algorithm.

- Loading of sEMG signal;
- Calculation of TFR matrix using S-transform;
- Selection of optimal threshold;
- Converting the ST image into a binary signal;

– Finally, detecting the onset/offset timing and calculating the stride duration.

3.3.1 S-transform technique

The S-transform is proposed to solve the Short-Time Fourier Transform (STFT) and Continuous Wavelet Transform (CWT) issues. For non-stationary signals, the STFT cannot track the signal dynamics correctly because of the constant window width.
The S-transform combines the STFT and CWT properties by using a frequency-dependent Gaussian time window. Moreover, it has good frequency resolution [62].

3.3.1.1 The short-time Fourier transform (STFT)

The STFT of the signal x(t) can be expressed as [63]:

$$STFT\left(\tau, f\right) = \int_{-\infty}^{+\infty} x\left(t\right) \omega\left(t-\tau\right) e^{-i2\pi ft} dt \tag{3.1}$$

Where τ is a time of spectral localization, f is Fourier frequency, and theω (t) is a window function.

3.3.2 The ST-STFT relationship

The S-transform is a particular case of STFT by replacing the window functionω (t) by the Gaussian window. The Gaussian window is defined as:

$$\omega\left(t\right) = \frac{|f|}{\sqrt{2\pi}} e^{\frac{-t^2 f^2}{2}} \tag{3.2}$$

Substituting Eq. (3.1). (2) in Eq.(3.2), we get Eq.(3.3)

$$S\left(\tau, f\right) = \int_{-\infty}^{+\infty} x(t) \frac{|f|}{\sqrt{2\pi}} e^{-\frac{(\tau-t)^2 f^2}{2}} e^{-i2\pi ft} dt \tag{3.3}$$

3.3.3 The Discrete S-Transform

The ST can be formulated as follow [64]:

$$S\left(\tau, f\right) = \int_{-\infty}^{+\infty} X(\alpha+f) e^{\frac{-2\pi^2\alpha^2}{f^2}} e^{i2\pi\alpha\tau} d\alpha; \;\; f \neq 0. \tag{3.4}$$

Where:

$$X(\alpha + f) = \int_{-\infty}^{\infty} x(t) e^{-i2\pi(\alpha+f)t} dt \tag{3.5}$$

Using the Eq.(3.4) to obtain the discrete ST (setting f $\rightarrow \frac{n}{NT}$ and $\tau \rightarrow$ kT):

$$S\left(kT, \frac{n}{NT}\right) = \sum_{m=0}^{N-1} X[\frac{m+n}{NT}] e^{-\frac{2\pi^2 m^2}{n^2}} e^{\frac{i2\pi mk}{N}} \tag{3.6}$$

Where T is the sampling time interval, and N is the total number of sampling points. With k=0, 1 ... N-1 denotes the discrete-time series, and n=0, 1 ... N-1 represents the discrete frequencies.

3.3.4 S-Transform Matrix

The time-frequency representation image can be defined as a complex ST matrix where its columns represent the discrete-time series and the rows are the frequencies of the signal. As we know the dominant energy of the sEMG signals concentrates in the range of 20-500 Hz [65]. So, we have restricted the ST matrix rows into $[21 - 500]$Hz.

3.3.5 The binary image of the S-transform matrix

During muscle activity, the Time-Frequency Representation becomes more intensive.After the assessment of different threshols, we empirically select the optimal threshold for separating these gray level distributions from the background and normalizing the intensity values (0 or 1).

$$\mathrm{Im}_{bin}(m,n) = \begin{cases} 1 & Im(m,n) > \delta \\ 0 & Im(m,n) \leq \delta \end{cases} \tag{3.7}$$

Where δ is given by:

$$\delta = SD2(Im(m,n)) \tag{3.8}$$

3.3.6 Binary signal

To convert the matrix Ibin (m, n) into binary vector, we calculated the sum of cells along each row using the following formula (Eq.(3.9)).
For n=1, 2 ... N.

$$s(n) = \sum_{m=1}^{M} I_{bin}(m,n) \tag{3.9}$$

Where m=1, 2...M (number of rows), and N the number of columns (length of the signal).
In Figure.3.1, The S-Transform-based detection algorithm was implemented on normal sEMG signal detected from Recto Femoral muscle during gait.

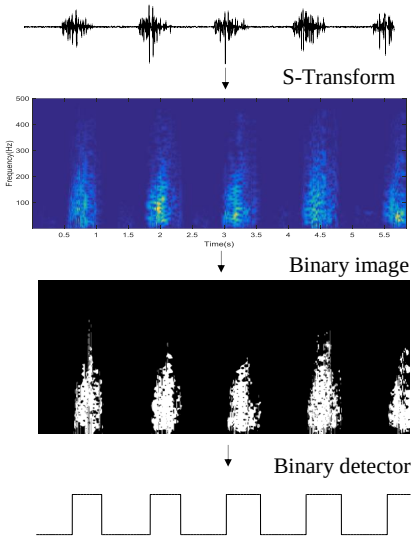

Figure 3.1: Scheme of the proposed ST image segmentation method.

3.4 Experimental setup

In order to validate the efficiency of our proposed detection method, we firstly test it on sEMG lower limb database (for more details, refer to Chapter 4), and then compare it to other recent methods i.e. TKEO, IP, SampEn.

3.4.1 Methods for Comparison

This section describes the muscle activation detection methods recently used in the literature, which will be compared with the proposed method.

3.4.1.1 Teager-Kaiser Energy Operator

The Teager-Kaiser Energy Operator (TKEO) calculates the energy of signal basing on its amplitude as follows.

$$\Psi\left[s(n)\right] = s^2\left(n\right) - s(n+1)s(n-1) \tag{3.10}$$

Where s (n) is the amplitude of signal s.
The onset/offset timing can be detected when the TKEO signals exceed the arranged threshold value defined as the standard deviation of the TKEO amplitude.

3.4.1.2 Integrated Profile

To obtain the discrete IP, a discrete integration of all rectified samples of signal (s) was calculated as follows.

$$IP\,(t) = \sum_{i=1}^{t} |s(i)| \tag{3.11}$$

With t =1, 2 . . . Length(s). The linear line L (t) is a linear function has the same maximum value of IP (N), can be defined as:

$$L\,(t) = IP\,(N) * t/N \tag{3.12}$$

Where N: Length(x).
To determine the onset and offset, the difference between L (t) and IP (t) should be calculated as follow:

$$D\,(t) = IP((t) - L(t) \tag{3.13}$$

The onset and offset were determined as the time points ton and toff at which D(t) reaches its minimum and maximum values, respectively.

3.4.1.3 Sample Entropy

Sample entropy measures the predictability of dynamic systems represented by time series. It was used in Cardiac variability time-series analysis [66], and in muscle onset detection from EMG signals with ECG artifact[59] and in another study with involuntary spikes [61].
The Sample entropy is the negative natural logarithm, with two essential parameters, the embedding dimension m, and tolerance r. It depends on the probability$B^m(r)$ that two sequences match for m points within a margin of r and $A^m(r)$ for m + 1 points. For finite time series x of length N. setting constant m=2 (m should be $\ll$ N) and r=0.25 *SD (standard derivation of the signal). The Sample entropy can be calculated as below:

$$SampEn\,(m, r,\ N) = -\log \frac{B^m\,(r)}{A^m\,(r)} \tag{3.14}$$

The sample entropy curve can be constructed by dividing the signal into sections with the same length (L) of the window. The sample entropy is calculated using

the signal sections multiplied by the overlapped sliding windows. To reduce the noise background and maintain a high temporal resolution, the sliding window and the window increment were empirically set at values 32 ms, 4 ms respectively. During the activation muscle, the SampEn curve obtained the important values, where the onset /offset can be detected when the SampEn signals exceed the arranged threshold value. Empirically, we set the optimal threshold as half of the standard deviation of the baseline amplitude.
The comparison between four onset/offset detection methods is shown in Figure.3.2. The real surface EMG signal from Recto Femoral muscle with the onset and offset time obtained by visual detection (vertical dashed lines), The curve of the proposed method. SampEn (with 32 ms sliding window and an increment window of 4 ms), (TKEO curve, and the final curve presents the integrated profile curve with the detected onset time (the minimum value) and detected offset time (the maximum value) (vertical solid lines).

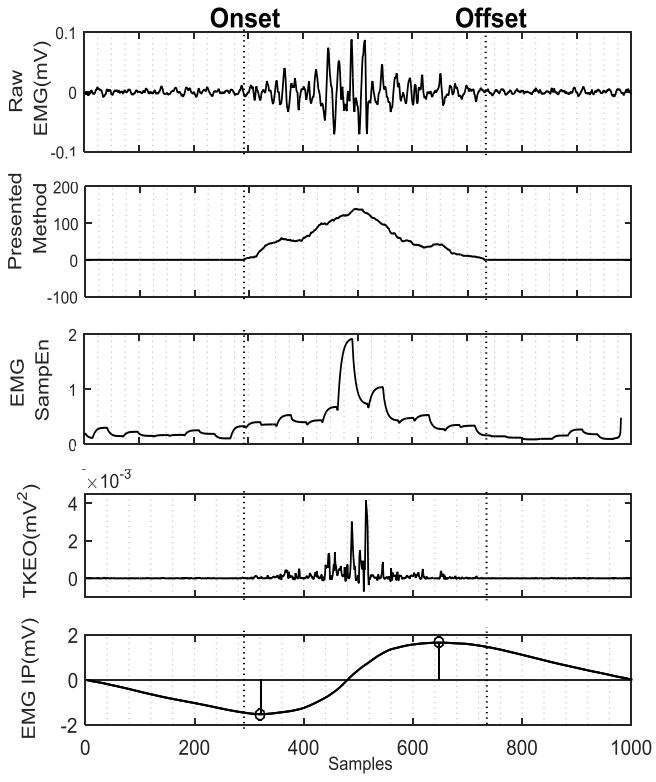

Figure 3.2: Onset and offset timing detection using ST, IP, SampEn and TKEO methods.

3.4.2 Performance evaluation metric

The latency is adopted to evaluate the onset/offset detection performance, can be defined as the absolute value of the difference between automatic (t_{auto}) and visual (t_v) detection.

$$\tau = \ |t_{auto} - t_v \ | \tag{3.15}$$

3.4.3 Muscle activation interval and onset timing-knee flexion correlation

The muscle activation interval and linear correlation between muscle activation and knee flexion are calculated to distinguish between normal and abnormal subjects, defined as follows.

3.4.3.1 The muscle activation interval (MAI)

The muscle activation interval and onset timing are very important indicators, especially in clinical applications. The onset time is the time of starting muscular activation, and the activation interval is the interval between onset and offset time. Also, it is the duration of one stride.

$$MAI\,(i) = Offset\,(i) - Onset\,(i) \tag{3.16}$$

3.4.3.2 Correlation between onset timing and maximum flexion of the knee

The linear correlation between the muscle and the maximum flexion of the knee was calculated by using Pearson's correlation coefficient (Eq.(3.17))

$$r_p\,(X, Y) = \frac{Cov(X, Y)}{\sigma_X \sigma_Y} \tag{3.17}$$

Where cov(X, Y) is the covariance.

$$Cov\,(X,\ Y) = \frac{1}{N}\sum_{i=1}^{N}\left(X\,(i) - \bar{X}\right)\left(Y\,(i) - \bar{Y}\right) \tag{3.18}$$

And σ_x, σ_y are the standard deviation of x and y respectively.

$$\sigma_x = \sqrt{\frac{1}{N-1}\sum_{i=1}^{N}\left|X\,(i) - \overline{X}\right|^2},\ \sigma_y = \sqrt{\frac{1}{N-1}\sum_{i=1}^{N}\left|Y\,(i) - \overline{Y}\right|^2} \tag{3.19}$$

$\overline{X}$, $\overline{Y}$ are the mean of X and Y respectively.
In this study, the X (i) is the onset timing vector and Y (i) is the instants of maximum knee flexion during swing phase (refer to Chapter 4), using peak detector algorithm with adapted threshold: $th = SD\,(s_{FXK}) + \frac{mean(S_{FXK})}{3}$.
Pearson's correlation varies between 1 and -1, when $r_p\,(X,\ Y)$ is close to 1 means there is a strong positive linear correlation, strong negative correlation when it's close to -1, and negligible or zero correlation when it is close or equal to 0.

3.5 Result and discussion

As shown in Figure.3.3, an example of a muscle activation interval using the four detection techniques i.e. ST, TKEO, SampEn, IP.

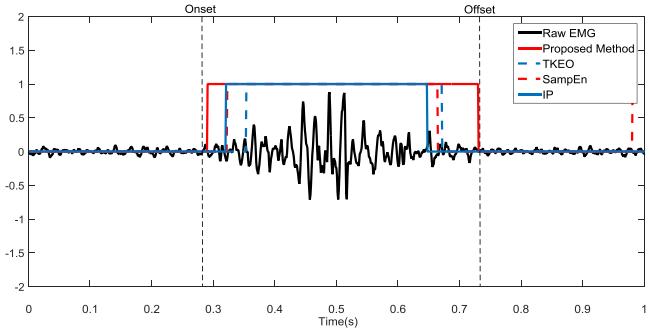

Figure 3.3: Comparison of MAI detection using ST, IP, SampEn and TKEO method.

In comparison with invasive technique (detection by using the needles), the surface EMG can be interfered with various undesirable spurious spikes due to adjacent muscles, tenuous skin-electrode displacement during the gait, ECG artifact, ambient interference. . . .etc. These spikes' characteristics change from low amplitude and long duration to high amplitude and short duration, lead to erroneous onset/offset detection.

In this situation, not only the time component but also the frequency is necessary, because during the contraction both amplitude in the time domain and the component of frequency increase.
TKEO was proposed for automatic detection, it can be valid just for signals with low noise and contractions of long duration. As well as SampEn was based on a sliding window with two necessary parameters: the window length and window increment. The choice of these parameters depends on a priori information of

undesired signals, it's very sensitive for ECG signal because this noise is periodic [60], but in our case, it's less efficient and the selection of these parameters is difficult because, in this dataset, it can be found in one record each muscle has different noise, some of them are low, some adversely are high. Also, the integrated profile has low latency, compared with the proposed method, along with the failed detection of the active muscle spasm, thus it can be reliable just for gait with normal cases and useless for pathologic cases.

There is another study based on wavelet transform [57], where the detection performance depends on the choice of mother wavelet that should be similar to the MUAP, for the real sEMG signals, it cannot be implemented.

The S-Transform used the Gaussian window, also it is not sensitive to the noise and has a good resolution, for this reason, the contractions in time-frequency presentation are distinguished clearly and easily with less error of detection, as confirmed in Figure.3.4.

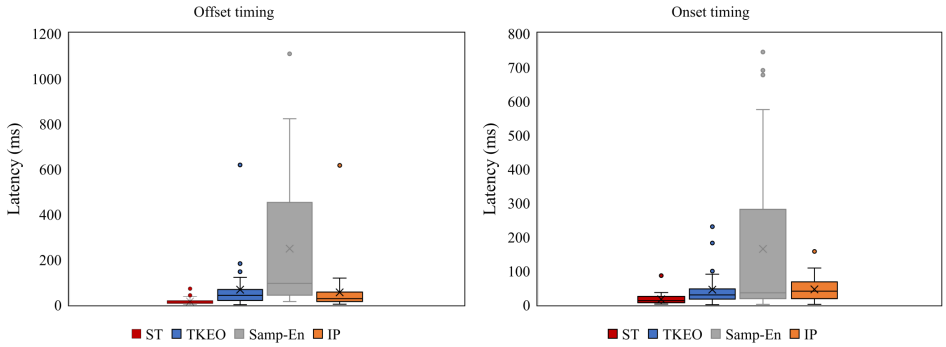

Figure 3.4: Statistical comparison of onset offset detection performance.

For the normal cases, it can be noticed that the activation intervals are quasi-homogeneous. As well as the number of strides is equal to the number of maximum knee flexion peaks during the swing.
However, for the abnormal cases, the activation intervals are very diverse; also, the number of strides and maximum peaks of knee flexion during the swing are not the same (see Figure.3.5).

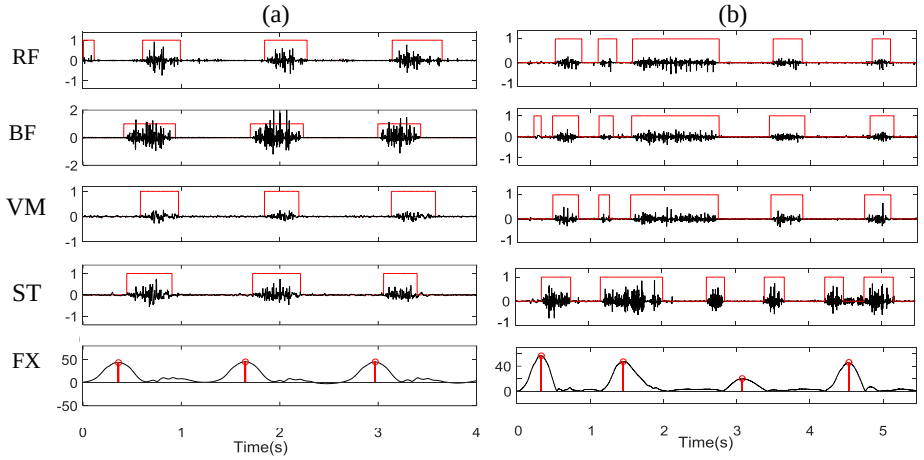

Figure 3.5: Detection of sEMG muscle activation and knee flexion peaks for normal (a) and abnormal (b) subjects.

Table 3.1 summarizes the statistical analysis results of MAI diversity and sEMG-knee relationship using Pearson's correlation coefficient (r_p). For the normal cases, the correlation between sEMG and knee flexion appears a very strong positive relationship with values of $r_p \geq 0.999$, meanwhile, it seems weak (less than 0.40) for the abnormalities, and This is due to the perturbation in the gait cycle where the contraction of the hamstrings and quadriceps muscles are inconsistent with the flexion and extension of the knee.
The MAIs are less diverse (lower than 60 ms) for normal than abnormal cases where diversity is more than 100 ms.
The MAI diversity is expressed by the standard deviation of strides for each muscle. In the same Table 3.1, the stride intervals during normal gait are quasi-homogeneous, their MAI diversity is less than 60 ms compared to abnormal gait, where the diversity is more than 100 ms.

Table 3.1: Statistical results of the sEMG-knee relationship and MAI diversity.

	Pearson's correlation coefficient (r_p)		**MAI Diversity**	
Muscles	*Normal cases*	*Abnormal cases*	*Normal cases*	*Abnormal cases*
	mean± SD	mean± SD	mean(SD)	mean(SD)
Recto Femoral	1.0000± 5.0000e-05	0.2120±0.1632	39.1848	159.7638
Femoral Biceps	0.9999±1.5000e-04	-0.1037±0.3829	36.6940	225.1532
Vastus Medialis	0.9999 ±8.1650e-05	0.2601±0.1873	50.8442	313.1644
Semitendinosus	0.9999 ±1.5000e-04	-0.2458±0.3543	35.1162	196.7390

3.6 Conclusion and future scope

Muscle activation detection is widely used in the diagnosis of neuromuscular diseases and kinesiology domain. Several methods have been applied and developed to facilitate automatic detection and reduce the error of detection.
In this chapter, the S-transform method has been proposed and compared with three recent methods: TKEO, SampEn, and integrated profile.
The results show that the S-transform method yielded better performance with the shortest average latency of τ_{onset} = 0.015 s, τ_{offset}= 0.014 s because it is less sensitive to noise and has good resolution. While TKEO method is valid for signals with low noise and long duration, and SampEn depends on a priori information of undesired signals such as ECG artifacts. Also, the integrated profile has low latency but failed to detect the short active intervals. Two statistical parameters were extracted for knee pathology diagnosis during gait:

- The standard deviation of strides duration in order to measure the diversity of activation intervals duration. During normal gait, the sEMG is quasi-periodic with quasi-homogeneous strides; when the strides duration becomes more diverse, it can be a sign of neuromuscular disorders, knee injuries, etc.

- The linear relationship between knee flexion and sEMG signals using Pearson's correlation coefficients. It is very strong for normal subjects and weak or negligible for the abnormalities.

In the future, these statistical parameters will be added to features extraction for classification.
In the next chapter, an automatic knee diagnosis method will be developed using sEMG signals together with the knee angle.

4

An automatic diagnosis of knee injuries using sEMG and goniometric signals

4.1 Introduction

Anterior Cruciate Ligament (ACL) and Meniscus (MN) injuries are common knee injuries that affect both active male and female athletes. These injuries are known to cause early joint knee arthritis and hence early diagnosis and treatments are critical to their clinical outcomes. In this chapter, we propose a diagnosis method for soft tissue-knee injuries using surface electromyographic (sEMG) and goniometric signals.
The signals associated with each pathology are collected and treated identifying the parameters indicative of joint anterior-posterior instability, loading bearing, impingement, and flexion-extension articular motion. Special features are extracted in time and frequency domain for responses associated with knee irregularities (knee injuries) and the relevant effects and their corresponding patterns are selected by feature selection methods. To validate such an approach and classification of different types of knee soft tissues injuries, cross-validation technique and supervised classifiers were used.

4.2 Knee Joint

Fluent and stable walking, running, and sitting, these daily activities could not be possible without a healthy knee joint; even simple yoga asanas such as tree

pose (Vriksasana) or chair pose (Utkatasana), playing football or other kinds of sports need bending and extending of this hinge joint.

4.2.1 Knee Joint Anatomy

The knee is the largest, complex, and bearing-weight joint in the human body; consists of bones, cartilages, meniscus, ligaments, tendons, and muscles (see Figure.4.1). They work all together to stabilize the movements.

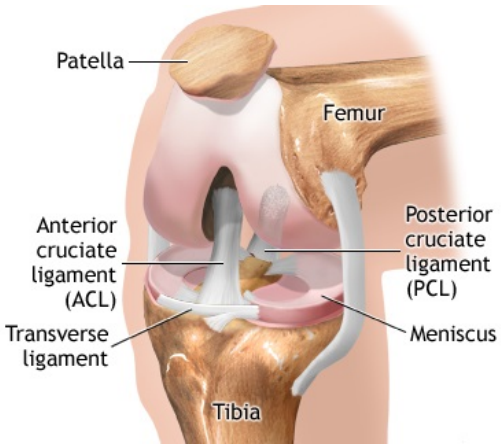

Figure 4.1: The knee joint anatomy [11].

4.2.1.1 Bones

Three major bones join together to form the knee joint; the thigh bone is also known as the femur is the strongest and longest bone in the human body, shin bone also called tibia is the second longest bone after femur and the kneecap a.k.a. patella.
Besides these three bones, the fibula is the calf bone located on the lateral side of the tibia, has the same length but thinner. Fibula itself plays a secondary role in supporting the knee joint stability, serving to attach ligaments and muscles, also to bear a little weight [67].

4.2.1.2 Articular Cartilages

The two convex condyles at the end of the femur with two asymmetrical concave condyles at the end of the tibia bone form together with the tibiofemoral articulation, whereas, the undersurface of the patella glides along the intercondylar groove of the femur, forming together the patellofemoral articulation.

Both articulations surfaces are covered by hyaline cartilage which is smooth, slippery, and flexibly designed to reduce the friction forces, which in turn protect the bones from rubbing on each other.
These articular cartilages become more slippery by synovial fluid. This viscous fluid is secreted by the synovial membrane located in the interior of the capsule to lubricate the knee joint [67].

4.2.1.3 Meniscus

On the tibial plateau, there are two crescent-shaped lamellae known as medial and lateral menisci. These fibrocartilaginous structures designed to adds stability to the joint, disperse the weight, and act as shock-absorbers to prevent the collision of the bones [67].

4.2.1.4 Ligaments

The ligaments are flexible, tough, fibrous connective tissue bans that join the knee bones in order to stabilize the joint and limit the movements [67]. There are four ligaments, each one provides a specific function described below.

1. The medial collateral ligament (MCL) is on the medial side of the knee, which connects the femur to the tibia and protects the joint from sliding sideways, resists the valgus stress, the lateral rotation and the anterior translation of the tibia relative to the femur.

2. The lateral collateral ligament (LCL) is located on the lateral side of the knee, connects the Femur to the fibula and resists the varus stress and the lateral rotation of the tibia relative to the femur.

3. Anterior and posterior cruciate ligaments (ACL & PCL) are cross-shaped located on the inside of the knee. The ACL role is to prevent the hyperextension and protect the tibia from sliding forward on the femur.

4. Whereas the PCL role is to prevent the posterior movement of the tibia relative to the femur.

4.2.1.5 Tendons and Muscles

The ligaments join the knee joint bone whereas the tendons join the muscles to the knee bones; there are two major muscle groups surround the knee and allow the movement of the knee [67]. The quadriceps and hamstrings muscles are responsible for the extension and flexion of the knee, respectively.

4.2.2 Knee Joint Biomechanics

In the knee motion, there six degrees of freedom as shown in Figure.4.2, three rotations, and three translations [68][69].

- Rotation
  1. Abduction/adduction: from 6° to 8° in extension.
  2. Flexion/extension from 3° to 135° of flexion.
  3. Medial/lateral rotation from 25° to 35° of flexion.
- Translation
  1. Anterior/posterior translation from 5 to 10 mm.
  2. Medial/lateral shift: 2-5 mm.
  3. Compression/distraction: 1-2 mm.

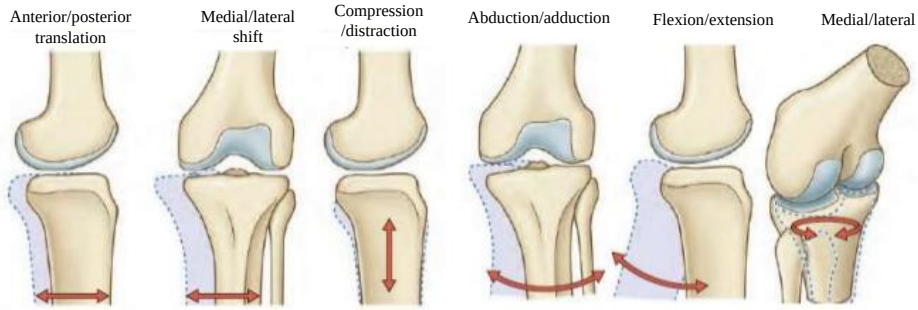

Figure 4.2: Six degrees of freedom of the knee [12].

4.2.3 Knee joint biomechanics and muscle activation during gait

The most habitual movements of the knee occur and repeated quasi-periodically, during the gait cycle. The single gait cycle a.k.a. stride consists of two phases: swing phase (40%) and stance phase (60%), which in turn subdivided into different subphases.

- Stance phase
  The stance phase represents the entire time that the foot is in contact with the floor, consists of three subphases: initial bipedal support represents 10%, single support from foot flat to heel off represents 40%, and terminal bipedal support (10%) [70].

1. Heel Strike (**HS**) is the initial contact of the heel with the reference floor due to dorsiflexors contraction, the knee extends because of quadriceps contraction.
2. Foot Flat (**FF**) is the loading response phase where the weight-bearing transfer to the reference leg, the quadriceps muscles is less active and the knee flexes to 15-20°.
3. Midstance phase, where the knee yields the maximum flexion then begins to extend, and the weight-bearing is aligned with the reference leg and the abductors fire for lateral support.
4. Heel Off (**HO**) is the terminal stance phase when the heel leaves the ground; the knee flexes to 0-5°.
5. Toe Off (**TO**) and pre-swing phase starts when the toe leaves the ground and the knee flexion increase to 35-40°.

– Swing phase
The swing phase is the period of time that the reference leg is off the floor consist of initial swing, mid-swing, and terminal swing.The swing phase is the period of time that the reference leg is off the floor consist of initial swing, mid-swing, and terminal swing.

1. Initial & mid-swing phase starts when the reference leg completely leaves the floor and swing in the air, the knee flexes up to 60-65° because of hamstrings muscles contraction but then extends to 30° due to quadriceps muscles contraction.
2. Terminal swing phase is the final phase, where the tibia is vertical to the floor. Simultaneously, the quadriceps contract to extend the knee, and the hamstrings provide the needed flexor force to protect the knee from hypertension.

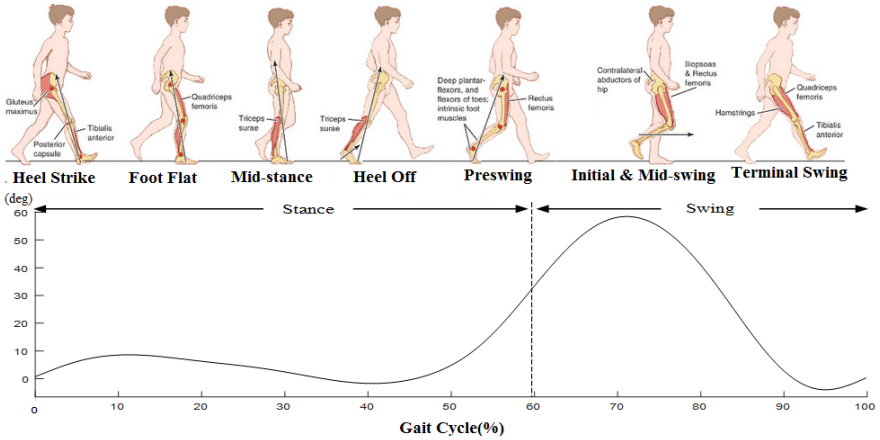

Figure 4.3: The phases and the knee angle of normal gait.

Table 4.1 shows muscle activity during the gait cycle.

Table 4.1: Muscle activation during Gait cycle.

Gait Cycle		Muscle activity
Heel Strike	0%	Quadriceps femoris, Tibialis Anterior, Gluteus Medius, Gluteus Maximus.
Foot Flat	0%-12%	Quadriceps femoris, Tibialis Anterior, Gluteus Medius, Gluteus Maximus Adductor Magnus, Tensor Fascia latae, Tibialis Posterior, Peroneus Longus.
Mid-stance	12-31%	Gastrocnemius, Soleus.
Heel Off	31-50%	Soleus, Gastrocnemius, Flexor digitorum longus , Flexor hallucis longus, Tibialis posterior, Peroneus longus, Peroneus brevis.
Toe Off	50-62%	Soleus, Gastrocnemius, Biceps Femoris, Adductor Longus.
Initial swing	62-75%	Extensor Hallucis Longus, Flexor Hallucis Longus, Sartorius, Iliacus, Tibialis Anterior, Tibialis Anterior, Extensor Hallucis Longus, Flexor Hallucis Longus, Sartorius, Iliacus, Tibialis Anterior, Tibialis Anterior.
Mid-swing	75-87%	Semimembranosus, Semitendinosus, Biceps Femoris, Tibialis anterior.
Terminal swing	87-100%	Quadriceps femoris, Semitendinosus, Semimembranosus, Biceps Femoris., Tibialis anterior.

4.2.4 Knee injuries and diagnosis techniques

Millions of people worldwide suffer from knee injuries e.g. cruciate and collateral ligaments injuries [71], meniscus tears [72][73], muscle strains, tendon ruptures, and osteoarthritis [74]. The PCL is more resilient to injury comparing to ACL, MCL, and LCL injuries. The LCL and MCL are vulnerable to lateral stresses. The anterior cruciate ligament (ACL) injury (see Figure.4.4) is the most commonly injured ligament for the athletes like footballers and skiers, typically occurs when the force directed anteriorly to the semi-flexed knee.

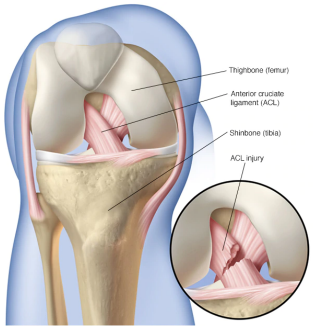

Figure 4.4: ACL injury [13].

Meniscus tear is among the most common knee injuries, especially for athletes, can be acute or chronic tears (see Figure.4.5), the chronic tear occur usually in the elderly patients could be treated by anti-inflammatory medications or by physical therapy, while the acute tear could be fixed by surgical treatment.

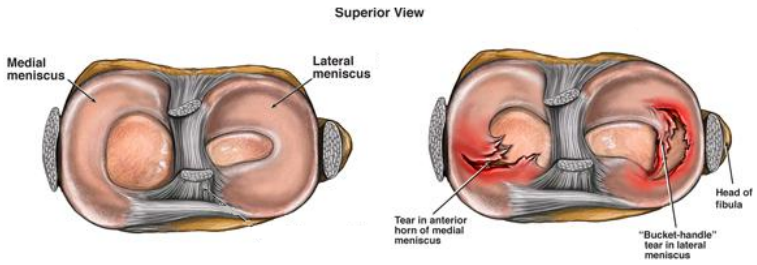

Figure 4.5: Meniscus tear.

These injuries cause significant pain, inflammatory conditions associated with the knee, and potential disability that become real if these injuries are not treated. The knee is a bony and soft tissue complex structure that requires an orthopedic surgeon equipped with X-rays [75], CT scans [76], and MRIs [77] to diagnose the problem properly. In addition to the aforementioned symptoms, an orthopedic

examination tests such as anterior Drawer, Lachman, vulgus and versus stress tests for ligamentous stability, McMurray's test and Thessaly tests [78][79] for meniscal tears or lesion are performed.
Early detection of knee injuries and pathologies prevents the pain and the damage of the knee structures. Besides the orthopedic tests, the diagnosis techniques are necessary to identify the pathologies and determine the injured structures. It's mostly based on diagnostic imaging techniques like radiography (X-ray), computed tomography (CT), and magnetic resonance imaging (MRI)] that we can pinpoint the source of the knee problem before a surgical treatment i.e. arthroscopic surgery [80][81], and rehabilitation plan are put in place.

4.3 Problem statement and motivation

The lack of imaging techniques in the diagnosis of knee pathologies such as MRI used for soft tissue exams and CT is simply a cost issue as most of the initial exams rely on X-rays. If the first exam is not decisive additional imaging will be ordered as is the case of osteochondral defects sizes, tumors, or some abnormalities that are not clearly diagnosed and identified by X-rays. This situation can be critically important in hospitals of developed countries where the CTs and MRI machines are not available or are heavily used and scheduling can delay the diagnosis.

The knee is a complex joint with a supporting structure composed of muscles/tendons and ligaments working together to maintain knee stability and performance. The femoral tibial articular surfaces move along medial and lateral conforming condyles. Any damage to the knee structures disrupts the functionality of the knee. The patella rides along a femoral groove to maintain the quadriceps forces and tibia tendon forces in such a way to increases the leverage that the quadriceps tendon can exert on the femur by increasing the angle at which it acts. The collateral ligaments are usually used to balance the knee and maintain side to side support to the knee joint. With such complexity, the knee becomes a real challenge to diagnose structural changes associated with pain, early degeneration (osteoarthritis), ACL tear, and any other unforeseen pathology that render the knee function abnormal.

Additional diagnostic tools could benefit the clinician if they are cost-effective and proven reliable. Surface Electromyogram can become a versatile tool for the diagnosis of certain knee pathologies.
In this study, we propose an automatic method to diagnose knee injuries by using surface electromyographic signals detected from four muscles (Rectus Femoris

RF, Vastus Medialis VM, Biceps Femoris BF, and Semitendinosus ST) and goniometric signal during dynamic movement i.e. Gait. The sEMG and Goniometric signals were preprocessed for feature extraction, the feature selection method was used, in order to reduce the database dimensionality and select the relevant signal parameters. Finally, the random forest classifier was applied to evaluate the performance.

4.4 Literature review

The human gait has been used for various applications: in medical diagnosis [82], rehabilitation [83], recognition and control of movements [84][85]. The gait parameters have been extracted by using the different sensors as accelerometer[86], goniometer[87] EMG [88][89] to facilitate the analysis of gait and aid in diagnosis.

Recently, Hurd et al. used the EMG, goniometer and plat force sensors for studying the effect of knee instability after ACL rupture on movement patterns during the midstance phase [90]. In another study, Wei applied the support vector machine (SVM) classifier to recognize the sub-phases of gait using eight leg muscles (6 muscles of right leg: Medial Gastrocnemius (MG), Soleus (SO), Tibialis Anterior (TA), Rectus Femoris (RF), Vastus Medialis (VM), Medial Hamstrings (MH) and 2 muscles of left leg: MG and TA), the sEMG signals of these muscles were processed for feature extraction in time and frequency domain; The results obtained showed that the performance recognition with Mean Absolute Value and Zero-Crossing features was better than other features with an average accuracy of 89,40% [91].

Janidarmian et al, using the time-domain features i.e. Mean, Minimum, Maximum, Median, Standard Deviation, Coefficients of variation, Peak-to-peak amplitude, Percentiles, Interquartile range, Zero crossings, Skewness, Kurtosis, Signal power, Peak intensity, Lag-one autocorrelation, Inter-axis Correlation Coefficient, RMS, Trapezoidal numerical integration; The best performance achieved by the Bagged Decision Trees classifier with an accuracy of 97.17% [92].
Interestingly, Herrera-Gonzalez et al. proposed an automatic diagnosis of knee injuries by using the sEMG and goniometric signals during gait, sitting and standing. The wavelet transform and spectrogram techniques were used for feature extraction and artificial neural network (ANN) for classification. The results obtained showed that the crossed internal and external muscles of the lower limb in combination with goniometry features achieved a higher performance with an accuracy of 95%, 95% and 100% for gait, standing, and sitting, respectively [93].

4.5 Methodology

The block diagram of the proposed methodology is shown in Figure.5.2. The sEMG signals were detected from four lower limb muscles simultaneously with the goniometric signal that measures the flexion-extension of the knee. These signals are pre-processed. Then the temporal and spectral features were extracted. The feature selection is applied in order to select the relevant features. Finally, the random forest classifier is used to classify the knee injuries, i.e. anterior cruciate ligament (ACL) injury, meniscus injury.

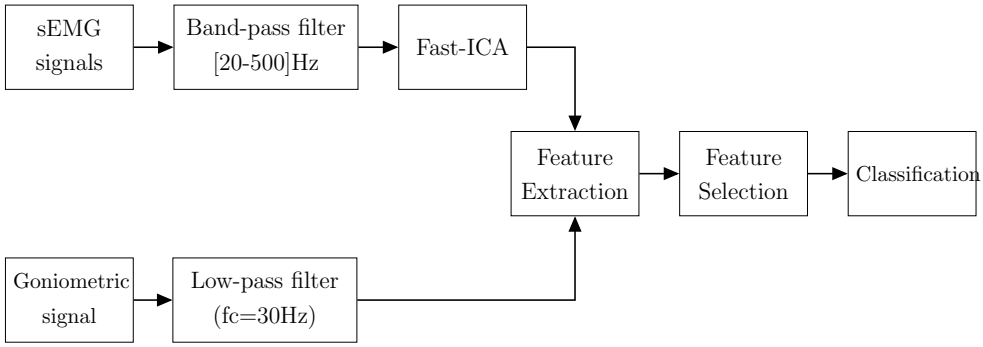

Figure 4.6: Block diagram of the knee injuries classification method.

4.5.1 Lower Limb sEMG Dataset description

The sEMG database is available at UCI. It consists of 21 male volunteers older than 18 years, with 11normal subjects and 11 with knee Abnormalities: 06 subjects with anterior cruciate ligament (ACL) injury, and 04 with meniscus injury; each subject underwent three different movements: gait, leg extension from a sitting position, and flexion of the leg up. These data were acquired from four lower limb muscles: Rectus Femoris RF, Vastus Medialis VM, Biceps Femoris BF, and Semitendinosus ST). Simultaneously, the flexion-extension angle was measured by placing the goniometer on the external side of the knee joint. All records were transmitted in real-time Datalog software through Bluetooth adapter, 14-bit resolution and sampling frequency of 1000Hz [94].

4.5.2 Data pre-processing

In order to reduce the influence of undesirable noises, a 3^{rd} order Butterworth low pass filter was applied on the goniometric signal with cut-off frequency of 30Hz; and a 2^{nd} order Butterworth bandpass filter with cut-off frequencies of [20- 460]

Hz (refer to Chapter 2) used for sEMG signals.
The filtered sEMG signals were supplied to FastICA [95] (Independent Component Analysis) algorithm for source estimation and removing the electrical cross-talk (refer to Chapter 2). All the data were segmented into data segments of the same length using a fixed window length of 5000 samples and an overlap of 90%.

4.5.2.1 Independent Component Analysis (ICA)

ICA is a statistical technique used for the separation of independent sources. In principle, the independent components (IC) can be obtained by maximizing the non-Gaussianity using the contrast functions i.e. Kurtosis and negentropy, or by minimizing the Mutual Information (MI) [128]. In a noise-free, the ICA model can be expressed as follows:

$$x(t) = As(t) \tag{4.1}$$

The latent sources $s(t) = [s_1(t), \ldots., s_p(t)]^T$ are mutually independent and have non-gaussian distributions; the linear mixing of these sources produce the observations $x(t) = [x_1(t), \ldots., x_p(t)]^T$, where $A \in R^{(n*p)}$ is the mixing matrix.
ICA aims to estimate the unmixing matrix $W = A^{-1}$, thereby recovering the sources $s^*(t) = [s_1^*(t), \ldots., s_p^*(t)]^T$.
In this study, the FastICA approach that is based on negentropy function was preferred to separate the EMG signals and reduce the cross-talk, due to its robust performance and fast convergence[128].

4.5.3 Feature extraction

In this study, several techniques have been used in order to extract the temporal and spectral features from goniometric and sEMG signals as described below.

4.5.3.1 Time Domain features

Goniometric signal — The single gait cycle consists of swing (40%) and stance (60%) phases, which in turn divided in knee swing/stance flexion and knee swing/stance extension intervals. The four extrema are the zero-crossing points of the knee angular velocity calculated by the first derivative of the knee angle (goniometric signal) as shown in Figure.4.7. These maxima and minima facilitate the calculation of different parameters.

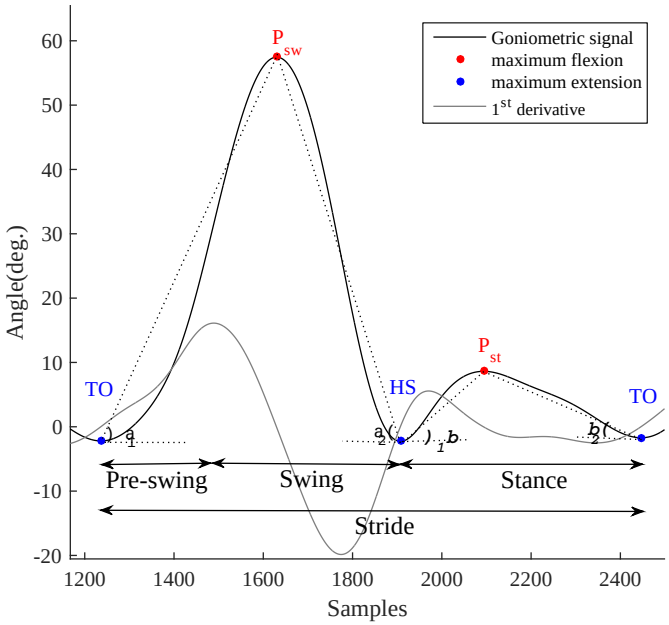

Figure 4.7: Knee angle and angular velocity signals.

- Maximum knee flexion during swing (P_{sw}).
- Maximum knee flexion during stance (P_{st}).
- $\frac{P_{sw}}{P_{st}}$ ratio.
- Duration between P_{sw} and P_{st}.
- Angles between maximum knee extension and maximum knee flexion during swing (α_1, α_2).
- Angles between maximum knee extension and maximum knee flexion during stance (β_1, β_2).
- Stance duration: from Heel Strike to begin of Toe Off (Pre-swing).
- Pre-swing + swing duration: From TO to HS.
- Stride length [96].

sEMG signal —From the four sEMG signals, we have extracted the following time-domain features.

– Absolute Mean Value

$$AMV = \frac{1}{N}\sum_{i=1}^{N}|s_i| \tag{4.2}$$

– Difference Absolute Mean Value

$$DAMV = \frac{1}{N}\sum_{i=1}^{N-1}|s_{i+1} - s_i| \tag{4.3}$$

– Root Mean Square

$$RMS = \sqrt{\frac{1}{N}\sum_{i=1}^{N}s_i^2} \tag{4.4}$$

– Shannon Energy

$$E_{Sh} = \frac{-1}{N}\sum_{i=1}^{N}s_i^2 \log s_i^2 \tag{4.5}$$

– Sample Entropy[97]

$$Samp - En(m, r, N) = \begin{cases} -\log \frac{C(r)^m}{C(r)^{m-1}} & C^m \neq 0 \wedge C^{m-1} \neq 0 \\ -\log \frac{N-m}{N-m-1} & C^m = 0 \vee C^{m-1} = 0 \end{cases} \tag{4.6}$$

Where N is the total number of sampling points. setting constant m=2 (m should be $\ll$ N) and r=0.25∗SD (standard derivation of signal).

4.5.3.2 Autocorrelation and linear correlation

During gait, sEMG and goniometric signals are quasi-periodic, this is because the contractions of extensor and flexor muscles and the knee extension/flexion are regularly repeated. Hence, the autocorrelation is a convenient technique to extract the cyclic patterns. Besides quasi-periodicity, the sEMG signals are quasi-random in nature and the use of smoothing technique is appropriate to closely reflect the goniometric signals. In this study, we have applied the integrated profile method (refer to chapter 3) on both sEMG and goniometric signals to obtain approximately similar shape (see Figure.4.8) and then calculated their autocorrelation using the following formula.

$$r_p(\tau) = \frac{cov(s_i, s_{i+\tau})}{\sigma_{s^2}} \tag{4.7}$$

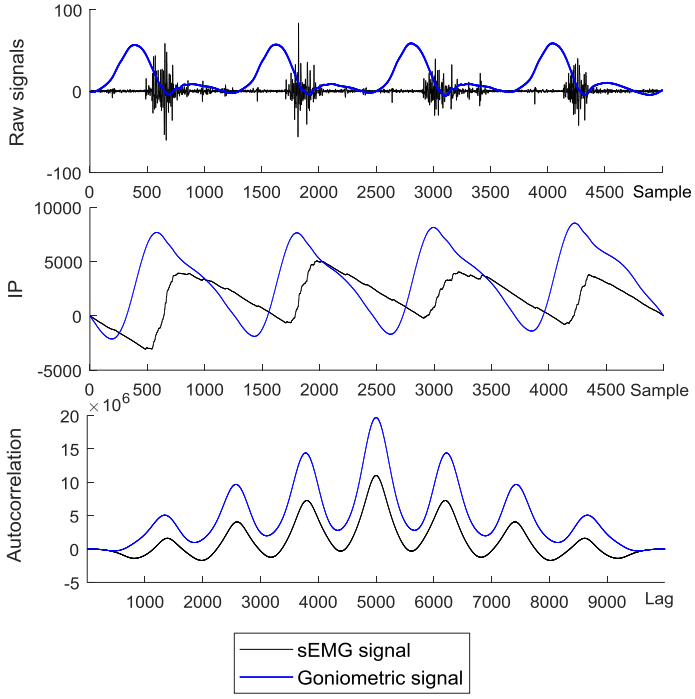

Figure 4.8: Integrated profile and autocorrelation of sEMG (from RF) and goniometric signal (healthy subject)

From the autocorrelation curves, we have extracted the following features.

- Zero-crossings of autocorrelation.
- Slope of maximum autocorrelation peaks.
- $\frac{\theta_i}{\theta_{i+1}}$ ratio.

As shown in Figure.4.9, the autocorrelation-based features extracted from the goniometric signal (healthy subjects), the same features are extracted from the four sEMG signal and then studying their linear relationship.

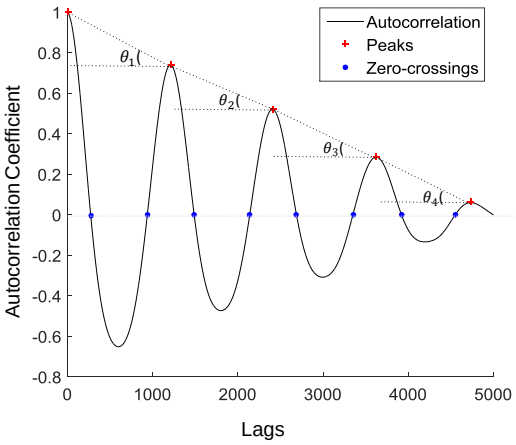

Figure 4.9: Autocorrelation-based goniometric features.

The relationship between signals is very important, for that reason the linear correlation has been used to determine the correlation between goniometric signal and sEMG signal of each muscle, the correlation between sEMG signals of quadriceps muscles, the correlation between sEMG signals of Hamstring muscles and correlation between sEMG signals of quadriceps muscles using the following equation (for further details, refer to Section 4.8 of Chapter 3).

$$C_p(s_1, s_2) = \frac{cov(s_1, s_2)}{\sigma_{s_1}\sigma_{s_2}} \tag{4.8}$$

4.5.3.3 Frequency Domain features

In the frequency domain, the PSD has been calculated using Welch's method in order to extract the following spectral features (for more details, refer back to Chapter 2).

- Mean frequency
- Median frequency
- Peak frequency.

4.5.4 Feature Vector

After segmentation and feature extraction the total matrix size is 271x 82 with 21 for normal case, 191 for ACL injuries, 59 for meniscus injuries. 82 represents the length of class with features vector which can be represented as follows.

Table 4.2: Feature vector description

Feature Vector			
No	***Feature***	***No***	***Feature***
1-4	RMS of RF, VM, BF, and ST	51-52	Pst (mean, SD)
5-8	AMV of RF, VM, BF, and ST	53-54	Pst (mean, SD)
9-12	DAMV of RF, VM, BF, and ST	55-56	Psw_Pst ratio (mean, SD)
13-16	ESh of RF, VM, BF, and ST	57-58	$Duration_{Psw-Pst}$ (mean, SD)
17-20	Samp-En of RF, VM, BF, and ST	59-60	α_1 (mean, SD)
21-24	fmed of RF, VM, BF, and ST	61-62	α_2 (mean, SD)
25-28	fmean of RF, VM, BF, and ST	63-64	β_1 (mean, SD)
29-32	fmax of RF, VM, BF, and ST	65-66	β_2 (mean, SD)
33-36	Cp(θ_G, θ_{sEMG}) of RF, VM, BF, and ST	67-68	Stance duration (mean, SD)
37-40	Cp (θ_G ratio, θ_{sEMG} ratio) of RF, VM, BF, and ST	69-70	Swing duration (mean, SD)
41-44	ZCratio (G, sEMG) of RF, VM, BF, and ST	71-72	$Stride_{st-st}$ (mean, SD)
45	Corr (RF,VM)	73-74	$Stride_{sw-sw}$ (mean, SD)
46	Corr (RF,BF)	75-76	θ_G(mean, SD)
47	Corr (RF,ST),	77-78	θ_G ratio (mean, SD)
48	Corr (ST, VM)	79	$fmed_G$
49	Corr (BF,ST)	80	$fmean_G$
50	Corr (BF,VM)	81	$fmax_G$

4.5.5 Feature Selection

Feature selection FS can be used for feature evaluation and optimal features selection by taking the irrelevant and redundant features out and keeping the relevant ones. This process can reduce the database dimensionality and the computational complexity, which in turn can improve the performance of classification and speed up the learning process in terms of computation time. Although several research works have been proposed to evaluate the relevant features for classification of EMG signals [98][99][100][101][102][103][104]. In this study, the ReliefF was used to select the effective features that influence on knee injury classification.

4.5.5.1 ReliefF

ReliefF is an extension of relief algorithm, was proposed by Kononenko [105] in order to deal with the multiclass problems. It randomly selects the instance Ri from training data and seeking to find the k nearest neighbor instances from the same class (nearest hits H_j), also the k nearest neighbors of each other classes (Near Misses M_j) [105]. The weight estimation function (W) is calculated as

follows.

$$W[f] = W[f] - \sum_{j=1}^{k} \frac{diff(f, R_i, H_j)}{m * k} + \sum_{\substack{u=1 \\ c \neq c(R_i)}}^{T} \frac{P(c_u)}{1 - P(c(R_i))} * \sum_{j=1}^{k} \frac{diff(f, R_i, M_j)}{m * k} \tag{4.9}$$

Where,
m is the number of instances ($1 \leq i \leq m$);
f is the number of features with f=1 ... F (the length of features);
P(cu): the probability of class;
T is the total number of classes;
P(c(R_i)): the probability of R_i class;
k: the number of the nearest neighbors;
diff() is the function that calculates the distance between the values of the feature f for two instances R_i and H_j or M_j;
The weight vector range between [-1 1], the important features accomplish the large positive weight.

4.5.6 Classification

Random Forest: is a combination of decision tree classifiers with similar quality. The subsets of features are randomly selected to split each tree node. The final decision is obtained by the majority vote of trees [106]. In this work, the optimal number of trees is 80.

4.5.7 Performance evaluation

In order to evaluate the performance of classification, there are different statistical metrics that can be used such as the overall classification accuracy (OCA), sensitivity, specificity, and the confusion matrix. The aforementioned metrics are described below.

– Confusion matrix: is also called the error matrix that represents the performance of classification in form of matrix CM, all the correct predictions are represented in the diagonal of the matrix, whereas the off-diagonal cells are for the incorrect predictions. In this study,we have three classes i.e. Healthy **H**, ACL injury **A**, and Meniscus injury **M** subjects, so the confusion matrix CM can be presented as follows.

$$\text{CM}= \begin{bmatrix} C_{HH} & C_{HA} & C_{HM} \\ C_{AH} & C_{AA} & C_{AM} \\ C_{MH} & C_{MA} & C_{MM} \end{bmatrix}$$

Where C_{HH}, C_{AA}, C_{MM} are the correct predictions (true positive TP) that are classified as healthy cases, ACL injury and meniscus injury, respectively. C_{HA} and C_{HM} are the numbers of healthy cases that are misclassified as ACL injury or meniscus injury, respectively
C_{AH} and C_{AM} are the numbers of cases with ACL injury that are misclassified as healthy cases or meniscus injury, respectively.
C_{MH} and C_{MA} are the numbers of cases with meniscus injury that are misclassified as healthy cases or ACL injury, respectively.

- The Overall Classification Accuracy **OCA** is the proportion of the number of correct predictions to the total number of predictions, expressed as follows.

$$OCA = \frac{Number\ of\ correct\ predictions}{total\ number\ of\ predictions} * 100\% \tag{4.10}$$

- Sensitivity is known as recall or true positive rate can be expressed as:

$$Se = \frac{TP}{TP + FN} \tag{4.11}$$

Where TP and FN are the true positive and false negative of considered class. For healthy class CH, Se_H is calculated as follows.

$$Se_H = \frac{C_{HH}}{(C_{HH} + C_{HA} + C_{HM}}) \tag{4.12}$$

- Specificity or the true negative rate calculated as:

$$Sp = \frac{TN}{TN + FP} \tag{4.13}$$

Where TN and FP are the true negative and false negative of considered class, respectively. For a healthy class,Se_H determined as follows.

$$Se_H = \frac{TN_H}{(TN_H + C_{NH} + C_{MH})} \tag{4.14}$$

With $TN_N = C_{AA} + C_{NM} + C_{MA} + C_{MM}$.

4.6 Results and discussion

The knee injuries database was divided into 02 databases of 2 classes: ACL injuries database consists of 191 ACL injuries and 21 normal (N) records, and

Meniscus injuries MN with 59 (MN).
The selection of relevant features is assessed by using reliefF algorithm. As shown in Figure.4.10 and Figure.4.11 the common relevant features in two databases are: in the frequency domain, the mean and median frequencies for sEMG and goniometric signals, and RMS, DAMV, Shannon entropy, AMV for sEMG and stance peak, stance-swing peaks ratio, $\alpha 2$, $\beta 2$, and stance duration in the time domain. Whereas The internal-external muscles of hamstring and quadriceps, also the goniometric and sEMG signals relationships are very important but it depends on injury type. For meniscus injury, BF-ST, VM-ST, G -RF, and G-BF correlation. Whereas, for ACL injuries only the goniometric and sEMG signals relationships that were selected.

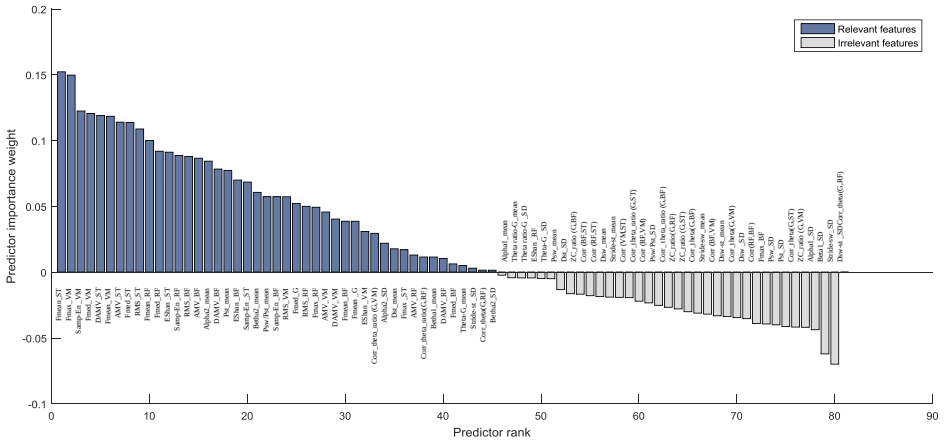

Figure 4.10: Ranking features of ACL injuries database.

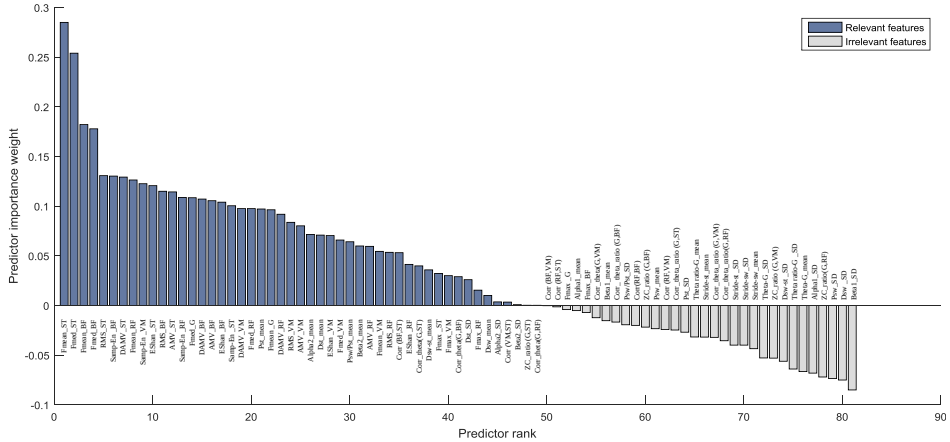

Figure 4.11: Ranking features selection of MN injuries database.

The comparison of five classifiers (i.e., Random Forest, Decision Tree (n-Trees=80), Diagonal-Linear Discriminant Analysis (DLDA), SVM with polynomial kernel function, and k-NN with k= 5) was realized using Matlab R2017a and performed on 1.99 GHz Intel Core i7-8550U based PC using a 64-bit Windows 10 operating system with 8 GB RAM. As shown in Table 4.3, The random forest with ReliefF achieved higher performance compared to other classifiers whereas the Decision Tree classifier has the lowest computation time. Adding the feature selection technique leads to remove the noised and irrelevant features which in turn reduce the computation time as shown in Tables 4.3 and 4.4.

Table 4.3: Classification performance of ACLI, and MNI databases with and without feature selection.

		Before FS				**After FS**			
Classifier	**Database**	***Acc(%)***	***Se(%)***	***Sp(%)***	***Computation time(s)***	***Acc(%)***	***Se(%)***	***Sp(%)***	***Computation time(s)***
Random	ACLI	97,16	76,19	97,38	1,95	97,16	76,19	100	1,88
Forest	MNI	96,25	85,71	100	1,80	98,75	95,23	100	1,75
Decision	ACLI	95,28	76,19	97,38	0,35	95,75	76,19	97,19	0,32
Tree	MNI	95,00	85,71	98,30	0,29	95,00	85,71	98,30	0,29
DLDA	ACLI	93,86	76,19	95,81	0,57	93,39	76,19	95,28	0,46
	MNI	83,75	85,71	83,05	0,46	91,25	85,71	93,22	0,45
	ACLI	93,86	76,19	95,81	1,10	92,92	61,90	96,33	0,94
SVM	MNI	90,00	85,71	91,52	0,93	95,00	85,71	98,30	0,92
	ACLI	93,44	38,09	99,47	1,58	92,96	28,57	100	1,14
k-NN	MNI	83,75	52,38	94,91	1,29	83,75	47,62	96,61	1,11

Figure.4.12 shows the relevant features of knee injuries database with 3 classes (Normal, ACL injuries, and MN injuries). Swing peak, stride, and $\beta 1$ are also selected as relevant features. The performance classification is shown in Table 4.4 and the prediction results are presented in the confusion matrix (see Table 4.5). It shows that 05 normal cases were misclassified as ACL injuries.

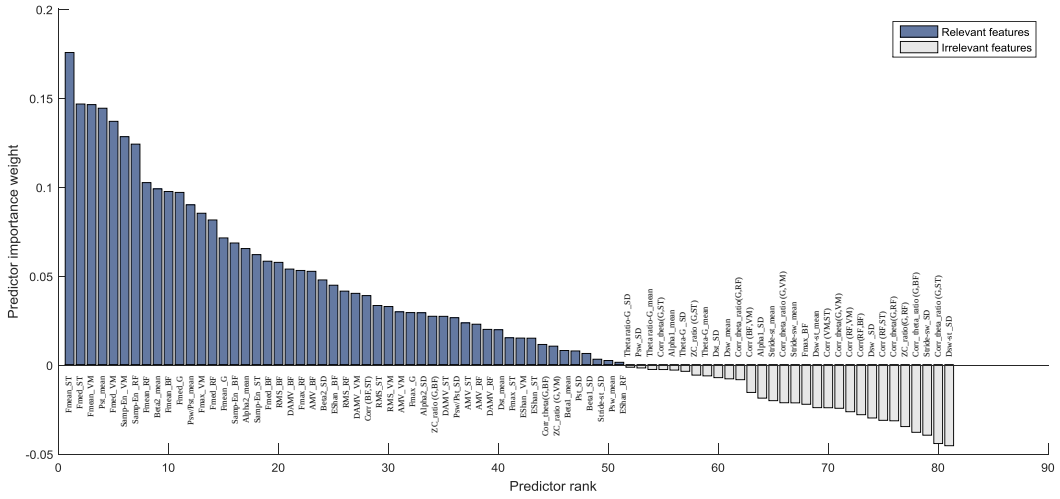

Figure 4.12: Ranking features selection of Knee injuries database.

Table 4.4: Classification performance of knee injuries database with and without feature selection.

	Before FS				**After FS**			
Classifier	***Acc(%)***	***Se(%)***	***Sp(%)***	***Computation time(s)***	***Acc(%)***	***Se(%)***	***Sp(%)***	***Computation time(s)***
Random Forest	97,27	61,90	100	2,06	**98,29**	**76,42**	**100**	2,02
Decision Tree	92,52	52,38	96,70	0,36	95,57	52,38	100	**0,33**
DLDA	84,99	61,90	94,13	0,55	86,05	57,14	96,33	0,50
SVM	85,37	71,42	98,53	1,37	94,21	61,90	99,26	1,35
k-NN	78,23	23,80	99,63	1,28	88,77	33,33	99,26	1,20

Table 4.5: Confusion matrix of classification results for random forest classifier and reliefF

	Classified as		
Actual class	***Normal***	***ACL injury***	***MN injury***
Normal	**16**	5	0
ACL injury	0	**191**	0
MN injury	0	0	**59**

4.7 Conclusion

In this chapter, we have developed an automatic knee injury diagnosis method using sEMG and goniometric signals. These signals were detected from four categories i.e. normal, ACL injuries, meniscus injuries subjects, the features were extracted from time and frequency domain and selected by ReliefF algorithm. The selection of relevant features improved the classification of knee injuries and performance, where the accuracy with random forest reached 98,29%, a slight increase from 97,27% before selection.
In the future study, we seek to enhance and improve the performance of the classification of different knee pathologies by extracting more parameters that are critical to the knee physical exam of the patient. There is more data testing needed and further validation for the proposed method to reach its full potential and becomes a tool readily available in clinics.
In the next chapter, we will develop an automatic diagnosis method for neuromuscular disorders i.e. neuropathy and myopathy by means of concentric needle.

5

An automatic diagnosis of neuromuscular disorders using iEMG

5.1 Introduction

Neuropathy and myopathy are the majority of neuromuscular disorders that inflict damage on nerves and muscles, which can be detected and evaluated by EMG. The purpose of this chapter is to develop an automatic diagnosis approach of neuropathy and myopathy disorders based on intramuscular electromyographic signals, using two sorts of iEMG database, the simulated iEMG signals that are used for evaluating and the clinical iEMG signals for validating our approach. These signals were decomposed by wavelet transform i.e. discrete wavelet transform DWT and wavelet packet transform WPT in order to decompose the signals and extract the statistical features. Then the feature selection methods such as ReliefF and fast correlation-based filter FCBF were employed for selecting the relevant features and classified by the linear discriminant analysis LDA.

5.2 Neuropathy and myopathy

Electromyography is a technique for measuring the electrical activities generated by skeletal muscle. The detection of electromyographic signals is acquired either by concentric needles or surface electrodes and can be recorded at a different percentage of maximal voluntary muscle contraction (MVC)[107]. The increase in voluntary force results in the additional firing of motor units (MUs) which in

turn complicate the separation of discrete waveforms i.e. motor unit action potentials (MUAPs), and the extraction of EMG characteristic metrics for diagnosis of neuromuscular disorders.
Any damage in structure or in the functionality of nerves, neuromuscular junctions, or muscles leads to neuromuscular disorders such as neuropathies and myopathies, which influence on the characteristic of MUAPs [108]. In neuropathy, due to peripheral nerves damage, the MUAPs having a longer duration and a higher amplitude compared to healthy cases. While in myopathy, because of the malfunction of muscle fibers, the MUAPs decrease in amplitude and duration [108](see Figure.5.1). However, the diagnosis in the early stage of neuromuscular disorders cannot be feasible, hence different quantitative methods and classification techniques have been developed in order to detect and minimize the progression of pathologies.

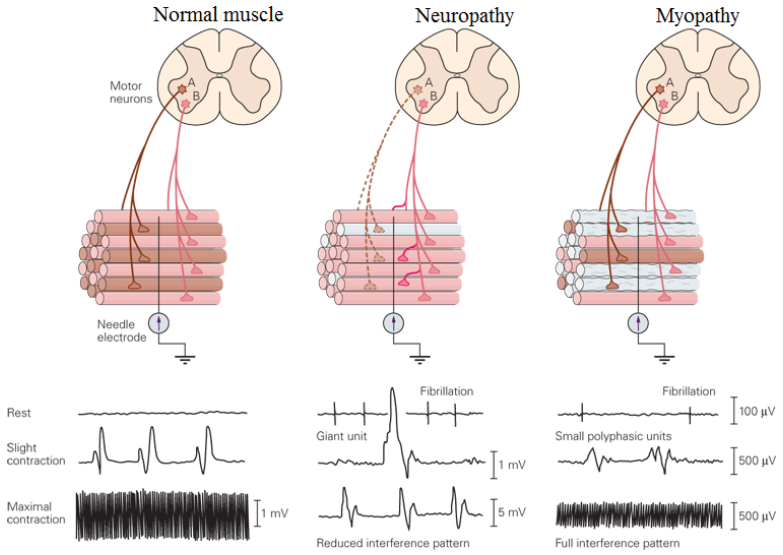

Figure 5.1: Neuropathic and myopathic disorders.

5.3 Literature review

In the literature, several feature extraction methods were proposed for neuromuscular disorders classification. Some of these methods based on the characteristic of MUAP using the morphological features i.e. amplitude, duration, area, numbers of turns, and numbers of phases [109][110], while others based on decomposition of EMG signals and extracting the statistical features [111][112].
Recently, Dostal et al.[113]extracted the number of turns, the amplitude of turns,

signal energy, and the permutation entropy to classify the neuropathic and normal individuals using support vector machine SVM. Koçer and Tümer [114] used the autoregressive (AR) and cepstral analysis for feature extraction and principal component analysis (PCA) for dimensional reduction, using Multilayer perceptron- (MLP) and radial basis function-based networks for classification, where the optimum performance was observed with the use of AR-PCA-MLP combination.

The wavelet transform is a very efficient tool for non-stationary signals analysis, has been adopted by many researchers in order to decompose the EMG signals and extract the time-frequency features. Barmpakos et al.[115] extracted the wavelet energies using discrete wavelet transform (DWT) along with Hudgins' set features[116]i.e. waveform length (WL), zero crossing (ZC), slope sign changes (SSC), Wilson amplitude (WA) and root mean square (RMS), with the purpose of increasing the classification performance. Also, Krishna and Thomas [117] extracted the DWT spectral features: total power, peak, median, and mean frequencies from the approximate coefficient to classify the normal, myopathic and neuropathic subjects of EMGLAB database using k-nearest neighbor classifier (k-NN), the obtained results showed that the DWT spectral features achieved a better performance compared to temporal and direct spectral features. As well as, Bhattacharya et al. [118] extracted the time features: mean amplitude value (MAV), RMS, ZC, WL, and the time-frequency features: average of absolute value, standard deviation, average power, and ratio of mean from each DWT sub-bands, and classified the signals of simulated EMG database using discriminator dependent decision rule-based classifier (D3R).

As well, Subasi [119] combined the swarm optimization (PSO) with SVM classifier using the statistical DWT features i.e. mean, standard deviation, average power, and the ratio of mean. While, Gakgoz et al., [120] employed the multiscale principal component analysis (MSPCA) method for EMG signals de-noising, and random forest for classification using the same statistical DWT features that were proposed in [119].

In this study, we have proposed a methodology for neuromuscular disorders classification using simulated EMG database for evaluation and clinical database for validation, the wavelet transform techniques i.e. discrete wavelet transform and wavelet packet transform have been employed in order to decompose the EMG signals and extracting the features. The feature selection methods: ReliefF and FCBF used for selecting the optimum features and linear discriminant analysis (LDA) classifier for classification.

5.4 Methodology

The block diagram in Figure.5.2 outlines our proposed method destined for the classification of neuromuscular disorders: neuropathy and myopathy using EMG signals. The EMG signals are firstly decomposed using wavelet transform, then the time-frequency features are extracted from each level which in turn are selected by the feature selection techniques, finally, the EMG signals with selected features are classified by linear discriminant analysis (LDA).

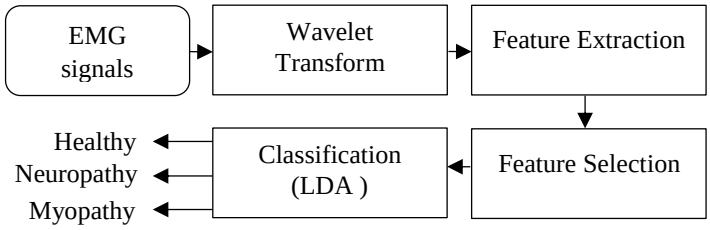

Figure 5.2: Block diagram of neuromuscular diseases classification.

5.4.1 Databases Description

5.4.1.1 Simulated EMG Database Description

The simulated EMG Data were generated using a physiologically based model that constructed to study the interrelationship between the structure and activation of muscle [121]. This EMG database contains three groups: Normal, Myopathy and Neuropathy, with 5 patients for each group. EMG signals were detected by the needle electrode from Biceps Brachii at five contraction levels of 5.0, 7.5, 10.0, 12.5, and 15.0 %MVC. Myopathic/ Neuropathic signals were simulated for 25, 50 and 75% muscle fiber/ motor-unit loss.
These signals were high-pass filtered by a 2^{nd} order Butterworth filter with cut-off frequency of 20 Hz and divided into 48457 samples using a fixed window without overlapping. This database contains 300 EMG signals with 100 recorders for each group

5.4.1.2 Clinical EMG Database

The simulated EMG signals are generated to evaluate and verify our methods whereas the clinical EMG signals are used for validation. In this study, to classify the neuromuscular disorders we used the accessible clinical EMG database that consists of 10 healthy subjects with 6 males and 4 females (age, mean $\pm$ SD: 27.2000 $\pm$ 4.5412 years), 07 myopathic patients with 5 males and 2 females (age,

mean±SD: 37.6667 ± 15.4876 years), and 08 neuropathic patients with 4 males and 4 females (age, mean± SD: 58.6667 ±5.2026 years).
These EMG signals were detected by inserting a concentric needle electrode into the long head of the biceps brachii muscle during a low isometric contraction, then amplified with a gain of 500 using an instrumentation amplifier DISA15C01 and filtered by a bandpass filter with cut-off frequencies of 2 Hz–10 kHz. The filtered signals were digitalized with 16-bit resolution and sampled at a sampling rate of 23438 Hz using Motorola DSP56ADC16 [122].
Figure.5.3 illustrates an example of EMG signals for normal (a), neuropathic (b) and myopathic(c) patients.

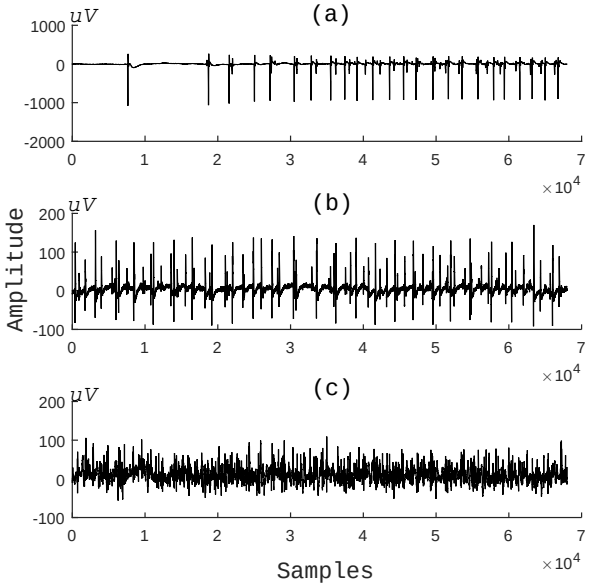

Figure 5.3: Example of iEMG signals for normal, neuropathic and myopathic subjects.

5.4.2 Feature extraction based on Wavelet Transform methods

Wavelet transform is a powerful tool for digital signal analysis, which decomposes the signal into a set of wavelets consisting of scaling (a) and shifting (b) of mother wavelet Ψ(t) that is well localized in frequency and time domain. The scaling process is stretching or shrinking of the signal in time, while the shifting means the translation of wavelet along the length of the signal. There are many different wavelets that can be selected as a mother wavelet: Daubechies, Haar, Meyer,

Coiflet, Mexican hat, Symlet, and Biorthogonal wavelets [123]. The choice of the right wavelet depends on the proprieties of the signal. In our case, we select Daubechies 4 (db4) wavelet that shaped similar to the MUAP form [120]. The wavelet transform of signal s(t) can be defined as follows.

$$w_s = \int_{-\infty}^{+\infty} s\,(t)\,\Psi_{a,b}\ \ (t)\ \ dt \tag{5.1}$$

Where:

$$\Psi\ _{a,b}\,(t) = \frac{1}{\sqrt{|a|}}\Psi(\frac{t-b}{a}) \tag{5.2}$$

5.4.2.1 Discret Wavelet Transform

Discrete wavelet transform is discrete in scale and time which decomposes the signal into a set of orthogonal wavelets. The detail and approximation coefficients are obtained by passing the signal (s) through the high pass (HPF) and low pass (LPF) digital filters and down-sampled by 2 factors as shown in Figure.5.4

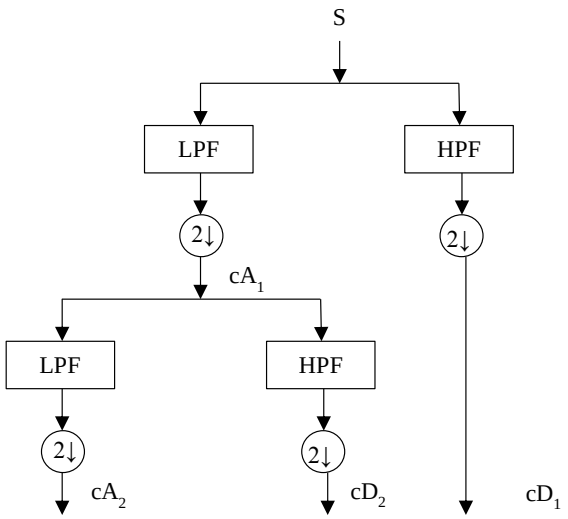

Figure 5.4: Discrete wavelet decomposition at 2^{nd} level.

The DWT can be expressed as follows.

$$Dwt\,(j,k) = \frac{1}{a}\sum_{i=0}^{i=N-1} s(i)\Psi(\frac{k-b}{a}) \tag{5.3}$$

Where N is the length of the signal. And a=2j, b= 2j k, j=0,1, 2,. . . , J-1, and k=0,1,2,. . . ,2j-1, (J is the level of decomposition $N = 2^J$).

5.4.2.2 Wavelet Packet Transform

Wavelet packet transform is an expansion of discrete wavelet transform which utilizes the quadrature mirror filters (QMFs). Where DWT decomposes only the approximation after the first level, the WPT decomposes both approximations and details at each level as shown in Figure.5.5, thus, it has a better resolution for a signal that contains important information in the high frequencies. As well as, WPT results in better filtering of the unwanted frequency components.

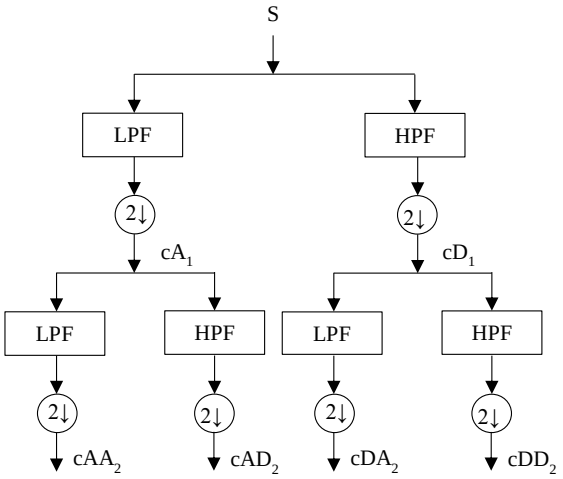

Figure 5.5: Wavelet packet decomposition at 2^{nd} level.

5.4.3 Feature Extraction

The discrete wavelet transform and the wavelet packet transform decompose the signal into sub-signals i.e. approximations and details. To represent the time and the frequency distribution, we extract the following statistical features that calculated from the reconstructed sub-signals in each level j.

1. Root Mean Square
2. Mean Absolute Value
3. Waveform Length **WL**: the sum of the absolute difference between consecutive values, given by Eq.(5.4)

$$WL = \frac{1}{N}\sum_{i=1}^{N} |s_{j_{i+1}} - s_{j_i}| \tag{5.4}$$

4. Standard deviation

5. Shannon Wavelet Entropy **SWE** and Shannon Wavelet Packet Entropy **SWPE**: the Shannon wavelet Entropy SWE was introduced firstly by Quian Quiroga et al. [124] in order to measure the disorder in EEG signal. Here, the Shannon Wavelet Entropy SWE and Shannon Wavelet Packet Entropy SWPE are calculated as follows.

$$SWE = -\sum_{i=1}^{N} p_j(i) * \ln p_j(i) \tag{5.5}$$

Where p_j is the ratio between the energy of the total signal (s) and the sub-signal (s_j) of each level J.

$$p_j = \frac{E_{s_j}}{E_s} \tag{5.6}$$

With $E_s = \sum_{i=1}^{N} {s_i}^2 = \sum_{j=1}^{J} \sum_{i=1}^{N} {s_{ij}}^2$, $E_{s_j} = \sum_{i=1}^{N} {s_{ji}}^2$, and N is the total number of samples.

6. Total Power, Mean Frequency, Median Frequency, Peak Frequency

5.4.4 Feature Selection

In case of dataset with a large number of features, the feature selection techniques are appropriate in order to avoid the overfitting problem, and dimensionality curse, as well as, reducing the computational complexity, speed up the training times and enhance the performance by selecting the important features and removing the irrelevant ones without loss of information. There are three various methodologies of FS i.e. filter, wrapper, and embedded methods. In this study, we used two methods of filter methodology: ReliefF and Fast Correlation-Based Filter FCBF described as below.

5.4.4.1 ReliefF

The ReliefF is a classical supervised filter approach that ranks the important features by computing their weights . The weight range varies between [-1 1], where the important features achieve the large positive weight.(for more details, refer back to Chapter 4)

5.4.4.2 Fast Correlation-Based Filter method (FCBF)

FCBF algorithm has been developed by Yu and Liu[125] in order to determine the class relevance and the dependencies of features using the Symmetrical Uncertainty (SU) correlation. The SU calculates the correlation between features and classes, and also the correlation between two features. It is computed by the entropy and conditional entropy, as expressed in Eq.5.7.

$$SU(X,Y) = 2\left[\frac{H(X) - H(X|Y)}{H(X) + H(Y)}\right] \tag{5.7}$$

Where,
H(X), and H(Y): are the entropy of random variables X and Y, with x_i and y_i values calculated as:
$H(X) = -\sum_i P(x_i)\log P(x_i)$; $H(Y) = -\sum_i P(y_i)\log P(y_i)$
H(X—Y): conditional entropy :$H(X|Y) = -\sum_j P(y_j)\sum_i P(x_i|y_j)\log P(x_i|y_i)$
With $P(x_i)$ and$P(y_i)$ are the prior probability of all x and all y, respectively.
And $P(x_i|y_j)$is the conditional probabilities of X given the values of Y.
The SU is normalized between 0 and 1, where the zero value for negligible or no correlation and one for strong correlation.

5.4.5 Classification

For the classification process, the choice of a classifier is very essential, depends on several factors such as the accuracy of prediction, and the computational time. Therefore, the chosen classifier should be an accurate and optimized tool in predicting novel patterns. For neuromuscular disorder diagnosis, We rely on linear discriminant analysis (LDA) classifier, which based on Mahalanobis distance calculates the between-class variance S_b and the within-class variance S_w in order to construct the lower-dimensional space by maximizing the between-class variance and minimizing the within-class variance [126]. The Sb and S_w can be express as follows.

$$S_b = \sum_{i=1}^{C} (\mu_i - \mu)(\mu_i - \mu)^T \tag{5.8}$$

$$S_w = \sum_{i=1}^{C}\sum_{j=1}^{N_i} (f_{i,j} - \mu_i)(f_{i,j} - \mu_i)^T \tag{5.9}$$

Where μ and μ_i are the overall mean and the mean of feature vectors of each class C,$f_{i,j}$ is the j^{th} feature of class i. Apropos of performance validation, we use the k-fold cross-validation technique, with being k= 10. this technique allows

us to ensure that all features were used for training and testing by resampling the data into k subsets. One subset is randomly chosen for test and others are kept for training, this step is repeated k times. In the sequel, the performance of classification is the mean of all the k trials.

5.4.6 Performance evaluation

To evaluate the performance of classification, the number of true positives (TP), true negative (TN), false positive (FP), and false-negative (FN) are used to calculate the Accuracy (Acc), Sensitivity (Se) and Specificity (Sp) which can be express as follows.

$$Acc = \frac{TP + TN}{TP + TN + FP + FN} \tag{5.10}$$

$$Se = \frac{TP}{TP + FN} \tag{5.11}$$

$$Sp = \frac{TN}{TN + FP} \tag{5.12}$$

5.5 Results and Discussion

The decomposition of EMG signals is a very important step to facilitate feature extraction and improve classification performance. In this study, Wavelet transform methods i.e. DWT and WPT have been applied for EMG decomposition and extracting the features, also ReliefF and FCBF used for selecting the relevant features, using the simulated EMG database.
The prediction of neuromuscular disorders is very higher at the advance stage compared to the early stage. In order to improve the classification performance at all stages, we search to find common and efficient techniques and procedures to get a better prediction percentage. As shown in Table 5.1, At level 5% MVC, the classification performance yielded a high overall classification accuracy of 87.7%, 91.7%, 97.3% for 25,50, and 75 fiber/motor-unit loss respectively, when using DWT with ReliefF and LDA classifier.

Table 5.1: The LDA overall classification accuracy (in %) of DWT and WPT methods for simulated EMG signals.

			Before FS		**After FS**			
		Methods			**ReliefF**		**FCBF**	
		MVC(%)	DWT	WPT	DWT	WPT	DWT	WPT
25 fiber/ Motor unit loss		05.0	85.0	81.7	**87.7**	83.3	79.3	79.0
		07.5	75.7	73.0	77.0	74.0	52.3	74.3
		10.0	78.9	79.6	80.0	79.3	69.6	77.9
		12.5	83.3	76.3	86.7	78.7	66.3	61.7
		15.0	74.0	70.0	77.3	76.3	49.7	62.0
50 fiber/Motor unit loss		05.0	89.3	82.0	**91.7**	82.7	68.7	75.0
		07.5	79.7	80.3	81.7	80.7	69.0	68.0
		10.0	89.3	83.9	90.0	87.5	76.4	77.1
		12.5	84.3	77.7	84.0	79.3	73.7	65.3
		15.0	92.7	83.3	84.3	83.3	57.3	65.3
75 fiber/ Motor unit loss		05.0	96.3	91.7	**97.3**	93.7	97.3	-
		07.5	95.3	88.0	95.3	87.7	87.6	-
		10.0	83.6	79.6	82.5	82.5	75.0	76.0
		12.5	93.0	83.7	90.3	85.7	73.0	76.4
		15.0	89.7	85.3	89.7	86.0	83.3	78.7

(-): No features selected.

To validate our method, we applied it to the clinical EMG database, Table 5.2 showed that the DWT with reliefF achieved a higher classification performance, the FCBF is a very efficient feature selection method but here, it failed in the selection and some important features were lost.

Table 5.2: The LDA overall classification accuracy (in %) of DWT and WPT methods for simulated EMG signals.

Performance metrics	**Before FS**		**After FS**			
			ReliefF		**FCBF**	
	DWT	WPT	DWT	WPT	DWT	WPT
Overall accuracy	93 .0	84.0	**97.5**	94.5	75.0	86.0
Average sensitivity	96.0	76.0	**98.0**	94.0	87.0	88.0
Average specificity	92.0	93.0	**98.0**	96.0	70.0	89.0
Number of features	78	397	52	50	13	47
Computation time (s)	5.5	6.1	4.5	4.5	4.6	4.7

The classification performance of the DWT method with and without feature

selection methods: ReliefF and FCBF have been presented in form of a matrix (see Tables 5.3), DWT with ReliefF has less prediction error compared to FCBF methods.

Table 5.3: The confusion matrix for LDA classifier

	Classified as								
	DWT			**DWT+ReliefF**			**DWT+FCBF**		
Class	***Normal***	***Neuropathy***	***Myopathy***	***Normal***	***Neuropathy***	***Myopathy***	***Normal***	***Neuropathy***	***Myopathy***
Normal	96	3	1	98	1	1	87	7	6
Neuropathy	5	43	2	1	48	1	21	22	7
Myopathy	3	0	47	1	0	49	9	0	41

Figure.5.6 represents the most common features that have been selected by ReliefF and FCBF, the Discrete wavelet frequency features: peak, mean, and median for details and the total power and also the Shannon wavelet entropy for approximation.

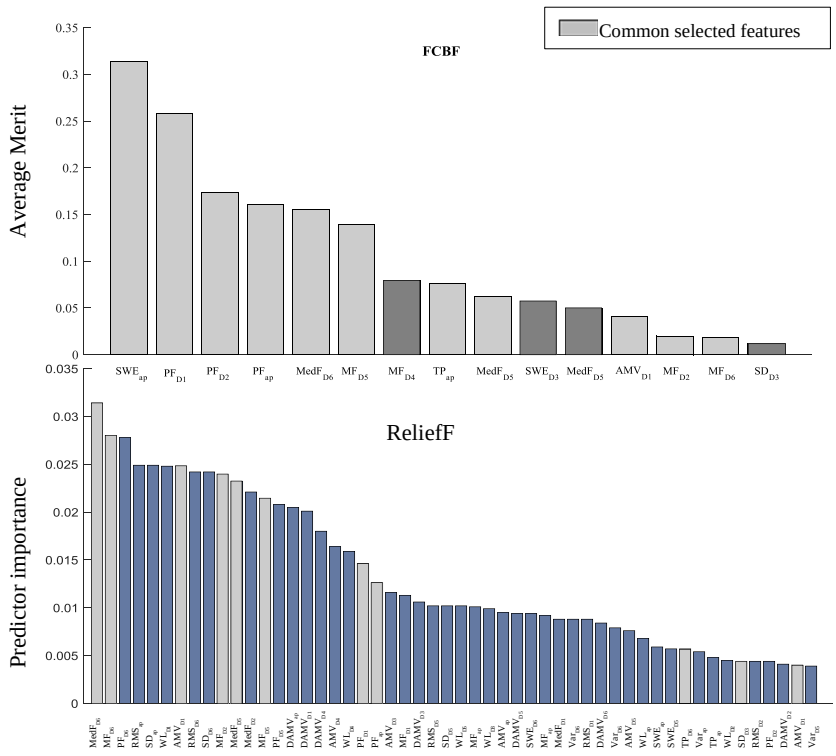

Figure 5.6: Ranking of relevant features using ReliefF and FCBF algorithms.

The five supervised classifiers i.e. LDA, random forest with 30 trees, decision tree with 30 trees, SVM, and k-NN (k=3) were compared using Matlab R2017a

and performed on 1.99 GHz Intel Core i7-8550U based PC with 8 GB RAM, 64-bit Windows 10. Table 5.4 shows that the LDA classifier with ReliefF achieved higher performance compared to other classifiers. As well as, the feature selection method improves the classification performance and also reduces the computation time.

Table 5.4: The classification performance for five supervised classifiers using clinical EMG signals

	Performance metrics	**LDA**	**Random Forest**	**Decision Tree**	**SVM**	**k-NN**
Before selection	Overall accuracy	93.0	90.5	80.5	84.0	79.0
	Average sensitivity	96.0	92.0	83.0	92.0	85.0
	Average specificity	92.0	90.0	80.0	79.0	78.0
	Computation time (s)	5.5	15.1	3.6	5.3	1.5
After selection (ReliefF)	Overall accuracy	97.5	91.5	81.5	82.5	79.5
	Average sensitivity	98.0	95.0	86.0	90.0	83.0
	Average specificity	98.0	89.0	79.0	76.0	81.0
	Computation time (s)	4.3	12.3	2.9	4.5	1.3

The overall classification accuracy of our proposed method was compared to other studies applying the same clinical EMG database. The relevant features with the right choice of classifier improve the classification performance, as shown in table 5.5, our proposed method achieved a higher overall classification accuracy of 97.5%.

Table 5.5: Comparison of feature extraction methods of other studies

Methods	**Classifiers**	**OCA(%)**
MSPCA + statistical DWT features[120]	Random Forest	88.0
DWT spectral features [117]	k-NN	80.5
wavelet energy and Hudgins' set features [115]	k-NN	79.0
Time-frequency and direct spectral features + ReliefF [127]	Random Forest	88.5
Our proposed method	LDA	**97.5**

5.6 Conclusion

In this chapter, we presented an approach for neuromuscular disorders classification based on decomposition methods i.e. wavelet transform. A set of features were extracted from decomposed signals then filtered by using reliefF and FCBF selection methods and classified by LDA classifier. This approach was first tested and evaluated on the simulated iEMG database then validated by iEMG clinical database,Where the DWT-ReliefF-LDA combination achieved a higher performance with an accuracy of 97.5%.
In future work, we will improve the classification performance by using more decomposition methods for feature extraction and selecting the optimum features by testing more feature selection methods. Finally, we will finish this dissertation by conclusion and putting forward some recommendations and research lines for our future studies.

Conclusion

In this Ph.D. Dissertation, we develop a real-time sEMG measurement system for recording and collecting the data. These collected data have been processed to study statistically the effect of age, gender, diabetes, handedness, and obesity on sEMG characteristics.
In medical applications, the onset and offset timing of muscle activation are very important parameters for detecting the functionality and dysfunctionality of muscle. For this purpose, we used The S-transform based detection method, The performance of this method has been compared with the recent methods: Teager-Kaiser Energy Operator, Integrated Profile, Sample Entropy, which reports a lower average latency of $\tau_{onset} = 0.015$ s, $\tau_{offset} = 0.014$ s.
During dynamic contraction especially for the gait, the muscle activation interval and the linear relationship between extensor/flexor muscles and the knee are reliable parameters used for knee pathology detection.
Moreover, we develop an automatic classification method for knee injury diagnosis i.e. ACL and meniscus injuries using sEMG and knee goniometry. Specific features are extracted from sEMG and goniometric signals in the temporal and spectral domains, also we have used the autocorrelation for extracting the cyclic features and linear correlation to determine the relationship between the knee.
The feature selection method is used to filter the irrelevant feature, enhance the prediction performance, and reduce the computation time. After selecting the relevant features by reliefF, we have employed five supervised classifiers i.e. Random Forest, Decision Tree, Diagonal-Linear Discriminant Analysis (DLDA), SVM with polynomial kernel function, and k-NN for classification and validating our results by cross-validation.
The higher classification performance (Acc= 98,29%) was obtained by the combination of random forest and the reliefF algorithm.
For neuromuscular disorders classification i.e. neuropathy and myopathy, we have developed an automatic diagnosis technique based on wavelet transform using iEMG signals. The wavelet transform techniques i.e. Discrete wavelet transform and Wavelet packet transform have been used for signal decomposition and

extracting the statistical features from each sub-band, then selecting the relevant ones using the filter methods i.e. ReliefF and Fast CorrelationBased feature FCBF. This approach was first tested and evaluated on the simulated iEMG database then validated by the iEMG clinical database, where the combination of DWT, ReliefF, and LDA classifier yieled a higher classification accuracy of 97.5%.

Future Directions

In the current studies, there are some limitations will be developed in the future.

- Development of wireless sophisticated sEMG measurement system and collect more data during dynamic movement.
- Enhance the prediction performance by exploiting more advanced signal processing techniques for feature extraction and testing other feature selection methods.
- Develop an automatic system for knee injuries diagnosis using deep learning.

Appendix A

Publications

During my Ph.D. study, some parts of my research have resulted in 1 peer-reviewed journal paper, 7 peer-reviewed international conference papers, and in 4 national conference papers listed as follows.

International Journal Papers

Benazzouz, A and Hadj Slimane, Z. E. (In press) "Knee pathology diagnosis based on muscle activation intervals detection and the relationship between knee flexion and surface emg", *International Journal of Medical Engineering and Informatics*, In press.

International Conference Papers

Benazzouz, A., Amirouche, F., Rieta, J.J., Guilal, R. (2019) "Knee injuries classification using sEMG and goniometric features during gait", *4th International Conference on Embedded Systems in Telecommunications and Instrumentation (ICESTI'19).* October 28th-30th, 2019. Annaba. Algeria. (Oral presentation).
Benazzouz, A., Guilal, R., Amirouche, F., and Hadj Slimane, Z. E. (2019) 'Emg feature selection for diagnosis of neuromuscular disorders', *In 2019 International Conference on Networking and Advanced Systems (ICNAS)*, IEEE, pp.1–5. (Oral presentation).
Benazzouz, A and Hadj Slimane, Z. E. (2018) "An automatic muscle activation detection using discrete wavelet and integrated profile: A comparative study", *in International Conference on Computer Science and its Applications.* Springer, 2018, pp. 169–178. (Poster presentation).
Benazzouz, A and Hadj Slimane, Z. E. (2018) "SEMG denoising and muscle

activation detection using wavelet transform", *The 1st International Workshop on Innovation in Biomechanics and Biomaterials (IWIBAB2018).* April 4th -5th, 2018.Oran, Algeria. (Poster presentation).
Benazzouz, A and Hadj Slimane, Z. E. (2017) "The SEMG-force relationship and the muscle weakness". *The 3rd International Conference on Electrical Engineering and Control Applications (ICEECA2017).* November 21st -23rd, 2017. Constantine, Algeria.(Oral presentation).
Benazzouz, A and Hadj Slimane, Z. E. (2017) "Study of the effects of the muscle weakness on surface EMG". *IEEE international conference on WIreless Technologies, embedded and intelligent Systems - WITS-2017.* April 19th -20th, 2017. Fez, Morocco. (Oral presentation).
Benazzouz, A and Hadj Slimane, Z. E. (2016) "Real-time acquisition of surface EMG signal system", *3rd International Conference on Embedded Systems in Telecommunications and Instrumentation (ICESTI'16).* October 24th -26th, 2016. Annaba. Algeria. (Oral presentation).

National Conference Papers

Benazzouz, A., Guilal, R., and Hadj Slimane, Z. E. (2019) "Detection of onset and offset of muscle contraction using sEMG signal". *9ème journée doctorale de Génie Biomédical (JD-GBM'19)*, Tlemcen. Algeria. (Poster presentation).
Benazzouz, A. and Hadj Slimane, Z. E. (2018) "sEMG signals classification for knee pathologies diagnosis using K-nn", *7eme Journée de maintenance biomédicale (JMB2018), Hopital central de l'armée, Dr Mohamed Sghir Nekkache*, October 4th , 2018, Algiers, Algeria. (Poster presentation).
Benazzouz, A. and Hadj Slimane, Z. E. (2018) "Denoising the real SEMG signal using wavelet transform".*8ème journée doctorale de Génie Biomédical (JD-GBM'18).* Tlemcen. Algeria. (Poster presentation).
Benazzouz, A. and Hadj Slimane, Z. E. (2016) "Design and realization of a surface EMG signal detection circuit".*6ème journée doctorale de Génie Biomédical (JD-GBM'16).* Tlemcen. Algeria. (Poster presentation).

Bibliography

[1] http://encyclopedia.lubopitko-bg.com/Functions-and-Types-of-Muscles.html. [Consulted on line 09-November-2019].

[2] https://www.healthpages.org/health-a-z/anatomy-major-anterior-muscles. [Consulted on line 17-January-2020].

[3] https://basicmedicalkey.com /anatomy-of-the-muscular-system. [Consulted on line 17-January-2020].

[4] http://www.me.umn.edu/labs/hmd/lab/docs/widmaier-samplech9. pdf. Consulted on line 17-January-2020.

[5] http://wifimovies.weebly.com/blog/motor-units-and-motor-unit-activation. [Consulted on line 17-January-2020].

[6] J. G. Betts, a. J. A. W. Kelly A., Young, J. Eddie, P. Brandon, K. Dean H., K. Oksana, J. Jody E., W. Mark, and D. Peter, *Anatomy and Physiology*. OpenStax, 2013. ISBN-13: 978-1-938168-13-0.

[7] https://www.edises.it/file/minicd/mart018/misc/assignmentfiles/nervous/IonChannels. pdf. [Consulted on line 17-January-2020].

[8] P. Konrad, "The abc of emg: A practical introduction to kinesiological electromyography.," 2005.

[9] G. Jenkins, C. Kemnitz, and G. J. Tortora, *Anatomy and physiology: from science to life*. John Wiley & Sons Incorporated, 2006.

[10] T. Rudroff, "Kinesiological fine wire emg: A practical introduction to fine wire emg applications," *Arisona: Noraxon USA*, 2008.

[11] http://www.leehealth.org/healthinformation/graphics/images. [Consulted on line 17-January-2020].

[12] https://image.slidesharecdn.com/kneejoint. [Consulted on line 17-January-2020].

[13] https://www.mayoclinic.org. [Consulted on line 17-January-2020].

[14] K. S. Saladin, "Anatomy & physiology: the unity of form and function," 2004.

[15] W. Scott, J. Stevens, and S. A. Binder-Macleod, "Human skeletal muscle fiber type classifications," *Physical therapy*, vol. 81, no. 11, pp. 1810–1816, 2001.

[16] G. S. Rash and P. Quesada, "Electromyography fundamentals," *Retrieved February*, vol. 4, 2003.

[17] C. Assaiante, M. Woollacott, and B. Amblard, "Development of postural adjustment during gait initiation: kinematic and emg analysis," *Journal of Motor Behavior*, vol. 32, no. 3, pp. 211–226, 2000.

[18] C. Steele, *Applications of emg in clinical and sports medicine*. BoD–Books on Demand, 2012.

[19] J. Romkes, C. Rudmann, and R. Brunner, "Changes in gait and emg when walking with the masai barefoot technique," *Clinical Biomechanics*, vol. 21, no. 1, pp. 75–81, 2006.

[20] A. Strazza, A. Mengarelli, S. Fioretti, L. Burattini, V. Agostini, M. Knaflitz, and F. Di Nardo, "Surface-emg analysis for the quantification of thigh muscle dynamic co-contractions during normal gait," *Gait & posture*, vol. 51, pp. 228–233, 2017.

[21] D. H. Sutherland, "The evolution of clinical gait analysis part l: kinesiological emg," *Gait & posture*, vol. 14, no. 1, pp. 61–70, 2001.

[22] A. B. Ajiboye and R. F. Weir, "A heuristic fuzzy logic approach to emg pattern recognition for multifunctional prosthesis control," *IEEE Transactions on Neural Systems and Rehabilitation Engineering*, vol. 13, no. 3, pp. 280–291, 2005.

[23] F. H. Chan, Y.-S. Yang, F. Lam, Y.-T. Zhang, and P. A. Parker, "Fuzzy emg classification for prosthesis control," *IEEE transactions on rehabilitation engineering*, vol. 8, no. 3, pp. 305–311, 2000.

[24] C. Cipriani, F. Zaccone, S. Micera, and M. C. Carrozza, "On the shared control of an emg-controlled prosthetic hand: analysis of user–prosthesis interaction," *IEEE Transactions on Robotics*, vol. 24, no. 1, pp. 170–184, 2008.

[25] M. A. Schweisfurth, M. Markovic, S. Dosen, F. Teich, B. Graimann, and D. Farina, "Electrotactile emg feedback improves the control of prosthesis grasping force," *Journal of neural engineering*, vol. 13, no. 5, p. 056010, 2016.

[26] M. Lucovnik, R. J. Kuon, L. R. Chambliss, W. L. Maner, S.-Q. SHI, L. Shi, J. Balducci, and R. E. Garfield, "Use of uterine electromyography to diagnose term and preterm labor," *Acta obstetricia et gynecologica Scandinavica*, vol. 90, no. 2, pp. 150–157, 2011.

[27] P. Namadurai, V. Padmanabhan, and R. Swaminathan, "Multifractal analysis of uterine electromyography signals for the assessment of progression of pregnancy in term conditions," *IEEE journal of biomedical and health informatics*, 2018.

[28] R. E. Garfield, W. L. Maner, L. B. MacKay, D. Schlembach, and G. R. Saade, "Comparing uterine electromyography activity of antepartum patients versus term labor patients," *American journal of obstetrics and gynecology*, vol. 193, no. 1, pp. 23–29, 2005.

[29] C.-F. Lin, S.-H. Hua, M.-T. Huang, H.-H. Lee, and J.-C. Liao, "Biomechanical analysis of knee and trunk in badminton players with and without knee pain during backhand diagonal lunges," *Journal of Sports Sciences*, vol. 33, no. 14, pp. 1429–1439, 2015.

[30] A. D. Vigotsky, I. Halperin, G. J. Lehman, G. S. Trajano, and T. M. Vieira, "Interpreting signal amplitudes in surface electromyography studies in sport and rehabilitation sciences," *Frontiers in Physiology*, vol. 8, p. 985, 2018.

[31] R. M. Howard, R. Conway, and A. J. Harrison, "A survey of sensor devices: use in sports biomechanics," *Sports biomechanics*, vol. 15, no. 4, pp. 450–461, 2016.

[32] S. Venugopalan, F. Juefei-Xu, B. Cowley, and M. Savvides, "Electromyograph and keystroke dynamics for spoof-resistant biometric authentication," in *Proceedings of the IEEE Conference on Computer Vision and Pattern Recognition Workshops*, pp. 109–118, 2015.

[33] Q. Li, P. Dong, and J. Zheng, "Enhancing the security of pattern unlock with surface emg-based biometrics," *Applied Sciences*, vol. 10, no. 2, p. 541, 2020.

[34] G. Yang, W. Tan, H. Jin, T. Zhao, and L. Tu, "Review wearable sensing system for gait recognition," *Cluster Computing*, vol. 22, no. 2, pp. 3021–3029, 2019.

[35] S. Kumar, *Electromyography in ergonomics*. Routledge, 2017.

[36] B. Steinhilber, S. Hoffmann, K. Karlovic, S. Pfeffer, T. Maier, O. Hallasheh, S. Kruck, R. Seibt, M. A. Rieger, M. Heidingsfeld, *et al.*, "Development of an arm support system to improve ergonomics in laparoscopic surgery: study design and provisional results," *Surgical endoscopy*, vol. 29, no. 9, pp. 2851–2858, 2015.

[37] O. Dostál, O. Vysata, L. Pazdera, A. Procházka, J. Kopal, J. Kuchyňka, and M. Vališ, "Permutation entropy and signal energy increase the accuracy of neuropathic change detection in needle emg," *Computational intelligence and neuroscience*, vol. 2018, 2018.

[38] W. G. Jung, "Op amp application handbook," 2002. ISNB0-916550-26-5.

[39] "Arduino uno." https://store.arduino.cc/arduino-uno-rev3. [Consulted on line 17-January-2020].

[40] M. H. Hayes, "Schaum's outline of theory and problems of digital signal processing," 1998. ISBN 0070273898.

[41] A. D. Association *et al.*, "Diagnosis and classification of diabetes mellitus," *Diabetes care*, vol. 36, no. Supplement 1, pp. S67–S74, 2013.

[42] J. Lexell, K. Henriksson-Larsén, B. Winblad, and M. Sjöström, "Distribution of different fiber types in human skeletal muscles: effects of aging studied in whole muscle cross sections," *Muscle & Nerve: Official Journal of the American Association of Electrodiagnostic Medicine*, vol. 6, no. 8, pp. 588–595, 1983.

[43] W. R. Frontera, V. A. Hughes, R. A. Fielding, M. A. Fiatarone, W. J. Evans, and R. Roubenoff, "Aging of skeletal muscle: a 12-yr longitudinal study," *Journal of applied physiology*, vol. 88, no. 4, pp. 1321–1326, 2000.

[44] K. Haizlip, B. Harrison, and L. Leinwand, "Sex-based differences in skeletal muscle kinetics and fiber-type composition," *Physiology*, vol. 30, no. 1, pp. 30–39, 2015.

[45] S. G. Wannamethee and J. L. Atkins, "Muscle loss and obesity: the health implications of sarcopenia and sarcopenic obesity," *Proceedings of the Nutrition Society*, vol. 74, no. 4, pp. 405–412, 2015.

[46] H. Wu and C. M. Ballantyne, "Skeletal muscle inflammation and insulin resistance in obesity," *The Journal of clinical investigation*, vol. 127, no. 1, pp. 43–54, 2017.

[47] F. W. King, *Hilbert transforms*, vol. 2. Cambridge University Press Cambridge, 2009.

[48] C. Hardyck and L. F. Petrinovich, "Left-handedness.," *Psychological bulletin*, vol. 84, no. 3, p. 385, 1977.

[49] A. M. VencesBrito, M. A. R. Ferreira, N. Cortes, O. Fernandes, and P. Pezarat-Correia, "Kinematic and electromyographic analyses of a karate punch," *Journal of Electromyography and Kinesiology*, vol. 21, no. 6, pp. 1023–1029, 2011.

[50] T. J. Limbird, R. Shiavi, M. Frazer, and H. Borra, "Emg profiles of knee joint musculature during walking: changes induced by anterior cruciate ligament deficiency," *Journal of orthopaedic research*, vol. 6, no. 5, pp. 630–638, 1988.

[51] S. Gallena, P. J. Smith, T. Zeffiro, and C. L. Ludlow, "Effects of levodopa on laryngeal muscle activity for voice onset and offset in parkinson disease," *Journal of Speech, Language, and Hearing Research*, 2001.

[52] T. Hortobágyi, S. Solnik, A. Gruber, P. Rider, K. Steinweg, J. Helseth, and P. DeVita, "Interaction between age and gait velocity in the amplitude and timing of antagonist muscle coactivation," *Gait & posture*, vol. 29, no. 4, pp. 558–564, 2009.

[53] F. Di Nardo, E. Maranesi, A. Mengarelli, G. Ghetti, L. Burattini, and S. Fioretti, "Assessment of the variability of vastii myoelectric activity in young healthy females during walking: A statistical gait analysis," *Journal of electromyography and kinesiology*, vol. 25, no. 5, pp. 800–807, 2015.

[54] A. Alves-Pinto, T. Blumenstein, V. Turova, and R. Lampe, "Altered lower leg muscle activation patterns in patients with cerebral palsy during cycling on an ergometer," *Neuropsychiatric disease and treatment*, vol. 12, p. 1445, 2016.

[55] J. Downar, D. J. Mikulis, and K. D. Davis, "Neural correlates of the prolonged salience of painful stimulation," *Neuroimage*, vol. 20, no. 3, pp. 1540–1551, 2003.

[56] J. Woods and B. Bigland-Ritchie, "Linear and non-linear surface emg/force relationships in human muscles. an anatomical/functional argument for the existence of both.," *American journal of physical medicine*, vol. 62, no. 6, pp. 287–299, 1983.

[57] G. Vannozzi, S. Conforto, and T. DAlessio, "Automatic detection of surface emg activation timing using a wavelet transform based method," *Journal of Electromyography and Kinesiology*, vol. 20, no. 4, pp. 767–772, 2010.

[58] S. Solnik, P. Rider, K. Steinweg, P. DeVita, and T. Hortobágyi, "Teager–kaiser energy operator signal conditioning improves emg onset detection," *European journal of applied physiology*, vol. 110, no. 3, pp. 489–498, 2010.

[59] X. Zhang and P. Zhou, "Sample entropy analysis of surface emg for improved muscle activity onset detection against spurious background spikes," *Journal of Electromyography and Kinesiology*, vol. 22, no. 6, pp. 901–907, 2012.

[60] P. Zhou and X. Zhang, "A novel technique for muscle onset detection using surface emg signals without removal of ecg artifacts," *Physiological measurement*, vol. 35, no. 1, p. 45, 2013.

[61] J. Liu and Q. Liu, "Use of the integrated profile for voluntary muscle activity detection using emg signals with spurious background spikes: A study with incomplete spinal cord injury," *Biomedical Signal Processing and Control*, vol. 24, pp. 19–24, 2016.

[62] P. Karthick, D. M. Ghosh, and S. Ramakrishnan, "Surface electromyography based muscle fatigue detection using high-resolution time-frequency methods and machine learning algorithms," *Computer methods and programs in biomedicine*, vol. 154, pp. 45–56, 2018.

[63] C. Aubel, D. Stotz, and H. Bölcskei, "A theory of super-resolution from short-time fourier transform measurements," *Journal of Fourier Analysis and Applications*, vol. 24, no. 1, pp. 45–107, 2018.

[64] Y. Wang, *Efficient stockwell transform with applications to image processing*. PhD thesis, University of Mathematics Waterloo, Ontario, Canada, 2011.

[65] J.-U. Chu, I. Moon, and M.-S. Mun, "A real-time emg pattern recognition system based on linear-nonlinear feature projection for a multifunction myoelectric hand," *IEEE Transactions on biomedical engineering*, vol. 53, no. 11, pp. 2232–2239, 2006.

[66] P. Marwaha and R. K. Sunkaria, "Cardiac variability time–series analysis by sample entropy and multiscale entropy," *International Journal of Medical Engineering and Informatics*, vol. 7, no. 1, pp. 1–14, 2014.

[67] F. Flandry and G. Hommel, "Normal anatomy and biomechanics of the knee," *Sports medicine and arthroscopy review*, vol. 19, no. 2, pp. 82–92, 2011.

[68] D. R. Peterson and J. D. Bronzino, *Biomechanics: principles and applications*. CRC press, 2007.

[69] S. Masouros, A. Bull, and A. Amis, "(i) biomechanics of the knee joint," *Orthopaedics and Trauma*, vol. 24, no. 2, pp. 84–91, 2010.

[70] D. A. Winter, *Biomechanics and motor control of human movement*. John Wiley & Sons, 2009.

[71] K. P. Spindler and R. W. Wright, "Anterior cruciate ligament tear," *New England Journal of Medicine*, vol. 359, no. 20, pp. 2135–2142, 2008.

[72] M. Majewski, H. Susanne, and S. Klaus, "Epidemiology of athletic knee injuries: A 10-year study," *The knee*, vol. 13, no. 3, pp. 184–188, 2006.

[73] J. N. Katz, R. H. Brophy, C. E. Chaisson, L. De Chaves, B. J. Cole, D. L. Dahm, L. A. Donnell-Fink, A. Guermazi, A. K. Haas, M. H. Jones, *et al.*, "Surgery versus physical therapy for a meniscal tear and osteoarthritis," *New England Journal of Medicine*, vol. 368, no. 18, pp. 1675–1684, 2013.

[74] D. T. Felson, "Osteoarthritis of the knee," *New England Journal of Medicine*, vol. 354, no. 8, pp. 841–848, 2006.

[75] G. W. Woods, R. F. Stanley JR, and H. S. Tullos, "Lateral capsular sign: x-ray clue to a significant knee instability," *The American journal of sports medicine*, vol. 7, no. 1, pp. 27–33, 1979.

[76] A. Hart, J. Buscombe, A. Malone, and G. Dowd, "Assessment of osteoarthritis after reconstruction of the anterior cruciate ligament: a study using single-photon emission computed tomography at ten years," *The Journal of bone and joint surgery. British volume*, vol. 87, no. 11, pp. 1483–1487, 2005.

[77] J. T. Bencardino, Z. S. Rosenberg, R. R. Brown, A. Hassankhani, E. S. Lustrin, and J. Beltran, "Traumatic musculotendinous injuries of the knee: diagnosis with mr imaging," *Radiographics*, vol. 20, no. suppl_1, pp. S103–S120, 2000.

[78] R. Rossi, F. Dettoni, M. Bruzzone, U. Cottino, D. G. D'Elicio, and D. E. Bonasia, "Clinical examination of the knee: know your tools for diagnosis of knee injuries," *Sports Medicine, Arthroscopy, Rehabilitation, Therapy & Technology*, vol. 3, no. 1, p. 25, 2011.

[79] K. J. McHale, M. J. Park, and F. P. Tjoumakaris, "Physical examination for meniscus tears," in *Meniscal Injuries*, pp. 9–20, Springer, 2014.

[80] F. Amirouche and G. F. Solitro, "Challenges in modeling total knee arthroplasty and total hip replacement," *Procedia IUTAM*, vol. 2, pp. 18–25, 2011.

[81] F. Amirouche, "Device and method of spacer and trial design during joint arthroplasty," Oct. 11 2007. US Patent App. 11/394,306.

[82] S. R. Hundza, W. R. Hook, C. R. Harris, S. V. Mahajan, P. A. Leslie, C. A. Spani, L. G. Spalteholz, B. J. Birch, D. T. Commandeur, and N. J. Livingston, "Accurate and reliable gait cycle detection in parkinson's disease," *IEEE Transactions on Neural Systems and Rehabilitation Engineering*, vol. 22, no. 1, pp. 127–137, 2014.

[83] N. Nazmi, M. A. A. Rahman, S.-I. Yamamoto, and S. A. Ahmad, "Walking gait event detection based on electromyography signals using artificial neural network," *Biomedical Signal Processing and Control*, vol. 47, pp. 334–343, 2019.

[84] Y. Cao, F. Gao, L. Yu, and Q. She, "Gait recognition based on emg information with multiple features," in *International Conference on Intelligent Information Processing*, pp. 402–411, Springer, 2018.

[85] G. R. Naik, S. E. Selvan, S. P. Arjunan, A. Acharyya, D. K. Kumar, A. Ramanujam, and H. T. Nguyen, "An ica-ebm-based semg classifier for recognizing lower limb movements in individuals with and without knee pathology," *IEEE Transactions on Neural Systems and Rehabilitation Engineering*, vol. 26, no. 3, pp. 675–686, 2018.

[86] D. Jarchi, J. Pope, T. K. Lee, L. Tamjidi, A. Mirzaei, and S. Sanei, "A review on accelerometry-based gait analysis and emerging clinical applications," *IEEE reviews in biomedical engineering*, vol. 11, pp. 177–194, 2018.

[87] I. N. Afiah, H. Nakashima, P. Y. Loh, and S. Muraki, "An exploratory investigation of changes in gait parameters with age in elderly japanese women," *Springerplus*, vol. 5, no. 1, p. 1069, 2016.

[88] V. Agostini, F. L. Fermo, G. Massazza, and M. Knaflitz, "Does texting while walking really affect gait in young adults?," *Journal of neuroengineering and rehabilitation*, vol. 12, no. 1, p. 86, 2015.

[89] T. Varrecchia, M. Rinaldi, M. Serrao, F. Draicchio, C. Conte, S. Conforto, M. Schmid, and A. Ranavolo, "Global lower limb muscle coactivation during walking at different speeds: relationship between spatio-temporal, kinematic, kinetic, and energetic parameters," *Journal of electromyography and kinesiology*, vol. 43, pp. 148–157, 2018.

[90] W. J. Hurd and L. Snyder-Mackler, "Knee instability after acute acl rupture affects movement patterns during the mid-stance phase of gait," *Journal of Orthopaedic Research*, vol. 25, no. 10, pp. 1369–1377, 2007.

[91] P.-n. Wei, R. Xie, R. Tang, C. Li, J. Kim, and M. Wu, "semg based gait phase recognition for children with spastic cerebral palsy," *Annals of biomedical engineering*, vol. 47, no. 1, pp. 223–230, 2019.

[92] M. Janidarmian, K. Radecka, and Z. Zilic, "Automated diagnosis of knee pathology using sensory data," in *2014 4th International Conference on Wireless Mobile Communication and Healthcare-Transforming Healthcare Through Innovations in Mobile and Wireless Technologies (MOBIHEALTH)*, pp. 95–98, IEEE, 2014.

[93] M. Herrera-González, G. A. Martínez-Hernández, J. L. Rodríguez-Sotelo, and Ó. F. Avilés-Sánchez, "Knee functional state classification using surface electromyographic and goniometric signals by means of artificial neural networks," *Ingeniería y Universidad*, vol. 19, no. 1, pp. 51–66, 2015.

[94] K. Bache and M. Lichman, "Uci machine learning repository [http://archive. ics. uci. edu/ml]. irvine, ca: University of california," *School of information and computer science*, vol. 28, 2013.

[95] A. Hyvärinen and E. Oja, "Independent component analysis: algorithms and applications," *Neural networks*, vol. 13, no. 4-5, pp. 411–430, 2000.

[96] M. Bernabei, J. H. Van Dieen, and H. Maas, "Longitudinal and transversal displacements between triceps surae muscles during locomotion of the rat," *Journal of Experimental Biology*, vol. 220, no. 4, pp. 537–550, 2017.

[97] A. Smrdel and F. Jager, "Separating sets of term and pre-term uterine emg records," *Physiological measurement*, vol. 36, no. 2, p. 341, 2015.

[98] R. Boostani and M. H. Moradi, "Evaluation of the forearm emg signal features for the control of a prosthetic hand," *Physiological measurement*, vol. 24, no. 2, p. 309, 2003.

[99] L. Yu and H. Liu, "Feature selection for high-dimensional data: A fast correlation-based filter solution," in *Proceedings of the 20th international conference on machine learning (ICML-03)*, pp. 856–863, 2003.

[100] J. Too, A. R. Abdullah, N. Mohd Saad, and W. Tee, "Emg feature selection and classification using a pbest-guide binary particle swarm optimization," *Computation*, vol. 7, no. 1, p. 12, 2019.

[101] A. Phinyomark, P. Phukpattaranont, and C. Limsakul, "Feature reduction and selection for emg signal classification," *Expert systems with applications*, vol. 39, no. 8, pp. 7420–7431, 2012.

[102] A. Phinyomark, S. Hirunviriya, C. Limsakul, and P. Phukpattaranont, "Evaluation of emg feature extraction for hand movement recognition based on euclidean distance and standard deviation," in *ECTI-CON2010: The 2010 ECTI International Confernce on Electrical Engineering/Electronics, Computer, Telecommunications and Information Technology*, pp. 856–860, IEEE, 2010.

[103] J. Liu, X. Li, G. Li, and P. Zhou, "Emg feature assessment for myoelectric pattern recognition and channel selection: a study with incomplete spinal cord injury," *Medical engineering & physics*, vol. 36, no. 7, pp. 975–980, 2014.

[104] H. Huang, H.-B. Xie, J.-Y. Guo, and H.-J. Chen, "Ant colony optimization-based feature selection method for surface electromyography signals classification," *Computers in biology and medicine*, vol. 42, no. 1, pp. 30–38, 2012.

[105] I. Kononenko, "Estimating attributes: analysis and extensions of relief," in *European conference on machine learning*, pp. 171–182, Springer, 1994.

[106] L. Breiman, "Random forests," *Machine learning*, vol. 45, no. 1, pp. 5–32, 2001.

[107] H. K.A, *Principles of electromyography.* The Biomedical Engineering Handbook, pp.244, CRC Press LLC, USA., 2002.

[108] F. Buchthal, *An introduction to electromyography.* Gyldendal, 1957.

[109] L. Pino, D. Stashuk, S. Boe, and T. Doherty, "Motor unit potential characterization using pattern discovery," *Medical engineering & physics*, vol. 30, no. 5, pp. 563–573, 2008.

[110] A. A. Brownell and M. B. Bromberg, "Effects of intramuscular needle position on motor unit action potential metrics," *Muscle & Nerve: Official Journal of the American Association of Electrodiagnostic Medicine*, vol. 35, no. 4, pp. 465–470, 2007.

[111] A. Hazarika, L. Dutta, M. Boro, M. Barthakur, and M. Bhuyan, "An automatic feature extraction and fusion model: application to electromyogram (emg) signal classification," *International Journal of Multimedia Information Retrieval*, vol. 7, no. 3, pp. 173–186, 2018.

[112] G. R. Naik, S. E. Selvan, and H. T. Nguyen, "Single-channel emg classification with ensemble-empirical-mode-decomposition-based ica for diagnosing neuromuscular disorders," *IEEE Transactions on Neural Systems and Rehabilitation Engineering*, vol. 24, no. 7, pp. 734–743, 2016.

[113] O. Dostál, O. Vysata, L. Pazdera, A. Procházka, J. Kopal, J. Kuchyňka, and M. Vališ, "Permutation entropy and signal energy increase the accuracy of neuropathic change detection in needle emg," *Computational intelligence and neuroscience*, vol. 2018, 2018.

[114] S. Koçer and A. E. Tümer, "Classifying neuromuscular diseases using artificial neural networks with applied autoregressive and cepstral analysis," *Neural Computing and Applications*, vol. 28, no. 1, pp. 945–952, 2017.

[115] D. Barmpakos, P. Kaplanis, S. A. Karkanis, and C. Pattichis, "Classification of neuromuscular disorders using features extracted in the wavelet domain of semg signals: a case study," *Health and Technology*, vol. 7, no. 1, pp. 33–39, 2017.

[116] B. Hudgins, P. Parker, and R. N. Scott, "A new strategy for multifunction myoelectric control," *IEEE Transactions on Biomedical Engineering*, vol. 40, no. 1, pp. 82–94, 1993.

[117] V. A. Krishna and P. Thomas, "Classification of emg signals using spectral features extracted from dominant motor unit action potential," *International Journal of Engineering and Advanced Technology*, vol. 4, no. 5, pp. 196–200, 2015.

[118] A. Bhattacharya, P. Pahari, P. Basak, and A. Sarkar, "Class discriminator-based emg classification approach for detection of neuromuscular diseases using discriminator-dependent decision rule (d3r) approach," in *Recent Trends in Signal and Image Processing*, pp. 49–56, Springer, 2019.

[119] A. Subasi, "Classification of emg signals using combined features and soft computing techniques," *Applied soft computing*, vol. 12, no. 8, pp. 2188–2198, 2012.

[120] E. Gokgoz and A. Subasi, "Comparison of decision tree algorithms for emg signal classification using dwt," *Biomedical Signal Processing and Control*, vol. 18, pp. 138–144, 2015.

[121] A. Hamilton-Wright and D. W. Stashuk, "Physiologically based simulation of clinical emg signals," *IEEE Transactions on biomedical engineering*, vol. 52, no. 2, pp. 171–183, 2005.

[122] M. Nikolic, *Detailed analysis of clinical electromyography signals: EMG decomposition, findings and firing pattern analysis in controls and patients with myopathy and amytrophic lateral sclerosis.* PhD thesis, 2001.

[123] M. Misiti, Y. Misiti, G. Oppenheim, and J.-M. Poggi, *Wavelets and their Applications.* John Wiley & Sons, 2013.

[124] R. Q. Quiroga, O. Rosso, and E. Basar, "Wavelet entropy: a measure of order in evoked potentials," *Electr. Clin. Neurophysiol.(Suppl.)*, vol. 49, pp. 298–302, 1999.

[125] L. Yu and H. Liu, "Feature selection for high-dimensional data: A fast correlation-based filter solution," in *Proceedings of the 20th international conference on machine learning (ICML-03)*, pp. 856–863, 2003.

[126] C. R. Rao, "The utilization of multiple measurements in problems of biological classification," *Journal of the Royal Statistical Society. Series B (Methodological)*, vol. 10, no. 2, pp. 159–203, 1948.

[127] A. Benazzouz, R. Guilal, F. Amirouche, and Z. E. H. Slimane, "Emg feature selection for diagnosis of neuromuscular disorders," in *2019 International Conference on Networking and Advanced Systems (ICNAS)*, pp. 1–5, IEEE, 2019.

[128] A. Tharwat, "Independent component analysis: An introduction," *Applied Computing and Informatics*, 2020.

Abstract: Electromyography is a technique for recording the electrical activity of skeletal muscles by means of either surface electrodes or concentric needles. The non-invasive technique surface electromyography (sEMG) has received significant attention in the past decade: in biomechanics, rehabilitation, control of prosthetic devices, for the development of emotion recognition systems, sports activities, and the science of exercise. On the other hand, the invasive technique in electromyography is employed for diagnosing neuromuscular disorders such as neuropathy and myopathy. The stochastic nature of these EMG signals complicates the interpretation, so it needs advanced methods for detection, processing, feature extraction, and classification.

This dissertation aims to extract the pertinent characteristics which are essential in the diagnosis and lead to correct prediction. During gait, the muscular activation interval, onset and offset timings are very important parameters used for studying the function of the muscle in healthy patients and detecting the abnormalities when the gait data is abnormal. These parameters have been precisely extracted by S-Transform.

We have also developed two automatic diagnosis approaches, one for soft tissue-knee injuries i.e. Anterior Cruciate Ligament ACL and Meniscus MN injuries using surface electromyographic sEMG and goniometric signals, and the other one for neuromuscular disorders i.e. neuropathy and myopathy using intramuscular electromyogram iEMG. These signals (sEMG/EMG) were collected and preprocessed for extracting the newly developed parameters associated with the different pathologies. The relevant features were selected using different criteria and methods classified by supervised classifiers. The newly developed algorithms are provided and shown through different applications and case studies.

Index Terms **_** Anterior ligament injury, classification, Electromyogram, feature extraction, feature selection, iEMG, knee injuries, meniscus injury, myopathy, neuromuscular disorders, neuropathy, sEMG, S-Transform.

Résumé: L'électromyographie est une technique qui permet d'enregistrer l'activité électrique des muscles soit par des électrodes de surface ou par des aiguilles concentriques. La technique non invasive sEMG reçoit une attention considérable dans différents domaines d'application tels que: biomécanique, réadaptation, contrôle des prothèses, développement d'un système de reconnaissance des gestes, sciences du sport… etc. Tandis que la technique invasive est utilisée pour diagnostiquer les maladies neuromusculaires comme la neuropathie et la myopathie. La nature aléatoire de ces signaux EMG complique l'interprétation. Alors dans ce cas, nous avons besoin des techniques avancées pour les détecter, les traiter, extraire les paramètres et les classifier. L'objectif de cette thèse de doctorat est d'extraire les caractéristiques les plus pertinentes du signal électromyogramme pour faciliter le diagnostic. Pendant la marche, l'intervalle d'activation musculaire, début et la fin et même l'intervalle d'activation musculaire sont des paramètres les plus utilisés pour étudier la fonction musculaire dans des cas sains et détecter les anomalies dans la démarche anormale, afin de détecter ces paramètres, en utilisant la transformée de Stockwell.

Nous avons également développé deux approches de diagnostic automatique, l'une pour les lésions des tissus mous du genou i.e. ruptures du ligament croisé antérieur LCA et les déchirures du ménisque, en utilisant les signaux EMG de surface et goniométriques, et l'autre pour les maladies neuromusculaires i.e. la neuropathie et la myopathie, en utilisant électromyogramme intramusculaire. Ces signaux (sEMG/iEMG) ont été collectés et prétraités pour extraire les paramètres pertinents. Les paramètres pertinents ont été sélectionnés selon différentes méthodes de sélection, enfin la classification a été effectuée par un apprentissage supervisé.

Mots clés**_** Ruptures du ligament croisé antérieur, classification, électromyographie, extraction des paramètres pertinents, la sélection, iEMG, lésion du genou, les déchirures du ménisque, myopathie, troubles neuromusculaires, neuropathie, sEMG, transformée de Stockwell.

ملخص: التخطيط الكهرو عضلي هو تقنية لتسجيل نشاط الكهربائي للعضلة إما بواسطة الأقطاب السطحية أو الإبر متحدة المركز. التقنية الغير باضعة (التخطيط الكهرو عضلي السطحي) عرفت اهتماما كبيرا وتطبيقات مختلفة في عدة المجالات مثل: الميكانيكا الحيوية، إعادة التأهيل، التحكم بالأطراف الاصطناعية، تطوير أنظمة التعرف الإماءات، الرياضة وعلم التمرين ... الخ. بينما التقنية الباضعة تستعمل غالبا في تشخيص الأمراض العصبية العضلية مثل الاعتلال العصبي والاعتلال العضلي. لكن الطبيعة العشوائية لهذه الإشارات تصعب علينا عملية التحليل والتفسير، لذا فهي تحتاج إلى تقنيات متقدمة للكشف، المعالجة، استخراج البيانات، والتصنيف.

الهف من هذه الأطروحة هو استخراج الخصائص المناسبة من الإشارة الكهرو عضلية لغرض تيسير وتسهيل عملية التشخيص. خلال المشي، فترة نشاط العضلي، وزمن البداية والنهاية من المعايير المهمة والمستعملة في دراسة عمل العضلة واكتشاف الخلل خلال المشي غير الطبيعي. قمنا بتطبيق التحويل ستوكوال من أجل استخراج هذه المعايير بدقة.

كذلك قمنا بتطوير طرق التشخيص التلقائي، الأولي من أجل تشخيص جروح في الأنسجة الرخوة للركبة خصوصا تمزق الرباط الصليبي الامامي والهلالة المفصلية، من أجل هذا الغرض استعملنا إشارات الكهرو عضلية السطحية وإشارات الزوايا الركبة. الطريقة الثانية من أجل تشخيص الأمراض العصبية العضلية (الاعتلال العصبي والاعتلال العضلي) باستعمال الإشارات الكهرو عضلية داخلية. هذه الإشارات جمعت وعولجت من اجل استخراج الخصائص. وأخيرا الخصائص والميزات الأكثر تأثير وأهمية انتقت وصنفت بواسطة مصنفات تحت الاشراف.

كلمات مفتاحية: التخطيط الكهرو عضلي، التحويل ستوكوال، جروح في الأنسجة الرخوة للركبة، تمزق الرباط الصليبي الامامي، تمزق الهلالة المفصلية، الاعتلال العصبي، الاعتلال العضلي، الأمراض العصبية العضلية، استخراج الخصائص، التصنيف.